AN INTEGRATED EXPERIMENTAL AND FINITE ELEMENT STUDY TO UNDERSTAND THE MECHANICAL BEHAVIOR OF CARBON REINFORCED POLYMER NANOCOMPOSITES

A Dissertation
Presented to
The Academic Faculty

by

Md Atiqur Rahman Bhuiyan

In Partial Fulfillment
of the Requirements for the Degree
Doctor of Philosophy in the
George W. Woodruff School of Mechanical Engineering

Georgia Institute of Technology
August 2013

AN INTEGRATED EXPERIMENTAL AND FINITE ELEMENT STUDY TO UNDERSTAND THE MECHANICAL BEHAVIOR OF CARBON REINFORCED POLYMER NANOCOMPOSITES

Approved by:

Dr. Kyriaki Kalaitzidou, Advisor
School of Mechanical Engineering
Georgia Institute of Technology

Dr. Raghuram V. Pucha
School of Mechanical Engineering
Georgia Institute of Technology

Dr. Suresh Sitaraman
School of Mechanical Engineering
Georgia Institute of Technology

Dr. Karl Jacob
School of Materials Science and
Engineering
Georgia Institute of Technology

Dr. Donggang Yao
School of Materials Science and
Engineering
Georgia Institute of Technology

Date Approved: May 17, 2013

To my wife Tamanna Rahman, daughter Sanika Mahdiya Neha,
brother-in-law Abir Ashfaqur Rahman
and
To my parents

ACKNOWLEDGEMENTS

I would like to sincerely acknowledge several individuals who helped me in many ways throughout my research and thesis writing process.

First, I would like to express my deepest gratitude to my advisor Dr. Kyriaki Kalaitzidou for her guidance, cordial suggestions and thought provoking directions to accomplish my thesis. Her mentorship and profound knowledge on the latest research topics have been invaluable resources throughout my graduate studies. Additional thanks to Dr. Raghuram V. Pucha for serving on my thesis committee and for helping me with the modeling part of my thesis. His expertise in finite element modeling has been invaluable and made this work possible.

I would also like to thank my other committee members, Dr. Suresh Sitaraman, Dr. Karl Jacob, and Dr. Donggang Yao for serving as my committee members and for providing me with insightful comments during my PhD proposal presentation.

I thank Dr. Jonathan Colton and Dr. Baratunde A. Cola for giving me access to the equipment in their labs. I also thank Johnny worthy for helping me with the image analysis part of my thesis. I am also grateful to Dr. Virendra Singh and Sarang Deodhar for helping me to prepare my samples for experimental characterization. I would like to thank all my colleagues in Dr. Kalaitzidou's lab, especially Mehdi Karavan, for their friendly support.

A special thanks to my family, my parents and parents-in-law, my two brothers Afzal and Arif, for all of the sacrifices they have made on my behalf. Finally, I would like to thank my beautiful wife Tamanna Rahman and to my brother-in-law Abir

TABLE OF CONTENTS

LIST OF TABLES

LIST OF FIGURES

xiv

SUMMARY

The exceptional properties of carbon nanomaterials make them ideal reinforcements for polymers. However, the main challenges in utilizing their unique properties are their tendency to form agglomerates, their non-controlled orientation, non-homogeneous distribution and finally the change in their shape/size due to processing. All the above are the result of the nanomaterial/polymer interfacial interactions which dictate the overall performance of the composites including the mechanical properties. The aforementioned uncertainties are the reason for the deviation observed between the experimentally determined properties and the theoretically expected ones. The focus of this study is to understand the reinforcing efficiency of carbon nanomaterials in polymers through finite element modeling that captures the effect of the interfacial interactions on the tensile modulus of polymer nanocomposites (PNCs). The novelty of this work is that the probability distribution functions of nanomaterials dispersion, distribution, orientation and waviness, determined through image analysis by extracting 3-D information from 2-D scanning electron micrographs, are incorporated into the finite element model allowing thus for fundamental understanding of how the nanostructure parameters affect the tensile modulus of the PNCs. The nanocomposites are made using melt mixing followed by either injections molding or melt spinning of fibers. Polypropylene (PP) is used as the polymer and carbon nanotubes (CNT) or exfoliated graphite nanoplatelets (xGnP) are used as nanoreinforcements. The presence of interphase, confirmed and characterized in terms of stiffness and width using atomic force microscopy, is also accounted for in the model. The dispersion and distribution of CNT within the polymer is experimentally

altered by using a surfactant and by forcing the molten material to flow through a narrow orifice (melt spinning) that promotes alignment of CNT and even of the polymer chains along the flow/drawing direction. The effect of nanomaterials' geometry on the mechanical behavior of PNCs is also studied by comparing the properties of CNT/PP to those of xGnP/PP composites. Finally the reinforcing efficiency of CNT is determined independently of the viscoelastic behavior of the polymer by conducting tensile testing at temperatures below the glass transition temperature of PP. The finite element model with the incorporated image analysis subroutine has sufficient resolution to distinguish among the different cases (dispersion, distribution, geometry and alignment of nanomaterials) and the predicted tensile modulus is in agreement with the experimentally determined one. In conclusion, this study provides a tool, that integrates finite element modeling and thorough experiments that enables design of polymer nanocomposites with engineered mechanical properties.

CHAPTER 1

INTRODUCTION

Polymer nanocomposites (PNCs) have received considerable interest in recent years both in academia and in industry. They have advantageous material properties such as improved mechanical properties, high electrical and thermal conductivity, resistance against corrosion, noise damping, thermal stability over metallic materials and many more, and in general their performance can be engineered for a wide range of applications (1, 2). The unusually large surface area to volume ratio and the small size (smaller than the critical flaw) of the nanomaterials, used as reinforcements in PNCs, are responsible for their unique properties. Despite their great potential, the property enhancement that is currently realized in PNCs is much lower than expected. Some of the key problems include difficulty in preparing structure-controllable nanomaterials with high purity and performance, non-uniform dispersion and random orientation of nanomaterials within the polymer, inefficient load transfer from matrix to nanomaterials, etc., (3, 4). Therefore, further work is required in order to realize the full potential of PNCs in engineering applications. This chapter aims to provide an overview of the background, advantages, and applications along with the current challenges that hinder the development of PNCs with engineered properties. The current experimental and modeling techniques employed to evaluate the properties of PNCs are also presented. This chapter serves to provide the motivation, challenges and opportunities that lead to the goals and objectives of this research study.

1.1 Polymer Nanocomposites

PNCs consist of a polymer or copolymer reinforced with nanomaterials (at least one dimension below 100 nm) of various shapes including platelets, fibers and spheres.

Nanocomposites combine the light weight, flexibility, and transparency of polymers with the excellent mechanical, physical, and other properties of nanomaterials. Prior research on PNCs has shown fruitful achievements in improving mechanical properties, thermal stability, electrical and thermal conductivities, dielectric performances, gas barrier property, and other attributes (5). Various types of nanomaterials have been used as reinforcement for polymers including ceramic materials such as zirconia (6), silica (7), and titanium oxide (8) , inorganic materials such as nanoclays (9) and organic materials such as carbon black (10), graphite nanoplatelets (11), carbon nanotubes (CNT) (12), and carbon nanofibers (CNF) (13). The majority of the studies are focused on carbon nanomaterials because in addition to their superior mechanical and thermal properties, they are also electrically conductive leading to multifunctional PNCs. Figure 1.1a shows the most common carbon nanomaterials used in polymers as reinforcements, the range of their characteristic dimension and their shape/size. The SEM images of the corresponding carbon nanomaterials are also presented in Figure 1.1b.
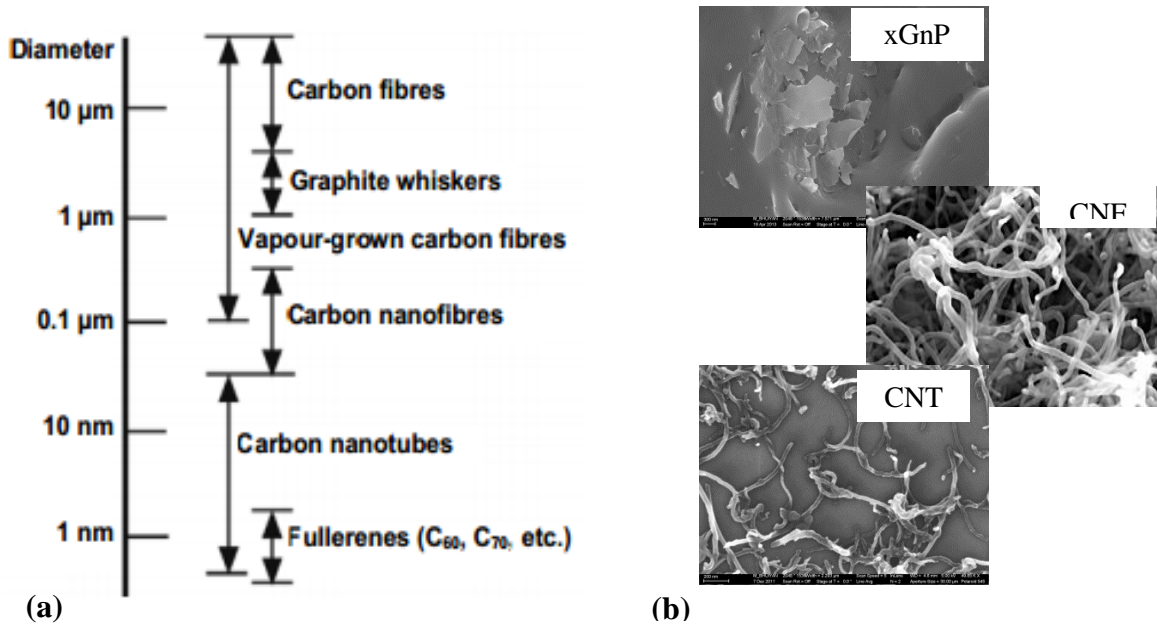
Figure 1.1 (a) Most common carbon nanomaterials used in polymers (14).(b) SEM images of carbon nanomaterials (15)

As reported in both theoretical and experimental studies CNT and exfoliated graphite nanoplatelets (xGnP) exhibit elastic modulus on the order of ~ 1 TPa and fracture strain of ~ 10-30% (16-18); thermal conductivity of ~6,000 W/m-K at room temperature (19), which is approximately three times the thermal conductivity of diamond and approximately 10^4 times that of most polymers (20) and electrical conductivity on the order of $10^4 \sim 10^7$ S/m, which is approximately 20 orders higher than that of most polymers (20, 21). These outstanding properties of CNT/xGnP, as well as their low density and high aspect ratio make them ideal candidate reinforcements for a wide range of polymer matrix composites (22, 23). It is expected that their addition can lead to multifunctional PNCs with enhanced overall performance (24-26). The wide range of applications of CNT/xGnP based composites includes aerospace structures, sporting goods, automotive components, consumers electronics, optical barriers, electromagnetic interference shielding, transmission line cables, nanosensors etc. (2, 27-29).

It is obvious that the only way to reach the maximum potential of the carbon reinforced PNCs is to replace the "error-trial" based approach commonly used with a systematic approach where using fundamental understanding of the nanomaterial-polymer interactions and the processing-structure-property relationship can lead to composites with engineered properties for targeted applications.

1.2 Current Challenges for the Fabrication of PNCs with Engineered Properties

The major challenges that need to be overcome are: i) poor dispersion and distribution of nanomaterials, ii) lack of controlled placement (orientation, alignment) of nanomaterials within the polymer, iii) alteration of the shape/size of the nanomaterial during processing and iv) limitations in characterizing/assessing phenomena at the nanoscale.

Uniform dispersion and homogeneous distribution of reinforcements in the case of nanomaterials is particularly challenging because they tend to form agglomerates due to their high specific surface area and consequently very strong van der Waals forces developed among them (30, 31). Non uniform dispersion limits the reinforcing efficiency of CNT/xGnP and can even lead to PNCs with properties worse than the neat polymer. Figure 1.2, shows the different dispersion and distribution combinations that are possible in PNCs. The ideal case of uniform dispersion and homogeneous distribution of nanomaterials, shown in Figure 1.2ai, is the one that is mostly used in the theoretical and numerical models leading to over-prediction of the PNCs properties. In the case of non-uniform dispersion with homogeneous distribution, shown in Figure 1.2aii, the agglomerates act as stress concentration sites and reduce the overall reinforcing efficiency because their modulus is less than that of the individual CNT/xGnP. Figure 1.2aiii shows the non-homogeneous distribution of nanomaterials with uniform dispersion, which can lead to uneven stress transfer between the polymer and the nanomaterials in presence of an applied mechanical load. The worst case of non-uniform dispersion and non-homogeneous distribution, shown in Figure 1.2aiv, is most commonly observed and its effect on the modulus of PNC is investigated in this research. A representative SEM image, captured from the fracture surface of 5 wt.% CNT/PP composites and presented in Figure 1.2b, shows presence of CNT non-uniform dispersion and non-homogeneous distribution within the PP matrix.
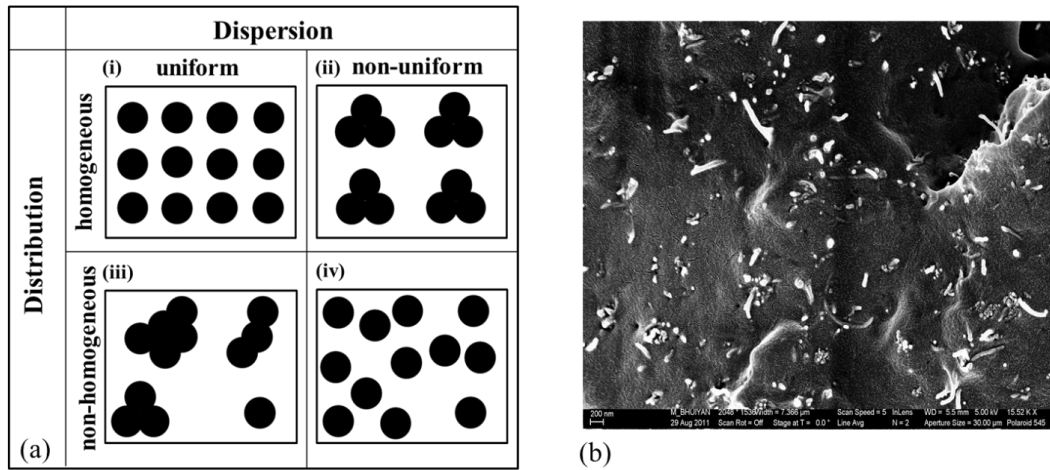
Figure 1.2 (a) Dispersion vs. distribution of carbon nanomaterials within the polymer matrix; (b) Non uniform dispersion and non-homogeneous distribution of CNT in PP matrix

The interfacial interactions between the nanoreinforcement and the host polymer are critical because they define the dispersion/distribution and dictate the performance of the PNC including modulus, strength, stiffness and fracture behavior. In terms of mechanical performance which is the focus of this research, strong interfacial interactions allow for effective load transfer across the nanoreinforcement/polymer interface which is necessary for enhancement of modulus and strength (22, 32). These interfacial interactions can lead to formation of interphase between the nanomaterials and the host polymer, which has finite thickness and has properties different than those of the two materials as reported elsewhere (33-37). Efforts to characterize the interphase in terms of its' thickness and modulus by using scanning electron microscopy (SEM) stereo imaging (38), atomic force microscopy (AFM) force modulation (39), AFM indentation (40, 41), nanoindentation (36) and phase imaging AFM and nanoindentation (42) have been reported. A summary of the results of these studies is presented in Table 1. Quantitative assessment of the interphase using these experimental techniques is still challenging because of the limitations of the characterization techniques at the nano-scale (37). In

this study, the AFM phase imaging technique was employed to determine the thickness and modulus of the interphase which was found to vary across the interphase.

Table 1.1 Interphase properties reported in literature for various composites

Composite system	Testing technique	Interphase thickness	Modulus relative to polymer	Ref.
AS4 carbon-EPON828	SEM stereo imaging	500 nm	Softer	(38)
HM carbon-PPS	Force modulation AFM	20- 80nm	—	(39)
EPON1001F coated AS-4 carbon-EPON 828	AFM indentation	Too small to detect	Similar	(40, 41)
γ-MPS and γ-GPS silane treated glass-vinylester	Nanoindentation	~1 μm	Harder	(36)
γ-APS/PU sized E-glass-PPm	Phase imaging AFM and nanoindentation	100- 300 nm	Softer	(42)

The interfacial interactions also dictate the orientation and waviness or buckling of nanomaterials within the polymer host. It is observed that due to their high aspect ratio, CNT/xGnP bend, buckle or roll up during the processing of the PNC (43-46). This waviness/buckling and the random orientation of nanomaterials, shown also in Figure 1.3, with respect to the direction of applied load as well as the formation of agglomerates drastically reduce the effective length of nanomaterials and thus their reinforcing efficiency (47-49). These phenomena impede the manufacture of PNCs with engineered properties (50-52).
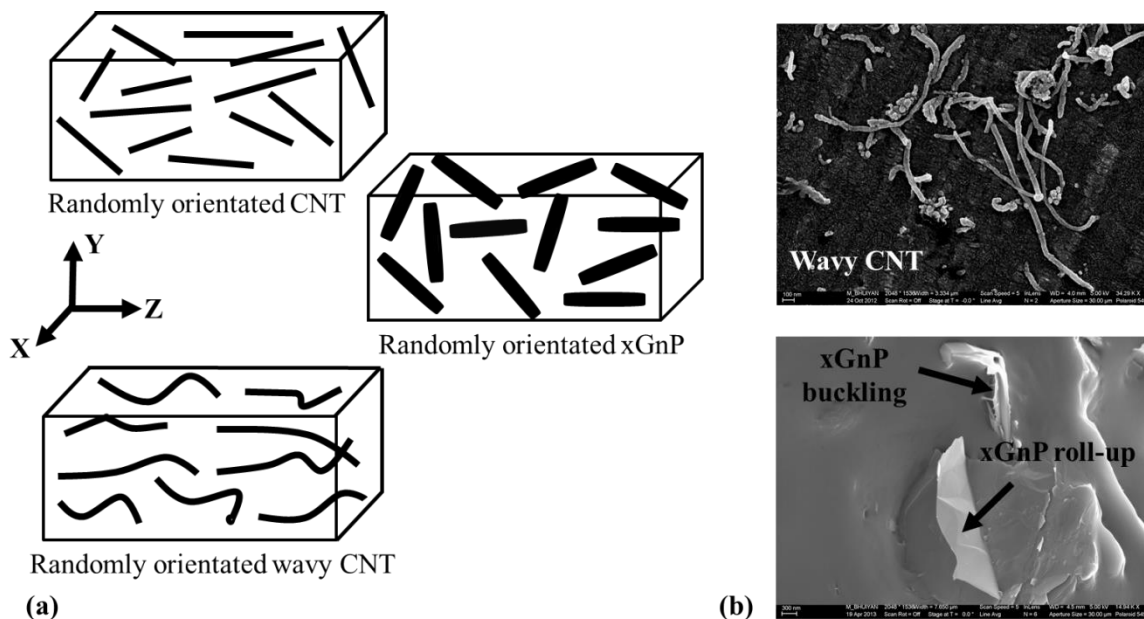
Figure 1.3 (a) Illustration of aligned and randomly oriented carbon nanomaterials in a polymer; (b) SEM images showing the presence of wavy CNT and buckled/rolled-up xGnP within the polymer matrix.

Numerous methods have been employed to ensure better aligning of the nanomaterials in the polymer including electro spinning, application of magnetic or electric field or high shear stresses during extrusion or injection molding, melt spinning and mechanical stretching (53, 54). However, control of nanomaterials' orientation and alignment and elimination of agglomerates within the polymer is practically not possible (31, 55-57); thus it is critical to be able to understand the effect these parameters have on the mechanical properties of PNC. The distribution functions of the orientation, spatial distribution and waviness of nanomaterials within the polymer needs to be determined and accounted for when design and modeling of the PNC is performed (58). Experimental methods used to determine these distribution functions include Raman spectroscopy, SEM, TEM, and AFM (44, 45, 52, 59, 60). However, these approaches provide only qualitative information. Image analysis techniques (58, 61) have also been used to quantitatively characterize nanomaterials dispersion, distribution and orientation state in polymer. But, these techniques are not automated and therefore are not suitable

for quantifying a large population of nanomaterials. In this study, an image analysis algorithm suitable for analyzing a large population of nanomaterials utilizing SEM micrographs is developed to determine the distribution functions of these parameters.

1.3 PNCs Characterization

Despite these challenges, the mechanical load carrying capacity of carbon nanomaterials in PNCs is undeniable. Preliminary experimental results demonstrate that the addition of a small amount, up to 3 wt.%, of CNT (44, 62-64) or xGnP (65-69) substantially improves the properties of the PNC compared to the properties of the host polymer. All these studies show that the load carrying capacity of the carbon nanomaterials in polymers is significant and that these materials have the potential to provide extremely strong, multifunctional and ultra-light composites (70). Therefore, substantial efforts, both experimentally and numerically, need to be undertaken in order to be able to understand the structure-property relationship in nano-scale carbon reinforced PNC in order to engineer their properties.

However, determining this structure-property relationship only experimentally is almost impossible because a "trial and error" approach has to be followed which is both time intensive and cost inefficient. In addition, experimental characterization of various parameters including dispersion, orientation, interphase geometry and modulus is very difficult even with the modern nanotechnology tools. Computational methods such as molecular dynamics (MD) simulations and continuum mechanics can play a significant role in order to overcome this issue.

MD simulation is one of the most reliable approaches to study the behavior of atomic interactions, interface load transfer mechanism, van der Waals bonding forces etc., and has provided enough results (71-73) to better understand the behavior of CNT, polymers and polymer-reinforced composites at the molecular level. Griebel and Hamaekers (71) used MD simulation to examine the elastic moduli of CNT/polymer

composites. In their study they have first derived the stress-strain plots for single-walled carbon nanotube reinforced polyethylene composites using MD simulations to evaluate the effective modulus. Odegard *et al* (73-75) also used MD simulations to account for interfacial interactions at the nanoscale between the CNT and the surrounding matrix. The findings of MD simulations are then used to develop a constitutive model to determine the mechanical properties of aligned and randomly oriented CNT reinforced polymer composites. However, the MD simulations are limited to small length and time scales and cannot be used for handling PNC with larger length and time scales (76), which is also a concern in the development of PNC for structural applications.

The introduction of continuum mechanics can overcome this issue making the task easier for characterizing large-scale models because of its high computational efficiency. Continuum mechanics based finite element methods (FEM) have been successfully used to investigate the mechanical behavior of PNC (77-80). Gade *et al* (81) used finite element analysis (FEA) to evaluate the effective material properties of CNT/polymer composites. They have validated their FEM results with the results obtained using constitutive modeling (75), MD simulations (23) and rule of mixtures and concluded that FEM can be used successfully to characterize PNC. Liu and Chen (70, 82) evaluated the effective mechanical properties of CNT based composites using a 3-D nanoscale representative volume element (RVE) based on continuum mechanics and using the finite element method (FEM). Their simulation results are consistent with the experimental results reported in (44, 83-85). Fukunaga *et al* (86) and Harnandez-Perez *et al* (78) also used FEM to evaluate the macroscopic elastic properties of CNT reinforced polymer composites under various loading conditions.

FEA has also been used to study the interfacial stress transfer and possible stress singularities in PNC (87) as well as the effect of interphase thickness on the elastic properties of PNC (77, 78). Xu *et al* (87) investigated the interfacial stress transfer and possible stress singularities arising at the interfacial ends of discontinuous

9

nanotubes/nanofibers that were embedded in a matrix subjected to tensile and shear loading using FEA. They concluded that load transfer efficiency of discontinuous nanofibers or nanotubes in composites is very low. Wang *et al* (77) studied the effect of CNT/polymer interphase on the effective modulus of the composites using FEA. In their study they used both soft and hard interphase of constant thickness and concluded that the CNT/polymer interphase plays an important role in load transfer efficiency but affects the effective moduli only slightly. Harnandez-Perez *et al* (78) also used FEA to investigate the influence of the CNT/polymer interphase on the effective properties of the composites and reported that the thickness of the interphase strongly affects the elastic properties of the composites.

The effect of nanoreinforcements waviness, orientation and random distribution in polymers and the failure of PNC have also investigated using FEA. Fisher *et al* (88) and Bradshaw *et al* (47) demonstrated the waviness effect on CNT-reinforced composites by constructing a numerical finite element RVE. They found that even slight nanotube waviness significantly reduces the effective stiffness of resulting composites. Similar approach was adopted by Anumandla and Gibson (49) to construct a closed form micromechanics model for estimating the effective stiffness of CNT-reinforced composites. Shi *et al* (48) investigated the effects of CNT waviness and agglomeration to the stiffness of CNT-reinforced composites and the results indicated that both CNT waviness and agglomeration significantly reduce the resulting composite stiffness. Luo *et al* (22) investigated the effects of CNT spatial distribution and geometry on the macroscopic stiffness and microscopic stresses on CNT reinforced composites using FEA. Li and Chou (89) also used FEA to investigate the effect of CNT waviness and random distribution on the tensile properties of CNT/polymer composites. They found that presence of CNT waviness and their random distribution within the polymer tend to reduce the elastic modulus of the composite.

Each of the methods discussed above provides important and unique contributions to the modeling of nano-scale carbon reinforced polymer nanocomposites. However, the majority of the studies reported assumed efficient load transfer at the nanoreinforcement/polymer interface thus over-predicting the mechanical properties of the PNC compared to those obtained experimentally. Therefore, more attention should be given to the stress transfer across the interphase. This research addresses the above mentioned challenges by developing a numerical model that accounts for all the parameters such as dispersion, distribution, orientation and waviness of carbon nanomaterials in polymers that are observed experimentally and by providing a systematic study of their comparative effect on the elastic properties of PNC.

1.4 Motivation

PNC reinforced with carbon nanomaterials have the potential to lead to a new class of multifunctional materials with enhanced mechanical performance. Although various studies have provided some insights into the reinforcing ability of carbon nanomaterials when added to polymers, the basic relationships among various parameters at the nano- or micro-scale and the macroscale properties of PNC remain unclear. Therefore, a reliable model to understand the mechanical behavior of PNC by linking the macroscopic properties of PNC with various morphological parameters such as nanoreinforcements dispersion, distribution, orientation, and waviness is highly needed. More detailed information regarding the statistical distribution of these parameters is also needed for refined predictive model development. So far, a series of modeling strategies has been developed to handle the effects of nanoreinforcement's geometry, content, orientation and waviness, as well as the presence of nanoreinforcement/polymer interphase on the mechanical properties of PNC. However, the majority of the studies have investigated the effect of one parameter at a time ignoring possible synergistic effects. In addition, almost all studies considered deterministic approaches to model the

distribution of various parameters when incorporated into the modeling. Therefore, it is necessary to introduce new techniques that are able to incorporate these experimentally determined parameters as well as to investigate their synergistic effects on the mechanical behavior of PNC. In order to accomplish this requirement, an integrated modeling strategy that combines experimental characterization and finite element modeling is implemented in this study to investigate the mechanical behavior of PNC subjected to uniaxial loading.

1.5 Research Goal and Objectives

The goal of this research is to provide design guidelines for fabrication of PNC with engineered mechanical properties by investigating the various parameters that affect the properties of PNCs through an integrated study that combines thorough experimental characterization and finite element modeling (FEM). The parameters of interest include nanomaterials dispersion, distribution, orientation and waviness within the polymer host and nanomaterial/polymer interphase characteristics. CNT (both pristine and SDBS modified ones) and xGnP reinforced PP composites are fabricated using various methods such as injection molding or melt spinning and are characterized using SEM, AFM and tensile testing. An elaborate image analysis is used to quantify the aforementioned parameters as observed in the captured SEM and AFM images of the fabricated composites. Three dimensional (3D) finite element models with multiple CNT or xGnP embedded within the polymer are generated using the experimentally determined parameters and are analyzed to predict the mechanical behavior of PNC subjected to tensile loading. Predicted results are then compared with the experimentally determined tensile modulus of the PNC to validate the FEM. The findings of this thesis can guide the manufacturers to tune the material processing conditions and characteristics in order to obtain PNC with desired performance. This can obviously accelerate the development of PNC for commercial applications.

The following objectives have been set to fulfill the research goal:

1.   Investigate the effects of manufacturing techniques (bulk vs. fiber composites) and of surface treatment of nanomaterials (non-modified vs. modified) on the nanomaterials/polymer interfacial interactions that are reflected by the nanomaterials state of dispersion, distribution, orientation, and waviness within the polymer matrix.

2.   Understand the effects of nanomaterilas/polymer interfacial interactions and nanomaterial/polymer interphase characteristics on the tensile modulus of PNCs. The effect of nanomaterials geometry on the tensile modulus of PNCs as well as their reinforcement effect at temperature below the glass transition temperature of polymer matrix is also investigated.

3.   Determine the distribution functions of nanomaterials characteristics such as dispersion, distribution, orientation and waviness within the polymer and characterize nanomaterial/polymer interphase through a novel image analysis approach that uses 2D SEM and AFM images.

4.   Develop finite element models using the distribution functions of nanomaterials characteristics and nanomaterial/polymer interphase as input to the model to understand and quantify their individual and synergistic effects on the tensile modulus of PNCs.

5.   Validate the proposed integrated model by comparing the model predictions with the data obtained from tensile experiments. The model is also validated in terms of its' ability to capture the effects of processing conditions and of nanomaterials geometry on the tensile modulus of PNCs.

Figure 1.4 shows an overview of the research presented in this thesis.

An integrated approach to fabricate PNCs with engineered properties

1. Characterization of bulk and fiber composites

2. Understand the effect of interfacial interactions

3. Use of the proposed model to predict the tensile modulus of PNC

CNT/PP and xGnP/PP (bulk, fibers)

(**A**) Mechanical properties (Tensile)
- Room temperature testing (bulk, fiber)
- Testing at a temperature below T_g (bulk CNT)

(**B**) Morphology characterization (SEM and image analysis)
- Dispersion and distribution (CNT, xGnP)
- Alignment/orientation (CNT, xGnP)
- Waviness (CNT)

(**C**) Interphase characteristics (AFM)
- Width and modulus (bulk, CNT and xGnP wt%)

(**D**) Finite element modeling and FEA
- Input parameters to the model
  - Interphase properties (fixed vs. property gradient profile)
  - Dispersion & distribution (random vs. pdf)
  - Alignment/orientation (random vs. pdf)
  - Waviness (random vs. pdf)

(**E**) Validation of the proposed models
- Experiment vs. FEA (Tensile modulus) (bulk, fibers)

* bulk: CNT/PP and xGnP/PP composites, bulk CNT: CNT/PP fibers; fiber: CNT/PP composites; random: random distribution of CNT and xGnP parameters; pdf: probability distribution function of CNT parameters. T_g: glass transition temperature of polymer

Figure 1.4 Overview of the proposed research for developing PNCs with engineered properties

1.6 Outline of the thesis

In this thesis an integrated approach that combines experimental characterization and finite element modeling is proposed to predict the tensile modulus of carbon reinforced PNCs. A brief introduction of PNCs along with a review of the previous research undertaken on modeling of PNCs is presented in Chapter 1. The motivation and the goal of this study are also explained and the objectives to achieve the goal are set.

Chapter 2 describes the various materials used in this study. Steps to manufacture PNCs are explained in detail followed by the various techniques used to characterize the fabricated PNCs in terms of their mechanical properties and morphology.

Chapter 3 deals with the mechanical and morphological characterization of PNCs. Tensile properties of carbon reinforced PNCs and the influence of various nanostructure parameters on the PNCs tensile properties are discussed. Effects of changes in the processing conditions and the environment on the tensile properties of PNCs are also presented. This chapter also discusses the techniques used to characterize nanomaterial/polymer interphase in terms of geometry and property.

Chapter 4 presents the image analysis technique used to determine the distribution functions of nanostructure parameters within the polymer matrix. Generation of 3D RVE for PNCs and the details of FEA are also discussed.

Chapter 5 presents the distribution functions of various CNT parameters within the polymer obtained from the image analysis. FEA predictions of tensile modulus of CNT/PP composites (both bulk and fiber), considering the distribution functions of CNT parameters obtained from the image analysis, are also presented. Validation of the proposed integrated approach is also performed at the end of this chapter by comparing the FEA predictions with the experimental data.

Chapter 6 presents a basic study on the mechanical reinforcing efficiency of two types of nanomaterials, CNT and xGnP, that have similar surface chemistry by different geometry.

Finally, in Chapter 7, conclusions are drawn based on the finding of this thesis and the key contributions of this work are summarized. The limitations of this work and scopes for future work are also discussed.

CHAPTER 2

MATERIALS, PROCESSING METHODS AND

CHARACTERIZATION

This chapter covers the details of the materials used and the processing methods employed for the fabrication of PNCs. Materials include the polymer matrix and two types of nanoreinforcements. Different compounding and molding methods were utilized to fabricate composite specimens as a function of nanoreinforcements loading (0 to 5 wt.%). The composites were characterized in terms of their mechanical properties and morphology.

2.1 Materials

The polymer used in this research is polypropylene (PP) homopolymer in powder form (pro-fax 6301, melt flow index 12 g/10 min) provided by LyondellBasell. The powder consisted of particles with diameters in the range of 100 μm to 300 μm. PP is among the most commonly used thermoplastics with a vast range of applications in the automotive and construction industries (90). In addition, PP is non-polar, so there are no chemical interactions with the nanoreinforcements, which simplifies the study. These are the two main reasons for using PP as polymer matrix in this study. The nanoreinforcements used are multi-walled CNT purchased from Cheat Tubes, VT, and xGnP purchased from XG Sciences, East Lansing, MI. Table 2.1 shows the specifications for both the CNTs and xGnPs, as provided by the supplier.

Table 2.1 CNT and xGnP specifications as provided by the supplier

Reinforcements	Specifications
CNT	Outer diameter (OD): 20-30 nm, Inner diameter (ID): 5-10 nm, Length: 10-30 μm, Purity: > 95 wt.%, Ash: < 1.5 wt.%, Specific surface area: 110 m^2/g, Density: ~2.1 g/cm^3, electrical conductivity: > 100 S/cm
xGnP	Average diameter: ~1 μm, Thickness: ~10-20 nm, electrical conductivity: 18,000 S/cm

2.2 Processing of PNCs

2.2.1 Compounding

Two compounding methods were used in this study to disperse the nanomaterials within the polymer matrix: direct melt mixing and coating with sonication. In addition to these, surfactants were used to improve the dispersion for the case of CNT.

Direct melt mixing was performed by manually mixing the polymer and the nanomaterials and then feeding the mixture into a twin screw extruder. The materials were mixed at different screw speeds (245 RPM for bulk composites and 170 RPM for fiber composites) for 3 minutes at 180º C inside the DSM Micro 15 cc compounder (vertical, co-rotating twin-screw micro extruder) shown in Figure 2.1. The melt was then fed to the injection molding unit.

The coating method reported in (65) and shown schematically in Figure 2.2, was used to achieve good dispersion of nanomaterials within PP. First, CNT or xGnP are dispersed in isopropyl alcohol (IPA) through sonication (ultrasonic processor UIP500hd from Heilscher Ultrasound Technology, 75% amplitude, 45 minutes). PP is then added to the solution and sonication is continued for 15 more minutes. The IPA is then filtered away and the carbon coated PP powder is collected, dried and fed to the injection molding unit.

Extruder

Barrel in open position with
the screw inside
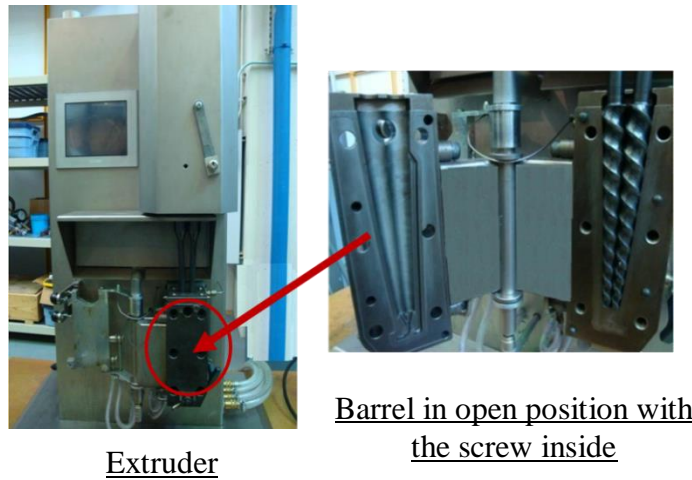
Figure 2.1 Melt mixing unit (DSM Micro 15cc compounder)

CNTs

xGnPs

IPA

+

Sonication of CNTs/
xGnPs solution

+

Neat PP

Vacuum filtration

CNTs/xGnPs coated PP
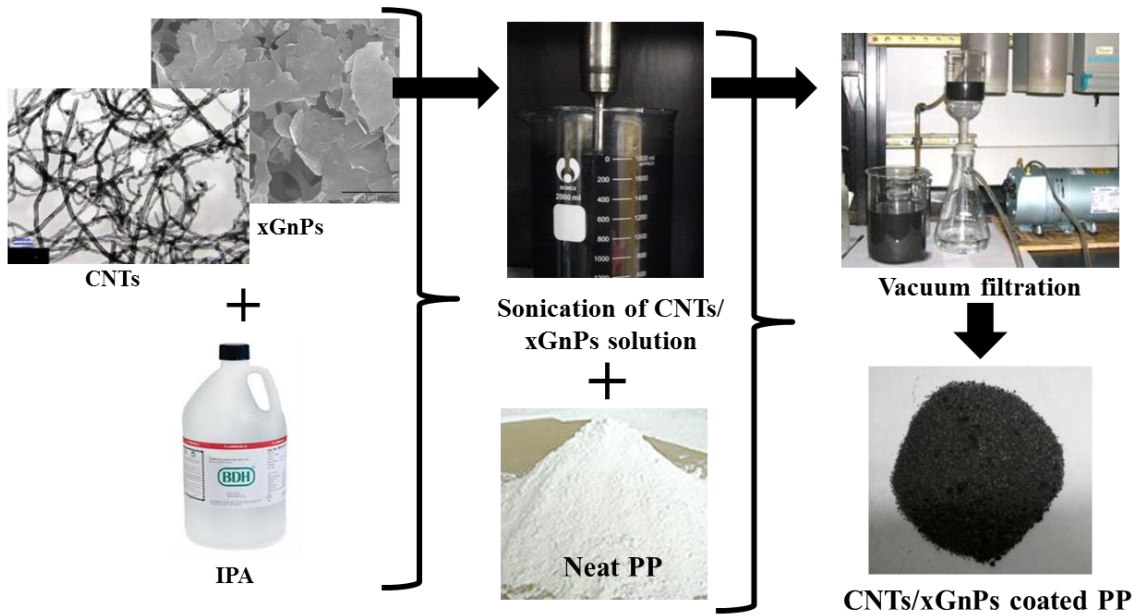
Figure 2.2 Procedure of the coating method

The use of surfactant is another approach to improve the dispersion. Sodium dodecylbenzene sulfonate (SDBS) (chemical formula C12H25C6H4SO3Na) and CNT at 1:1 weight ratio were dispersed in 100 ml of H_2O using sonication (model, 2 hours at room temperature). The suspension was then dried in a vacuum oven at 60 ℃ and the

dried mixture of CNT and surfactant was mixed with PP powder manually and fed into the extruder.

2.2.2 Injection Molding

Injection molding is used to fabricate bulk CNT/PP and xGnP/PP composites of dog bone shape. Figure 2.3 shows the injection molding unit used. The melt is injected directly to a mold placed at the injection molding unit using a transfer mold that is set at 170 ºC. The mold temperature was $T_{mold} = 80$ ºC, and the injection pressure is set to 758 kPa.

Transfer mold

Mold to make dog bone shape coupons
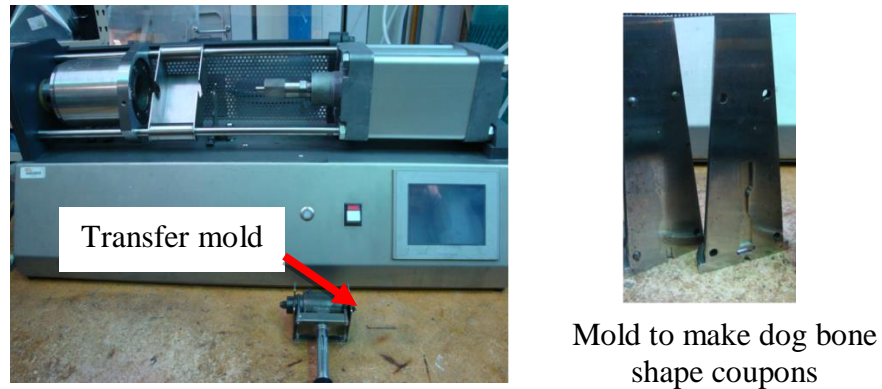
Figure 2.3 Injection molding unit

2.2.3 Melt Spinning

CNT/PP fibers are made using a fiber spinning set up, shown in Figure 2.4, that consisted of two 10.5 cm diameter rolls (take-up and collection rolls) with independent speed controls. Between the rolls there is a heating zone that the fiber is passed through as it is drawn. The temperature of the heating zone is set to 80° C. The molten CNT/PP compound is pushed through a single holed spinneret of 1mm diameter. Fiber take-up and collection is accomplished at a speed of 200 m/min and 800 m/min, respectively, (draw ratio of 4). The neat polymer specimens (bulk and fibers) are processed in the same way as above except that the polymer in this case does not undergo through the coating process (sonication in IPA and filtration).
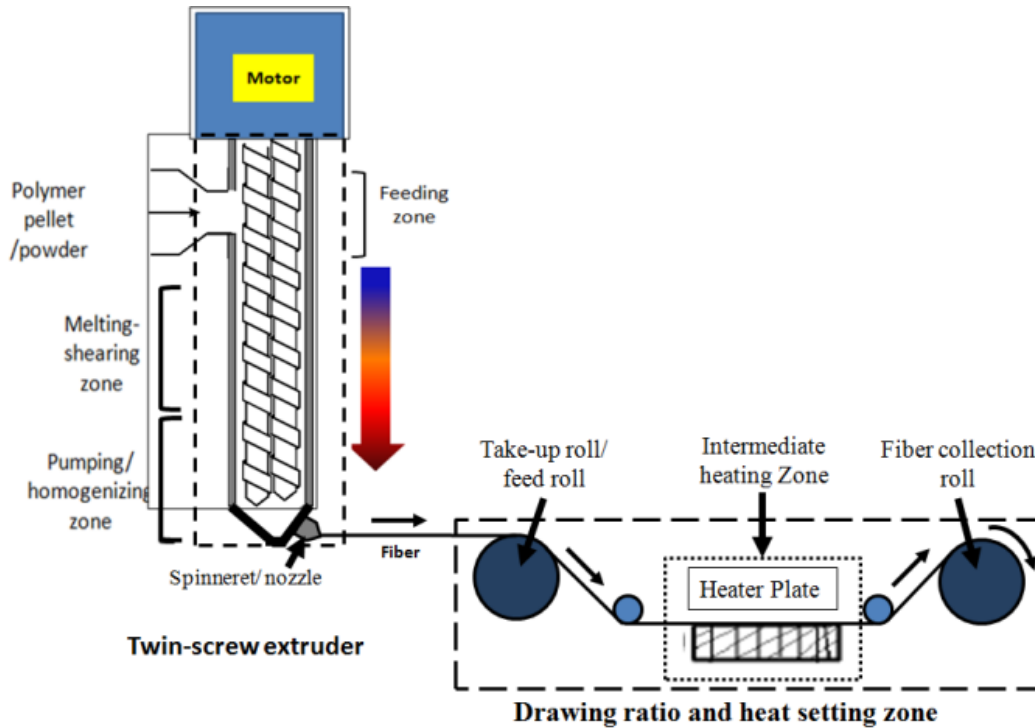
Figure 2.4 Schematic of fiber spinning set up

2.3 Characterization Methods

Bulk composites are tested for their tensile properties both at ambient temperature and at temperature below the glass transition temperature (T_g) of PP. Ambient temperature testing is done according to ASTM D638 using an Instron 33R- 4466 apparatus. A 500N load cell and an extensometer (Instron 2630-101) with a gage length of 10 mm are used. A displacement control with a velocity of 2.54 mm/s is applied. Tensile testing of CNT/PP bulk composites at temperature below T_g of PP is performed using the tensile clamp of dynamic mechanical analyzer (DMA). A constant temperature of -10 ℃, which is well below the T_g of neat PP (~5 ℃), is maintained throughout the test. A controlled force condition is maintained at a force ramp of 1 N/min to the maximum force limit of the DMA, which is 18 N.

CNT/PP fibers are tested at ambient temperature for their tensile properties according to ASTM D3822 using an Instron tensile testing machine with a 2.5 N load

cell. A single fiber is fixed on the specific fiber test tab with test length of one inch (25.4 mm) and the test is performed at a crosshead speed of 25.4 mm/min.

SEM study is conducted on samples prepared in two ways: (i) cryogenic fracture of manufactured composites in liquid nitrogen, and (ii) polishing and etching of composites surfaces using permanganate reagent. The composites surfaces are polished to 1 μm diamond finish and are dried for 24 hours at room temperature. The dried specimens are then etched for 1 hr with a 1.0 wt.% solution of potassium permanganate in a 2:1 mixture of concentrated sulphuric acid and phosphoric acid in an ultrasonic bath at room temperature (91-93). After etching the specimens are washed sequentially in dilute sulphuric acid, distilled water and acetone and are dried at room temperature. Both the fractured and etched surfaces are then examined under SEM (Zeiss Ultra 60- SEM, operated at an accelerating voltage of 5 kV) in order to extract information on the statistical distribution of CNT and xGnP dispersion, distribution, orientation and waviness within the polymer. The existence of voids and imperfect contact at the nanoreinforcement/polymer interface is also examined using SEM. All samples are cleaned with IPA and coated with a thin gold layer to avoid charging during SEM imaging.

The nanoreinforcement/polymer interphase is characterized using AFM in terms of its' thickness and stiffness. A Veeco AFM with Nanoscope V controller, operated in tapping mode using an aluminum coated cantilever (length 225 μm, spring constant 45 N/m, resonance frequency 190 kHz, silicon tip radius 2nm) provided by Nanoscience Instruments Inc. Phoenix, AZ, is used. The PNC samples are used as received from the injection molder for AFM experiment, and no special sample preparation is employed prior to AFM.

CHAPTER 3

TENSILE PROPERTIES AND MORPHOLOGY

CHARACTERIZATION OF POLYMER NANOCOMPOSITES

PP composites (in form of bulk specimens and fibers with an average diameter of ~ 30 microns), reinforced with either CNT or xGnP, are made and characterized according to the methods described in Chapter 2. The composites are tested for their tensile properties and morphology characteristics. Tensile testing is performed both at room temperature (temperature above glass transition temperature, T_g, of PP) and at temperature below the T_g of PP. The tensile properties below the T_g of PP are determined in the case of CNT/PP bulk composites in order to mask the polymer viscoelastic effects and to investigate only the reinforcing effects of CNT. The effect of the CNT dispersion within the host polymer on the tensile properties of PNC is also investigated by altering the dispersion state using surfactants. The tensile modulus and strength results of the PP nanocomposites are found to be in agreement with the dispersion state of the nanomaterials within the polymer as observed by SEM. Furthermore, the distribution of either CNT or xGnP within PP and the presence of agglomerates and defects in the composites were also studied using SEM. Fracture surfaces of CNT/PP and xGnP/PP composites or surfaces obtained by polymer etching are investigated during the morphology study. Finally, the CNT-PP and xGnP-PP interphase is assessed in terms of modulus and width using phase images of AFM obtained in tapping mode as described in Chapter 2. The details of the mechanical and morphological characterization are presented in the following sections.

3.1 Tensile Properties of PNCs

3.1.1 Tensile Properties above T_g

Tensile stress–strain curves of PP composites (bulk), reinforced with CNT and xGnP, obtained at room temperature tensile testing are presented in Figure 3.1. It is noted that the Tg of PP used in this study is ~ 5º C, as determined by DMA experiments. The strength and modulus (calculated as the slope of the curves in the linear regime) along with the corresponding standard deviation are also presented in Table 3.1. For all cases, each data point reported is an average of five tests. Tensile moduli of CNT/PP composites (bulk) obtained using theoretical micromechanical models such as Halpin-Tsai (H-T) (94) and Tandon-Weng (95)(T-W) as a function of CNT content are also presented in Table 3.1 for comparison.
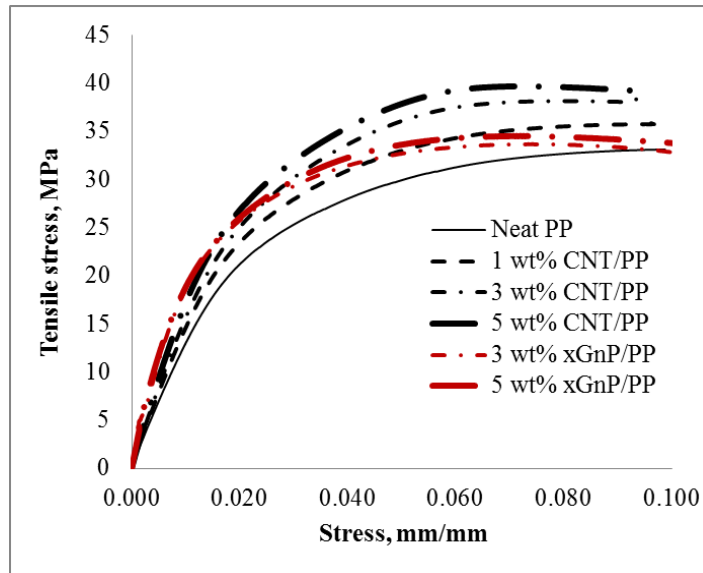
Figure 3.1 Tensile stress-strain plots of CNT/PP and xGnP/PP (bulk) composites as a function of nanomaterials content

Table 3.1 Tensile properties of CNT/PP and xGnP/PP composites (bulk) obtained from tensile experiment performed at temperature above T_g and from theoretical models

Nano	Experimental				Theoretical models	
material	CNT/PP		xGnP/PP		CNT/PP	
s wt.%	Modulus, GPa	Strength, MPa	Modulus, GPa	Strength, MPa	Modulus (H-T), GPa	Modulus (T-W), GPa
0	1.38±0.04	33.14±0.45	1.38±0.04	33.14±0.45	1.38	1.38
1	1.55±0.03	35.78±0.43			1.93	1.98
3	1.68±0.05	38.2±0.65	1.70±0.05	32.83±1.57	2.6	2.74
5	1.87±0.04	39.72±0.83	1.83±0.03	33.15±0.80	3.24	3.26

[*]H-T: Halpin-Tsai model and T-W: Tandon-Weng model

From the results presented, it can be seen that the tensile properties (strength and modulus) of both the bulk and fiber composites increase with the increase of nanomaterials' content, except for the tensile strength of xGnP/PP composites. Although the properties of PNC increase with the increase of nanomaterials' content, these properties are much lower than the properties predicted by the theoretical micromechanical models such as H-T(column 6, Table 3.1) and T-W (column 7, Table 3.1). The factors that contribute to this discrepancy are the existence of imperfect contact at the nanomaterial/polymer interface as well as the presence of nanomaterials agglomerates and their random orientation and waviness in the polymers. SEM observation of CNT/PP and xGnP/PP composites also supports the existence of weak nanomaterial/polymer interface and the presence of nanomaterials agglomerates within the PP. Representative SEM images captured from the fracture surfaces of 4 wt.% CNT/PP (bulk) and xGnP/PP (bulk) composites are presented in Figure 3.2a and 3.2b, respectively, where presence of wavy and/or buckled nanomaterials as well as their agglomerates (circled in the SEM images) is observed. Agglomerates reduce the reinforcing efficiency of nanomaterials since they act as stress concentration sites within

the polymer and result to PNCs with lower tensile properties. The existence of voids at the nanomaterial/PP interface (as pointed by arrow in the SEM images) that led to inefficient load transfer from nanomaterial to polymer is also observed.
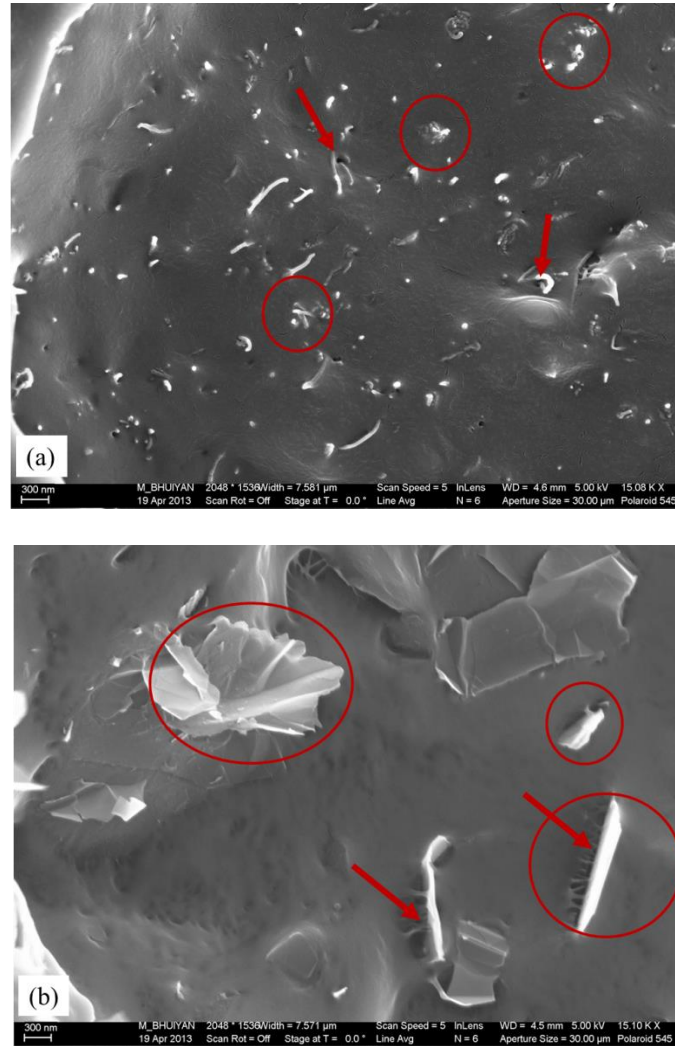
Figure 3.2 Representative SEM images captured from the fracture surface of (a) 4 wt.% CNT/PP composites; and (b) 4 wt.% xGnP/PP composites showing the presence of nanomaterials agglomerates (circled) and the existence of voids at the nanomaterial/PP interface (arrow)

Room temperature tensile testing of CNT/PP fiber composites is also performed to understand the effect of processing conditions on the composites' tensile properties. Figure 3.3 presents the tensile stress-strain curves obtained from the tensile testing of CNT/PP fiber composites. It is noted that for CNT/PP fiber composites, the maximum

CNT concentration used is 3 wt.%. Since the fiber diameter is small (~ 30 µm) spinning

of fiber with CNT concentration higher than 3 wt.% resulted in fiber breakage.
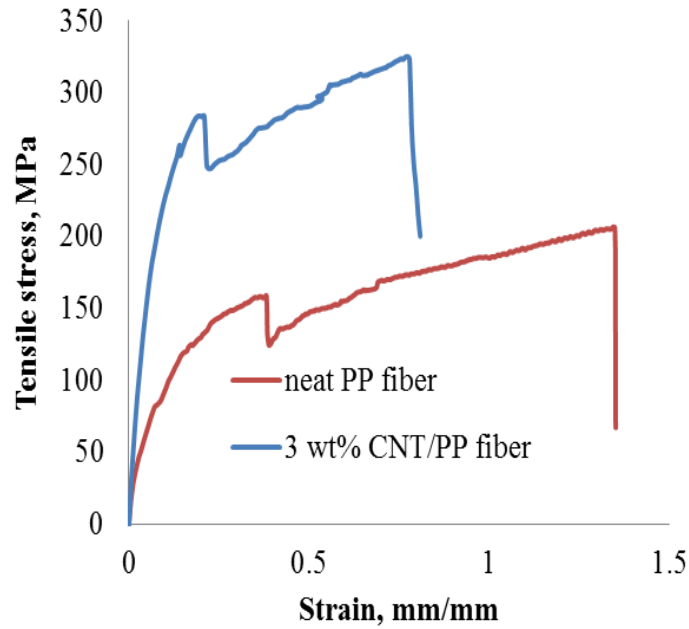
Figure 3.3 Tensile stress-strain curves of CNT/PP fiber composites obtained from the
tensile testing performed at room temperature

Table 3.2 Tensile properties of CNT/PP composites (bulk and fiber) obtained from tensile
experiment performed at temperature above T_g

Nano	**Experimental**			
materials	**CNT/PP (bulk)**		**CNT/PP (fiber)**	
wt.%	Modulus, GPa	Strength, MPa	Modulus, GPa	Strength, MPa
0	1.38±0.04	33.14±0.45	2.24±0.20	209±37.92
3	1.68±0.05	38.2±0.65	3.27±0.42	310±46.45

From Figure 3.3, it can be seen that the PP fiber has a very high initial modulus

followed by a very sharp yield. This sharp yield is due to the formation of necking during

the tensile testing of fiber. The stress decrease after yield corresponds to the intrinsic

softening of the polymer. The yielding, which is due to the nucleation of shear bands at

the necked zone, controls the plastic deformation of the polymer. Similar behavior of

27

CNT/PP fibers is reported elsewhere (96). The elongation at the break of the PP fiber is also higher than that of the bulk PP specimen (see figure 3.1), which is due to the alignment of amorphous chains during tensile stretching. As shown in Figure 3.3, a sharp drop of tensile stress at break is also observed which corresponds to the brittle fracture of fiber. This can be explained by the increase crystallinty of PP fiber (96).

The addition of CNT results in significant improvement in the tensile properties with a lower elongation at break, which means that the addition of CNT makes the fiber brittle. Table 3.2 presents the tensile properties of CNT/PP fibers (both strength and modulus) with the corresponding standard deviation. For all cases, each data point presented is an average of ten tests. Tensile properties of CNT/PP bulk composites presented in Table 3.1 are also presented in Table 3.2 for comparison. As can be seen from Table 3.2, the modulus of CNT/PP fiber composites is approximately twice than the modulus obtained for bulk CNT/PP composites with same CNT content. The improvement of tensile strength for CNT/PP fiber composites is even higher, which is more than eight times than the strength of CNT/PP bulk composites with same CNT content. This significant enhancement is attributed to the alignment of CNT and polymer chains along the applied load direction as well as the increased crystallinity of the polymers due to the addition of CNT, as reported elsewhere for CNT/PP fiber composites (96).

Another factor that contributes to this large improvement in the tensile properties of CNT/PP fiber composites is the CNT dispersion. A representative SEM image captured from the fracture surface of 3 wt.% CNT/PP fiber composite is presented in Figure 3.4 in order to examine the dispersion and alignment of CNT in fiber composites. As shown, the dispersion of CNT within the PP matrix is almost uniform with very few CNT agglomerates present. In addition, no evidence of CNT pull out is observed, which indicates good interfacial interactions between the CNT and the PP matrix. The CNT that are aligned along the applied load/spinning direction restrict the shrinkage of

polymer chains, which results in strong CNT-polymer interaction. As a result no CNT pull out occur during the fracture of CNT/PP fiber composites. Uniform dispersion of CNT within the PP matrix along with the good interfacial interactions results in CNT/PP fiber composites with modulus higher than that of CNT/PP bulk composites.
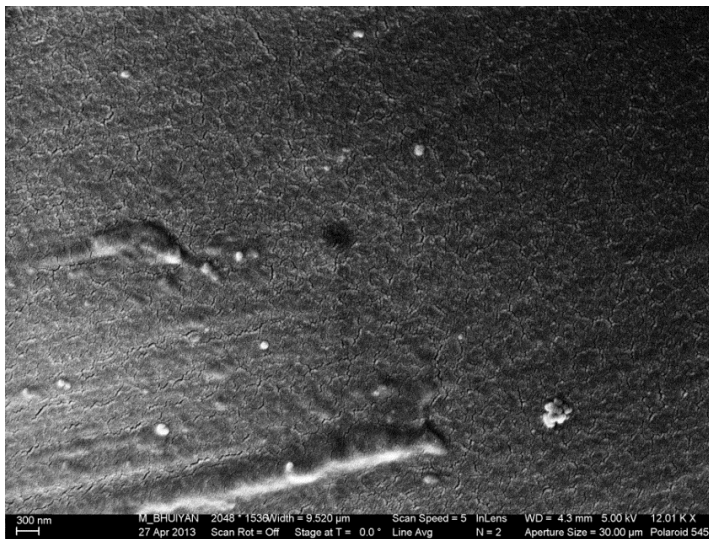
Figure 3.4 Fracture surface of 3 wt.% CNT/PP fiber composite

3.1.2 Tensile Properties below T_g

The reinforcement effect of CNT on PP composites at $-10°$ C, which is below the T_g of PP, is also investigated in this study. Since the polymer molecules are immobilized below the T_g, their viscoelastic effects on the tensile properties of PNCs are not present at this temperature. Therefore, tensile experiment at temperature below T_g is performed in order to understand the effects of nanomaterials alone on the PNCs tensile properties. Figure 3.5 shows the tensile modulus of CNT/PP composites tested at temperature below T_g. Tensile modulus of CNT/PP composites obtained from tensile experiment performed at temperature above T_g, using both DMA and Instron machine, is also presented in Figure 3.5 for comparison. As shown, the modulus of CNT/PP composites at temperature below T_g is significantly higher than that at temperature above T_g at the same CNT content. Two main observations can be made: i) As expected the modulus of neat PP is

higher below T_g because of tighter arrangement of the polymer molecules (97, 98) and decreased polymer chain mobility which suppresses the viscous and enhances the elastic behavior of the polymer. The interfacial interactions between CNT and PP also become stronger at low temperature due to the compressive stress caused by the different thermal expansion coefficients of CNT and PP (99). ii) The reinforcing efficiency of CNT is higher at temperatures below T_g,
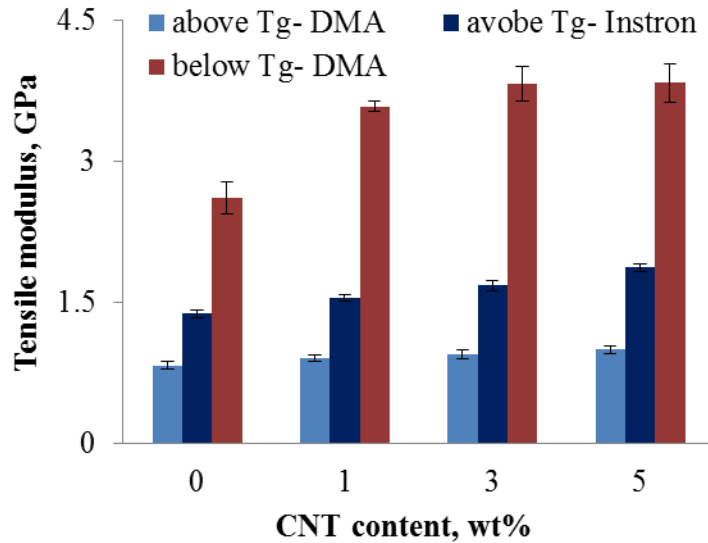
Figure 3.5 Tensile modulus of CNT/PP composites tested at temperature above and below T_g

From the results presented in Figure 3.5, it is also observed that for the tensile testing performed at temperature above T_g of neat PP, the modulus obtained using Instron machine is higher than that of obtained using DMA. This can be explained by the difference in testing conditions specifically testing speed for the two cases. In DMA the speed at which the tensile testing is performed is ~<0.04 mm/see whereas it is 2.5 mm/sec for the case of Instron machine. The high speed, in other words high strain rates, for the case of Instron tend to favor the elastic properties of materials instead of viscoelastic properties that results in higher modulus than that of obtained using DMA.

3.1.3 Effect of Nanomaterials Dispersion on the Composites Tensile Properties

Tensile testing of CNT/PP composites has also been performed to study the effect of nanomaterials dispersion on the composites effective modulus. In this study, the dispersion of nanomaterials is altered by using surfactant materials. Sodium dodecylbenzene sulfonate (SDBS) is used as surfactant to help the dispersion of nanomaterials uniformly within the PP matrix. Better dispersion of CNT within the polymer due to the addition of surfactants is confirmed by both the tensile properties and the morphological study using SEM.

The effect of CNT dispersion on the tensile modulus and strength of CNT/PP composites as a function of CNT content up to 5 wt.% determined at ambient temperature (temperature above T_g) are presented in Figure 3.6. As shown, for all CNT contents the modulus and strength of SDBS-modified CNT/PP composites is higher than the modulus and strength of non-modified CNT/PP composites with the same CNT content. This may be explained by the good dispersion of CNT within the PP matrix due to the addition of SDBS (98). SDBS that consist of hydrophilic head groups and hydrophobic hydrocarbon chain molecules act as an intermediate agent to improve the interfacial interactions between CNT and PP, resulting in better dispersion of CNT within the PP matrix (100). In addition, modification of the surface of CNT using SDBS reduces their surface tension, thereby preventing the formation of CNT agglomerates (101, 102).
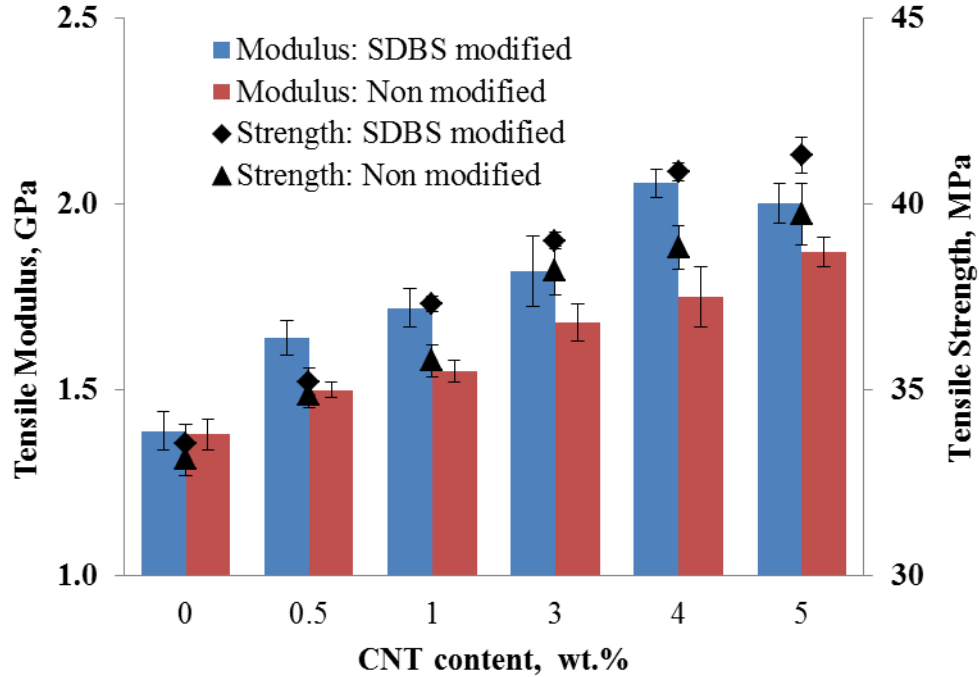
Figure 3.6 Effects of CNT dispersion on the tensile properties of CNT/PP composites

Another important observation that can be made from Figure 3.6 is that the tensile modulus of the SDBS modified CNT/PP composites reaches its' maximum at CNT content of 4 wt.% and further increase of CNT content does not increase the composites modulus. This can be explained by the presence of CNT agglomerates at higher CNT content, which lead to the decrease of composites tensile modulus. SEM images captured from the fracture surface of 5 wt.% SDBS modified CNT/PP composites, as shown in Figure 3.7, also support the presence of CNT agglomerates within the PP matrix (circled) at higher CNT content. Although use of SDBS results in good dispersion of CNT, at higher CNT content the surface of CNT increases significantly and CNT are closer together so the resultant van der Waals forces act against the improved dispersion induced by the surfactants. The presence of wavy CNT within the PP matrix is also observed. Waviness of CNT is another factor that contributes to the reduction in composites tensile modulus. As the ratio of CNT/SDBS used is 1:1, at 5 wt.% of CNT,

there is also 5 wt.% of SDBS which means that the high molecular weight (MW) PP is replaced by the low MW SDBS and this significantly affects the strength and modulus of the composites with modified CNT at high CNT contents.
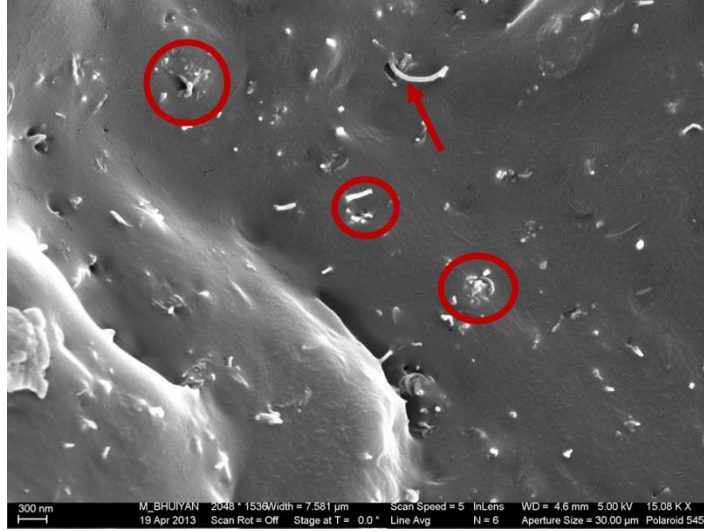
Figure 3.7 SEM image captured from the fracture surface of 5 wt.% SDBS treated CNT/PP composites showing the presence of CNT agglomerates (circled) and wavy CNT (arrow)

Tensile strength of CNT/PP composites is also presented in Figure 3.6. As can be seen the strength of SDBS modified CNT/PP composites is higher than the strength of non-treated CNT/PP composites for all CNT content. Better dispersion of SDBS modified CNT within PP that results from strong interfacial interactions between CNT and PP, compared to the non-modified CNT, is responsible for the tensile strength enhancement. Better dispersion of CNT in PP, for the case of SDBS modified CNT/PP composites, is confirmed by SEM experiments. Representative SEM images captured from the fracture surfaces of 4 wt.% CNT/PP composites, with modified and un-modified CNT, are presented in Figure 3.8a and 3.8b, respectively. As shown in Figure 3.8a, uniform dispersion of CNT within the PP is obtained for the case of SDBS modified CNT/PP composites. However, this is not the case for CNT/PP composites reinforced with non-treated CNT. As can be seen in Figure 3.8b, a large number of CNT agglomerates that are distributed non-homogeneously are present within the PP matrix
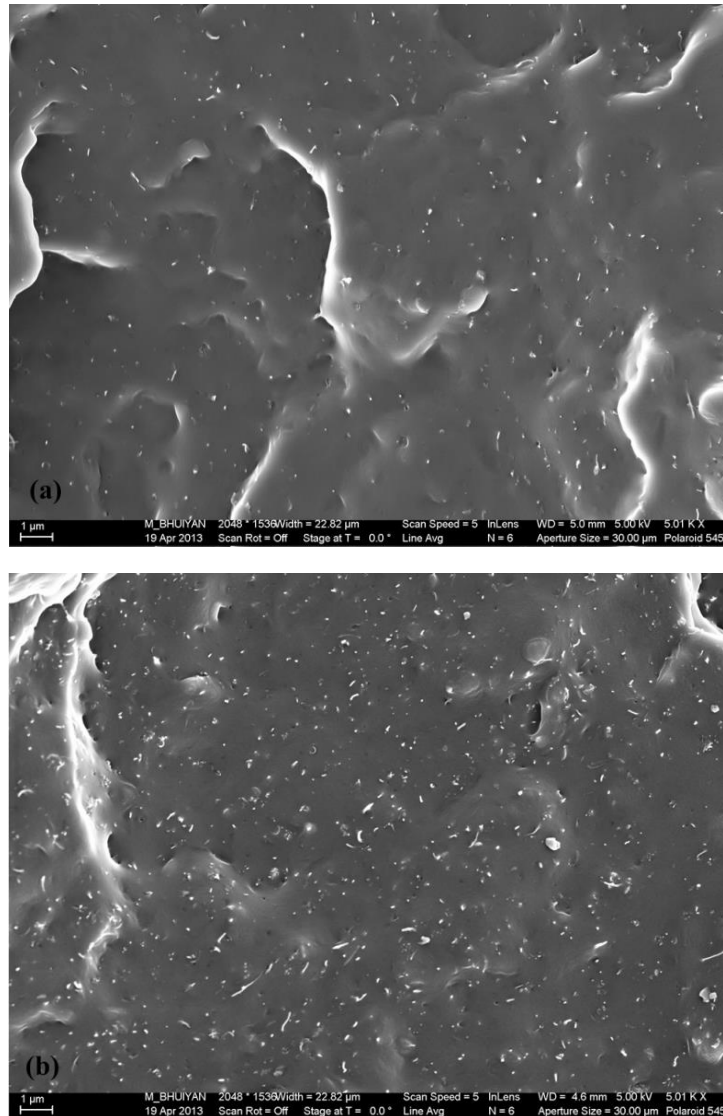
Figure 3.8 SEM micrographs captured from the fracture surfaces of 4 wt.% CNT/PP composites: (a) SDBS modified CNT/PP composites; and (b) non- modified CNT/PP composites

From the results (tensile properties of PP composites reinforced with CNT and xGnP and their SEM micrographs) presented in this section, it is obvious that the presence of non-uniformly dispersed wavy and/or buckled nanomaterials within the polymer matrix, as well as the existence of voids at the nanomaterial/polymer interface, are the key parameters that contributes to the lower tensile properties of PNCs. Other factors, in addition to these parameters, that result to PNCs with lower tensile properties

include non-homogeneous distribution of nanomaterials and their random orientation within the polymer matrix. SEM images presented in Figure 3.8 and Figure 3.9 confirm the non-homogeneous distribution and randomly orientation of nanomaterials within the PP matrix.
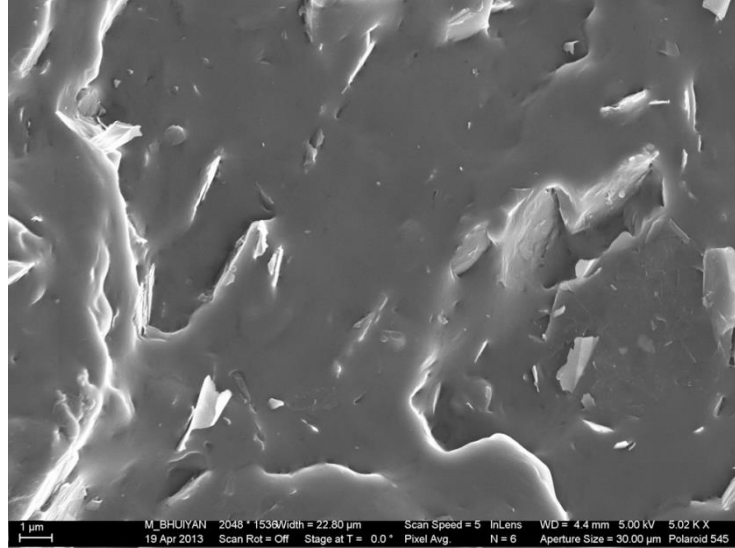
Figure 3.9: SEM image captured from the fracture surface of 4 wt.% CNT/PP composites showing the non-homogeneous distribution of xGnP within PP

Although the SEM micrographs, presented in this section, offer useful qualitative information about the dispersion, distribution, orientation and morphology of nanomaterials within the PP matrix, they do not allow extraction of statistical information about the distribution of these nanostructure parameters within the polymer, yet this information, is essential to this effort to understand and quantify the effects of these parameters on the tensile properties of PNCs. Therefore, an elaborate image analysis technique, using the polished and etched surfaces of all the composites studied in this research i.e., CNT/PP (bulk and fiber) and xGnP/PP (bulk) composites, is developed as part of this study that can provide information on nanomaterials dispersion, spatial distribution, alignment/orientation and waviness within the PP matrix. This qualitative information which is dictated, for a given material system, by the manufacturing method and processing conditions used and strongly affects the performance of the composites

35

including the tensile modulus was analyzed using an image analysis approach (described in Chapter 4). The output of the image analysis was used as input in the finite element models developed and employed in this study in order to understand how phenomena at micro-scale related to the nanomaterials characteristics can affect the macro-scale properties of the composites that is the tensile modulus.

3.2 Nanoreinforcement/Polymer Interphase Characterization

Another important parameter that affects the tensile properties of PNCs and has received considerable attention is the nanomaterial/polymer interphase (103, 104). A possible cause of the interphase formation is the reduction in polymer chain mobility near the reinforcements (24, 104). It has been observed that the interphase region has finite thickness and properties different than those of the matrix and the nanoreinforcements (33, 34, 105). In this study, the CNT/PP and xGnP/PP interphase is characterized in terms of its' width and modulus. AFM phase images obtained in tapping mode and captured from the surfaces of CNT/PP and xGnP/PP bulk composites were used to extract information about the nanomaterial/PP interphase, which was also used in the finite element models.

Phase imaging measures the phase lag in oscillation frequency when the AFM tip interacts with areas of different material properties (stiffness). It is an extremely sensitive method for differentiating materials of different moduli. A representative phase image of the top surface of 4 wt.% CNT/PP composite is presented in Figure 3.10a, where a clear transition area, the CNT/PP interphase, is observed between the CNT and the PP matrix. The width of this transition area (CNT/PP interphase) is determined using the AFM software by measuring the phase lag across the lines (profiles) that are drawn from one material to the other on the phase image. Four such lines that are initiated from the CNT pass through the interphase and end at the PP matrix are shown in Figure 3.10a. The phase lag across each line (profile) is shown in Figure 3.10b. Based on the analysis

described and using AFM phase images taken at various locations (five in an average) on the CNT/PP composites surfaces, the average width of the CNT/PP interphase measured is ~ 20 to 30 nm. This is the width of the interphase that is used in this study to model CNT/PP interphase while generating representative volume element (RVE) for finite element analysis. It is noted that CNT/PP composite with low CNT contents (e.g. 0.1 wt.%) is also examined through AFM in order to understand the effects of CNT contents on the thickness of CNT/PP interphase. And it is found that the thickness of the interphase falls within the range mentioned above. Representative AFM phase image and the corresponding property gradient profile obtained from the surface of 0.1 wt.% CNT/PP composites is presented in Figure 3.11.
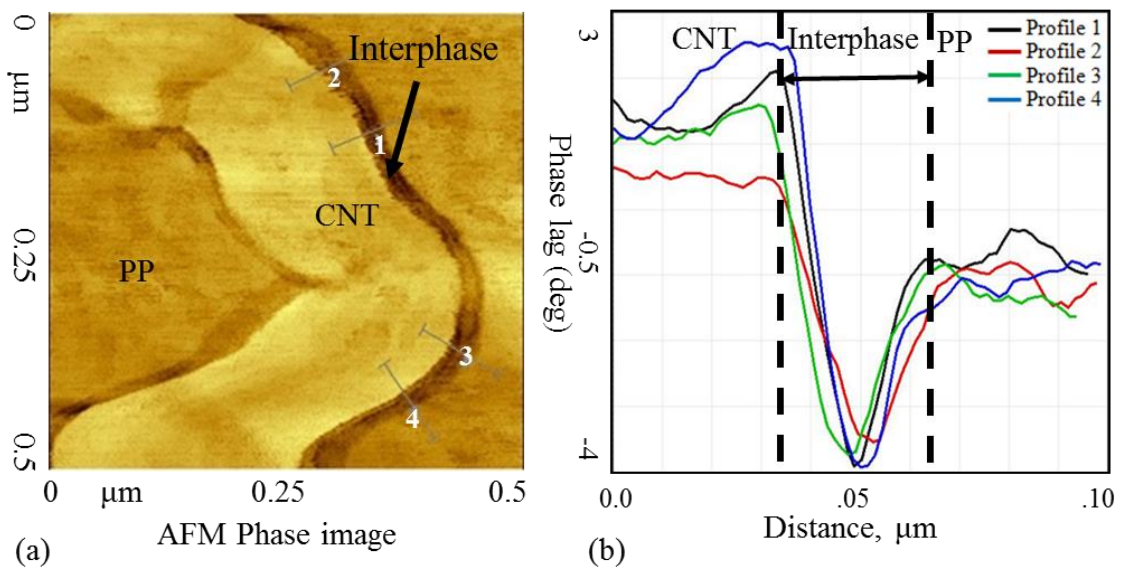
Figure 3.10 AFM observations: (a) AFM phase image of the surface, and (b) stiffness (modulus) gradient across the CNT/PP interphase with 4 wt.% CNT

37
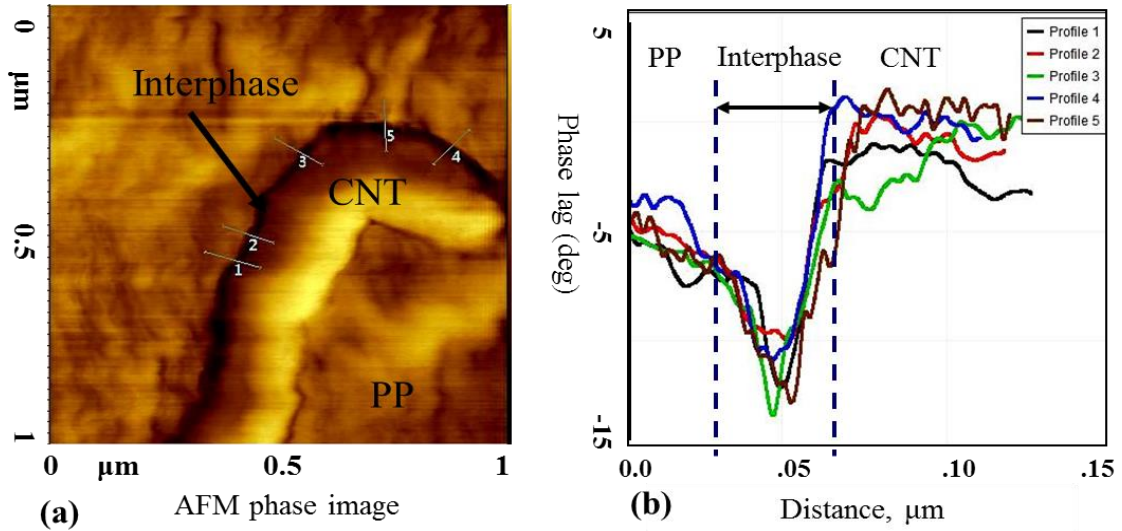
Figure 3.11 AFM observations: (a) AFM phase image of the surface, and (b) stiffness (modulus) gradient across the CNT/PP interphase with 0.1 wt.% CNT

Using the similar approach the average width of the xGnP/PP interphase for 0.1 wt.% and 1 wt.% xGnP/PP composites measured is ~ 30 to 50 nm. A representative AFM phase image of 1 wt.% xGnP/PP composites with the corresponding property gradient profile across the interphase is presented in Figure 3.12. It is noted that the width of the xGnP/PP interphase is larger than the width of the CNT/PP interphase. Although xGnP and CNT have the same surface chemistry, a variation in the width of the interphase formed around them is expected; this is mainly due to the difference in geometry of the nanomaterials e.g., xGnP are platelet shape whereas CNT are tubular in shape. It might be possible that the larger continuous surface of xGnP give rise to a deeper penetration of the influence of the surface resulting in an interphase with larger width (106).
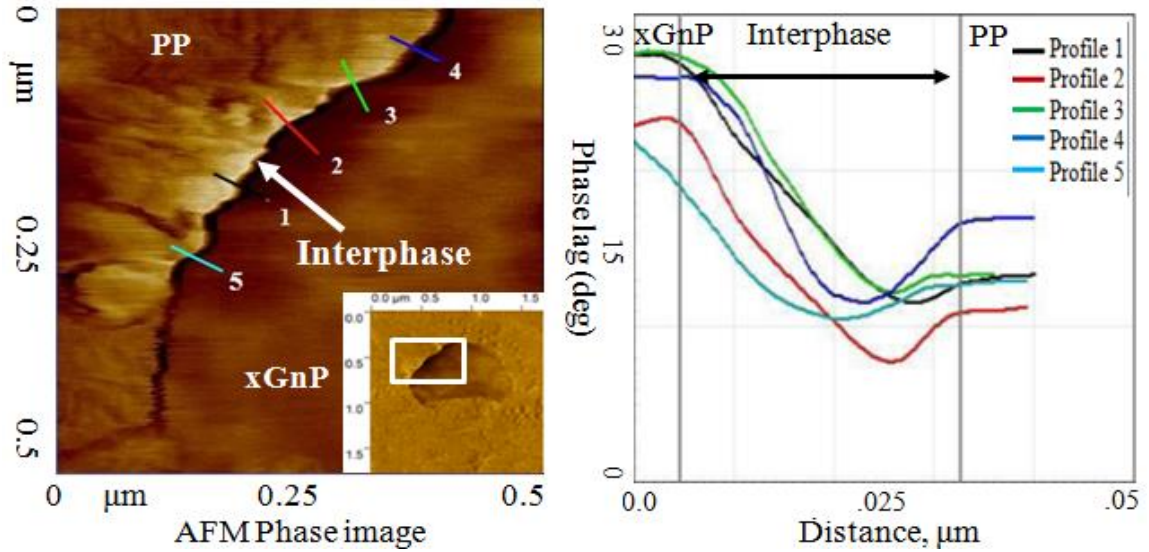
Figure 3.12 AFM observations: (a) AFM phase image of the surface, and (b) stiffness (modulus) gradient across the xGnP/PP interphase with 1 wt.% xGnP.

The modulus of interphase is determined qualitatively based on the observations made on AFM phase lag images. The phase lag reflects differences in stiffness and thus in modulus of the two materials. The phase lag across the CNT/PP interphase and xGnP/PP interphase is presented in Figures 3.10b and 3.12b, respectively. From the figures it can be seen that the phase lag (stiffness) across the interphase is not a step function or a smooth transition between the phase lag (stiffness) of CNT (Figure 3.10b) or of xGnP (Figure 3.12b) and the polymers but it's significantly lower than the stiffness of polymer indicating existence of voids and imperfect interfacial contact.

The interfacial interactions between the nanomaterials and the PP matrix are also investigated through the utilization of SEM images. Figure 3.13a and 3.13b show the SEM images of the fracture surfaces of the 4 wt.% CNT/PP composites and 4 wt.% xGnP/PP composites (bulk), respectively. The presence of pulled out CNT and the holes left behind on the fracture surfaces of CNT/PP composites (as indicated by arrows in Figure 3.13a) as well as the voids along the xGnP/PP contact area (as pointed out by arrows in Figure 3.13b) indicate the presence of weak interfacial interactions between the CNT and the PP matrix. This weak interfacial bonding results in inefficient load transfer

39

from the polymer to the nanoreinforcements when the mechanical load is applied to the composites and implies the presence of a soft interphase, one that has modulus lower than that of the polymer matrix. Presence of soft interphase in polymer matrix composites is also reported in the literature (35, 36). In this study the property gradient profile across the nanomaterial/PP interphase as obtained from the AFM phase lag images is directly used as input in the finite element models.
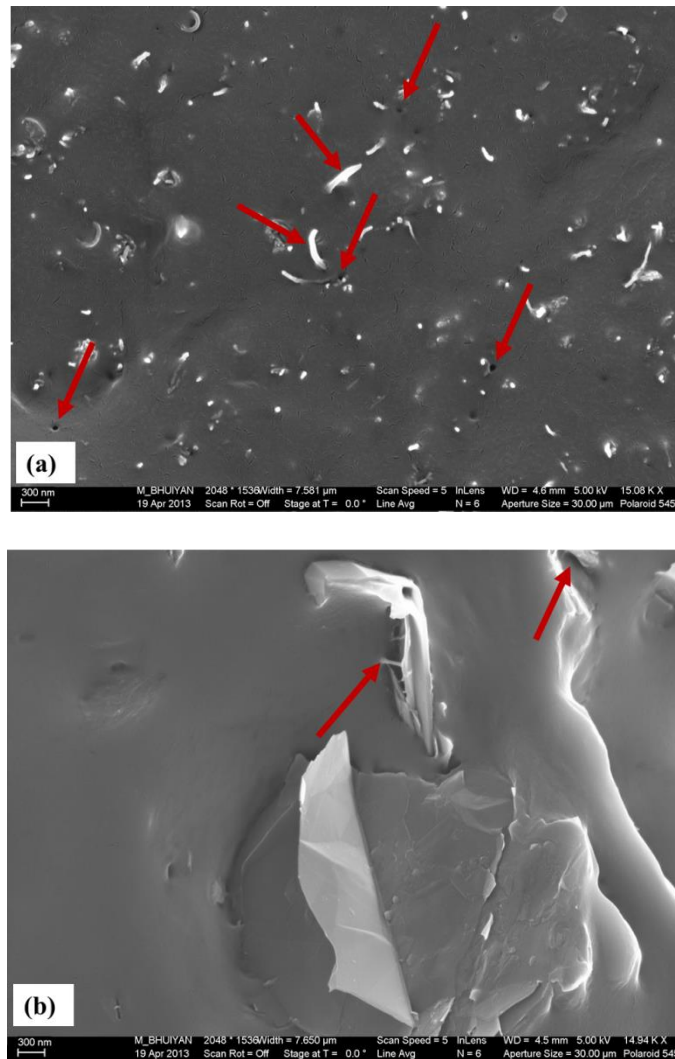
Figure 3.13 SEM images captured from the fracture surfaces of 4 wt.% (a) CNT/PP composites; and (b) xGnP/PP composites showing the presence of holes left behind by the pulled out CNT and existence of voids at the xGnP/PP interface (arrows)

3.3 Conclusions

In this chapter, PP composites (both bulk and fiber) reinforced with CNT and xGnP are investigated in terms of their tensile properties and the factors that affect the tensile properties of the PNCs most are identified. The effects of processing (CNT/PP bulk vs. CNT/PP fiber) and testing conditions (testing at temperature above and below T_g) as well as nanomaterials dispersion on the tensile properties are studied. It is observed that the reinforcing efficiency of nanomaterials is higher at temperature below T_g which can be explained by the enhanced nanomaterial-polymer interactions that occurs at that temperature due to the shrinkage of polymer chains on to the surface of the nanomaterials. Higher reinforcing efficiency of nanomaterials is also observed for the case of fiber composites, which is due to the presence of aligned naomaterials and polymer chains along the applied load direction. Strong interfacial interactions between nanomaterial and polymer matrix, which is an effect of processing conditions, also contribute to this property enhancement. Dispersion of CNT within the PP matrix is improved by using SDBS and an improvement in the tensile properties of SDBS modified CNT/PP composites compared to those of non-modified CNT/PP composites is observed. The reinforcing efficiency of two types of nanomaterials that have similar surface chemistries but different geometry (tube shape CNT vs. platelet or disc shape xGnP) within the PP matrix is also investigated. It is found, by comparing the tensile properties obtained from the room temperature tensile testing, that the reinforcing efficiency of both CNT and xGnP is approximately same although higher tensile properties for the case of CNT/PP composites were expected. In addition the property enhancement was not significant and was much lower than expected as confirmed by comparing the modulus obtained from experiments with the modulus predicted by theoretical models. The existence of non-uniform dispersion and non-homogeneous distribution of nanomaterials within the polymer, the presence of randomly oriented wavy/buckled nanomaterials and the existence of voids at the nanomaterial/polymer

41

interface are the key problems that resulted PNCs with lower tensile properties. SEM images captured from the fracture surfaces of CNT/PP and xGnP/PP composites are also examined to support the experimental findings as well as to extract information qualitatively on the distribution pattern of these nanostructure parameters within the polymer matrix. Finally, AFM experiment is performed to characterize the nanomaterial/polymer interphase in terms of width and modulus. It is found that the width of the nanomaterial/polymer interphase is independent of the nanomaterials' wt,% and the modulus across the of interphase varies exponentially. The findings of this chapter are summarized in Table 3.3 (tensile modulus) and Table 3.4 (tensile strength).

Table 3.3 Tensile modulus of CNT/PP (bulk and fiber) and xGnP/PP (bulk) composites

Nano materials wt.%	Tensile modulus of PNCs, GPa				
	CNT/PP (bulk)		CNT/PP (bulk)	CNT/PP (fiber)	xGnP/PP (bulk)
	non modified		modified	non modified	non modified
	above Tg	below Tg	above Tg	above Tg	above Tg
0	1.38 ± 0.04	2.61 ± 0.16	1.38 ± 0.05	2.24 ± 0.20	1.38 ± 0.04
0.5	1.5 ± 0.02	3.44 ± 0.09	1.64 ± 0.05		
1	1.55 ± 0.03	3.59 ± 0.06	1.72 ± 0.05		
3	1.68 ± 0.05	3.77 ± 0.18	1.82 ± 0.09	3.27 ± 0.42	1.70 ± 0.05
4	1.75 ± 0.08	3.83 ± 0.08	2.06 ± 0.04		
5	1.87 ± 0.04	3.83 ± 0.20	2.00 ± 0.05		1.83 ± 0.08

Table 3.4 Tensile strength of CNT/PP (bulk and fiber) and xGnP/PP (bulk) composites

Nano materials wt.%	Tensile strength of PNCs, MPa			
	CNT/PP (bulk)	CNT/PP (bulk)	CNT/PP (fiber)	xGnP/PP (bulk)
	non modified	modified	non modified	non modified
	above Tg	above Tg	above Tg	above Tg
0	33.14 ± 0.45	33.54 ± 0.52	209 ± 38	33.14 ± 0.45
0.5	34.93 ± 0.48	35.22 ± 0.36		
1	35.78 ± 0.43	37.3 ± 0.21		
3	38.2 ± 0.65	39.01 ± 0.23	310 ± 47	32.83 ± 1.57
4	38.67 ± 0.59	40.85 ± 0.24		
5	39.72 ± 0.83	41.30 ± 0.47		33.15 ± 0.80

CHAPTER 4

IMAGE ANALYSIS AND FINITE ELEMENT MODELING

This chapter covers the details of the image analysis approach and finite element modeling employed in this study to determine the effective modulus of the carbon nanomatrials reinforced PP composites. The probability distribution functions of the nanoreinforcements' various parameters such as orientation, spatial distribution, dispersion and waviness within the PP matrix are determined using two dimensional (2D) SEM images captured from the polished and etched or fractured surfaces of the fabricated composites (both bulk and fiber). The image analysis approach used in this study is suitable for characterizing large amounts of nanomaterials in a time effective way, and hence increases the statistical confidence. 3D finite element models (FEM) are then generated, using the distribution functions obtained from the SEM image analysis as input to the mode,l and analyzed for the PNC effective modulus. The details of the image analysis approach and FEM are presented in the following sections for a model composite system (bulk) with CNT as reinforcements.

4.1 Image Analysis

As mentioned above, the image analysis is performed on the SEM images captured from the polished and etched surfaces of CNT/PP composites. In order to obtain a statistically meaningful distribution of the CNT orientation, diameter, distribution and waviness, a set of about 15 SEM images are captured from various locations of the composite's surface. It is noted that since the composites are fabricated through extrusion and injection molding it is generally expected that the CNT in the skin layers of the composites will be more aligned to the applied load direction than the CNT in the core. However, considering that relatively low pressure of 785 kPa was used in injection

43

molding the difference in CNT orientation in the core and the skin is not expected to be significant. In this study, the focus was placed on determining the overall orientation of the CNT distribution and orientation in the polymer. Therefore, SEM images captured from both the skin and core layers of the composites are used together in the image analysis to extract the overall distribution of CNT orientation within the polymer. Representative SEM images of polished and etched surfaces of 4 wt.% CNT/PP composites normal and parallel to the injection molding/applied load direction are shown in Figure 4.1a and 4.1b, respectively. The 4 wt.% CNT/PP composite is used in the image analysis because phenomena such as agglomeration, orientation, waviness etc. are expected at a large extent when CNT content is high.
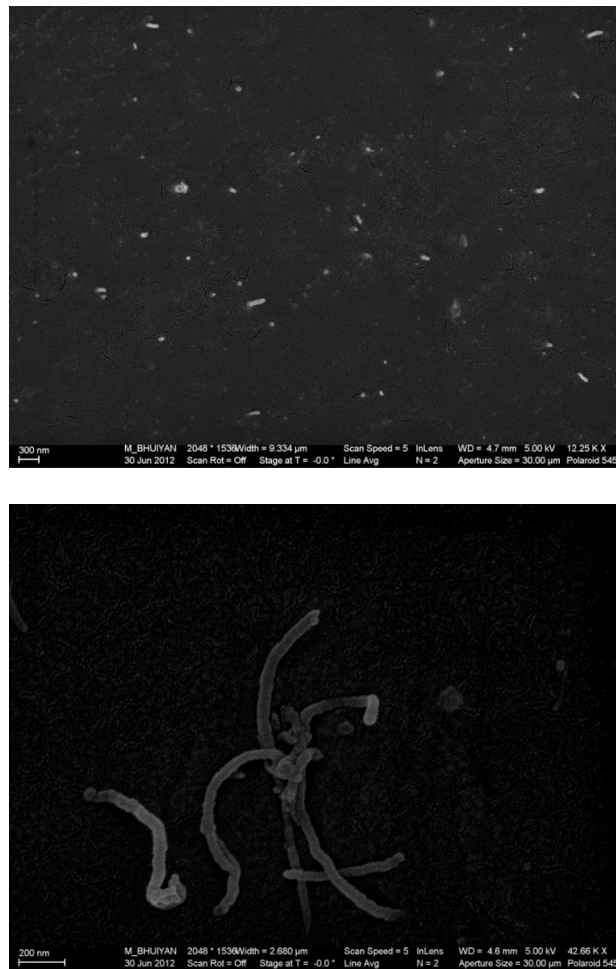
Figure 4.1 Representative SEM image of 4 wt.% CNT/PP composites captured from the surface a) normal/perpendicular to the b) parallel to the injection/applied load direction

The method of ellipses, most commonly used technique in the literature (107) to determine the 3D microstructure or reinforcements' orientation in composites, is employed to determine the nanoreinforcements' three dimensional (3D) orientation distribution. Using the geometric parameters measured in the method of ellipses the distribution functions of nanoreinforcements' diameter, a measure of CNT dispersion/agglomeration, and spatial distribution are determined. An image analysis algorithm described in (108) is employed in this study, after modification, to determine the nanoreinforcements' waviness distribution.

4.1.1 Distribution Function for CNT Orientation

The distribution of CNT orientation within the polymer is determined using the CNT footprint and geometry just below the polished surface of the SEM images. CNT intersect the plane (polished surface) as ellipses or circular disks depending on their inclination below the surface. By measuring the elliptical parameters, one can obtain two angles θ (out-of-plane angle) and φ (in-plane angle) that specify the 3D orientation of each CNT. A typical elliptical footprint of a CNT intersecting the polished plane is shown in Figure 4.2a and the θ and φ angles for a single CNT embedded in the polymer are shown schematically in Figure 4.2b. The geometric parameters that are measured from each elliptical feature are the center of the ellipse (x_c, y_c), the major ($2a$) and minor ($2b$) axes of the ellipse and φ, which is defined as the angle that the ellipse's major axis makes with the x-axis in the x-y plane. The second directional angle, θ, is defined as the angle that the CNT form with the injection/applied load direction (z axis) and is determined using the following geometrical relation:

$$\theta = cos^{-1}\frac{b}{a} \qquad\qquad (4.1)$$
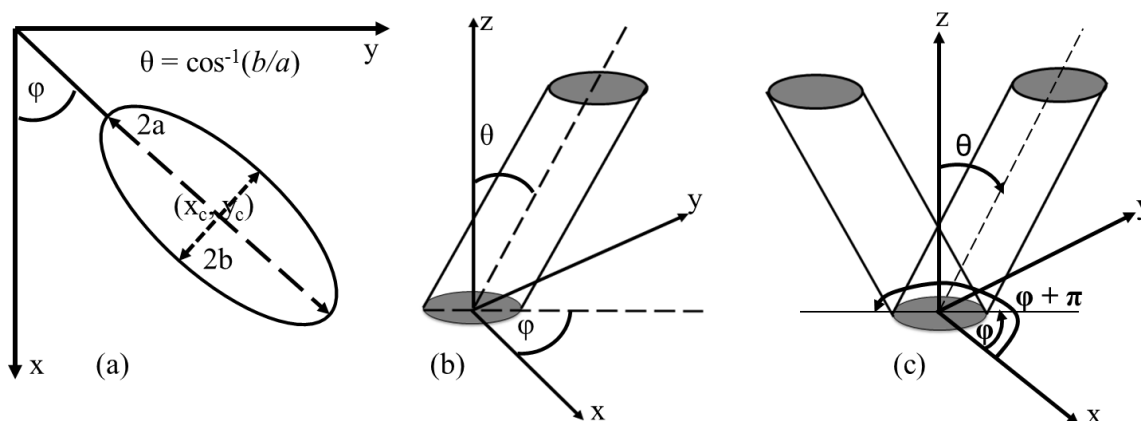
Figure 4.2 Definition of (a) geometrical parameters measured from the elliptical cross-sections of CNT: coordinates of the center of the ellipse (x_c, y_c), minor axis $(2b)$, major axis $(2a)$, and in-plane angle (φ); (b) in-plane (φ) and out-of-angle (θ) used to describe the orientation of CNT; and c) Ambiguity in nanoreinforcements' orientation. Two different in plane angles $(\varphi$ and $\varphi+\pi)$ in the x-y plane are possible for the same elliptical footprint and θ.

However, using just the elliptical marks creates ambiguity in the determination of the CNT in-plane angle φ (109, 110). Figure 4.2c depicts the problem of ambiguity. As shown in the figure, there can be two possible orientation configurations, (θ, φ) and $(\theta, \varphi+\pi)$, for the same elliptical cross section in the x-y plane that cannot be distinguishable. This ambiguity is resolved by using the dark regions, henceforth referred to as "etch marks", around the CNT cross-sections as can be seen in the representative SEM image presented in Figure 4.3a. These etch marks are revealed or amplified by chemical etching of the polished surface, which removes a thin polymer layer exposing some portion of the CNT underneath the surface being studied. These etch marks next to the major axis of the elliptical cross sections of the inclined CNT, shown in the SEM images, Figure 4.3a, are used to correct the in-plane-angle. The way the etch marks are related to the CNT orientation and the correction methodology for the in-plane angle are also shown in Figure 4.3. If the etch mark is located at the opposite side with respect to the measured in plane angle then no correction is required (Figure 4.3b). A correction of $\varphi = \varphi + \pi$ is

46

applied when the etch mark is in the same side with the measured in-plane angle (Figure 4.3c).
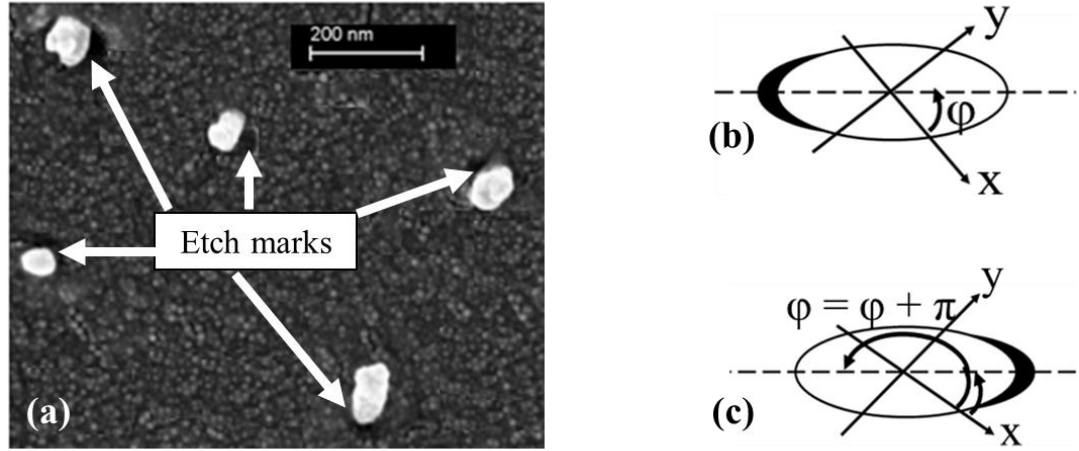
Figure 4.3 (a) Representative SEM images taken from the polished and etched surface of 4 wt.% CNT/PP composites showing the etch marks (dark regions) next to the CNT cross sections; (b and c) correction of CNT in-plane angle.

4.1.2 Distribution functions for CNT diameter and spatial distribution

The CNT diameter is usually determined using SEM and TEM (111, 112). Such techniques however, are either not automated to analyze large number of CNT or cannot account for CNT agglomerates and therefore are not capable of measuring CNT diameter distribution function. In this work, these limitations are overcome by using the major (*2a*) and minor (*2b*) axes, see Figure 4.2a, of the CNT elliptical cross-sections that are seen in the SEM images. The CNT diameter is calculated using the following three criteria: (i) if the major and minor axes are equal for a CNT cross section, *2a=2b=*CNT diameter; (ii) if the major axis is larger than *2*2b,* then CNT diameter = *2b*; (iii) for all other cases, CNT diameter= *(2a + 2b)/2*.

To determine the spatial distribution of CNT within the polymer, a method used for determining the spatial distribution of fibers is adopted (113) . The spatial position of the CNT is described in a polar coordinate system using two parameters R and α, shown in Figure 4.4, which are chosen in a convenient relation to the coordinates of the CNT

centroids within the SEM images. Specifically, R is the distance of the CNT cross-section centroid (x_c, y_c) from the origin, defined as $R = \sqrt{x_c^2 + y_c^2}$, and α is the angle between the x axis and R defined as $\alpha = \tan^{-1}\frac{y_c}{x_c}$. In this schematic, circular cross-sections represent CNT perpendicular to the plane while the elliptical cross-sections represent CNT at an angle with the plane.
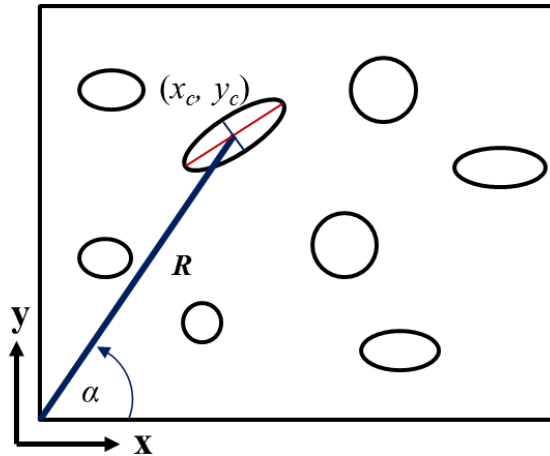
Figure 4.4 CNT cross sections extracted from the SEM image through binary conversion.

4.1.3 Distribution Function for CNT Waviness

Figure 4.5 shows the CNT parameters measured, to determine CNTs waviness distribution, from the SEM images captured from the surfaces that are parallel to the injection/applied load direction of CNT/PP composites (see Figure 4.1b). These parameters are the distance between the endpoints of a CNT (l_{ep}) and the length of the CNT (l_{CNT}) and are measured using a modified image analysis algorithm originally developed for extracting the network geometry of three dimensional (3D) collagen gels (108). The algorithm is based on a principle of nucleation and local maxima points. Using the distance function and parameters set by the user; the program finds nucleation points and maps the CNT network through the local maxima points. The concept is then extended to output both the length and the endpoint to endpoint distance of the CNT. The

48

straightness parameter (P_s) (114), defined by Equation (3.2), is used to characterize the CNT waviness. The P_s value is bounded from 0 to 1, with $P_s \sim 1$ indicating a totally straight CNT whereas $P_s \sim 0$ indicates high degree of waviness.

$$P_s = \frac{l_{ep}}{l_{CNT}}$$ (4.2)

where, l_{ep} = distance between the CNT endpoints, l_{CNT} = Length of the CNT, P_s = straightness parameter (CNTs are very wavy if $P_s = 0$; and CNTs are straight if $P_s = 1$)
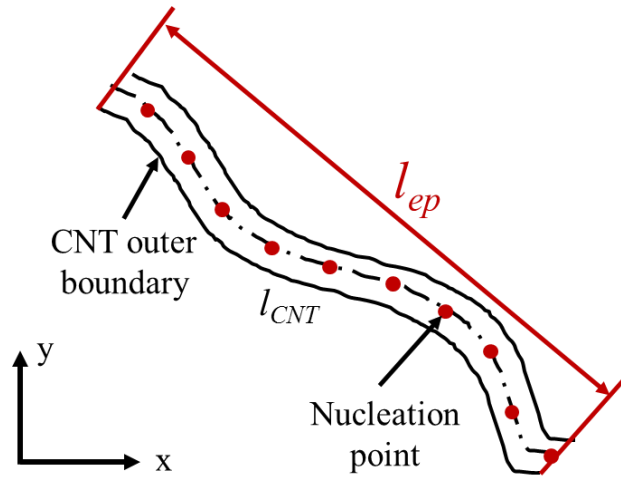
Figure 4.5 Schematic of a wavy CNT with the definition of measured parameters used to determine CNT waviness

4.1.4 Image Analysis Algorithm

This section presents the image analysis algorithm used to extract the distribution functions of various CNT parameters from SEM images that are accounted for in the finite element model.

4.1.4.1 CNT orientation, diameter and spatial distribution

The analysis of SEM images of 4 wt.% CNT/PP bulk composite surfaces prepared by polishing and etching, in order to determine the probability distribution functions of CNT characteristics, is performed using a program developed with MATLAB$^{\circledR}$ and the image processing toolbox. The algorithm implemented to determine the distribution functions of CNT parameters within PP matrix consists of the following general steps:

selection, classification and characterization of the CNT cross-sections, correction of orientation angles (out-of plane angle (θ) and in-plane angle (φ)) and determination of distribution functions for CNT orientation, diameter and spatial distribution. The flowchart shown in Figure 4.6 outlines the process.

Specifically, each SEM image is read into MATLAB® first. The image is then converted to a gray scale image from an RGB image. From the gray scale image, the locations of the etch marks are determined with a binary conversion factor. Since the etch marks are very dark on the image, if present, it is relatively easy to separate them with a binary image conversion. The image containing the extracted etches is then stored. Figure 4.7 shows a representative SEM image used in the image analysis. The etch marks obtained from the SEM image after binary conversion (as pointed by arrow) are presented in Figure 4.8.
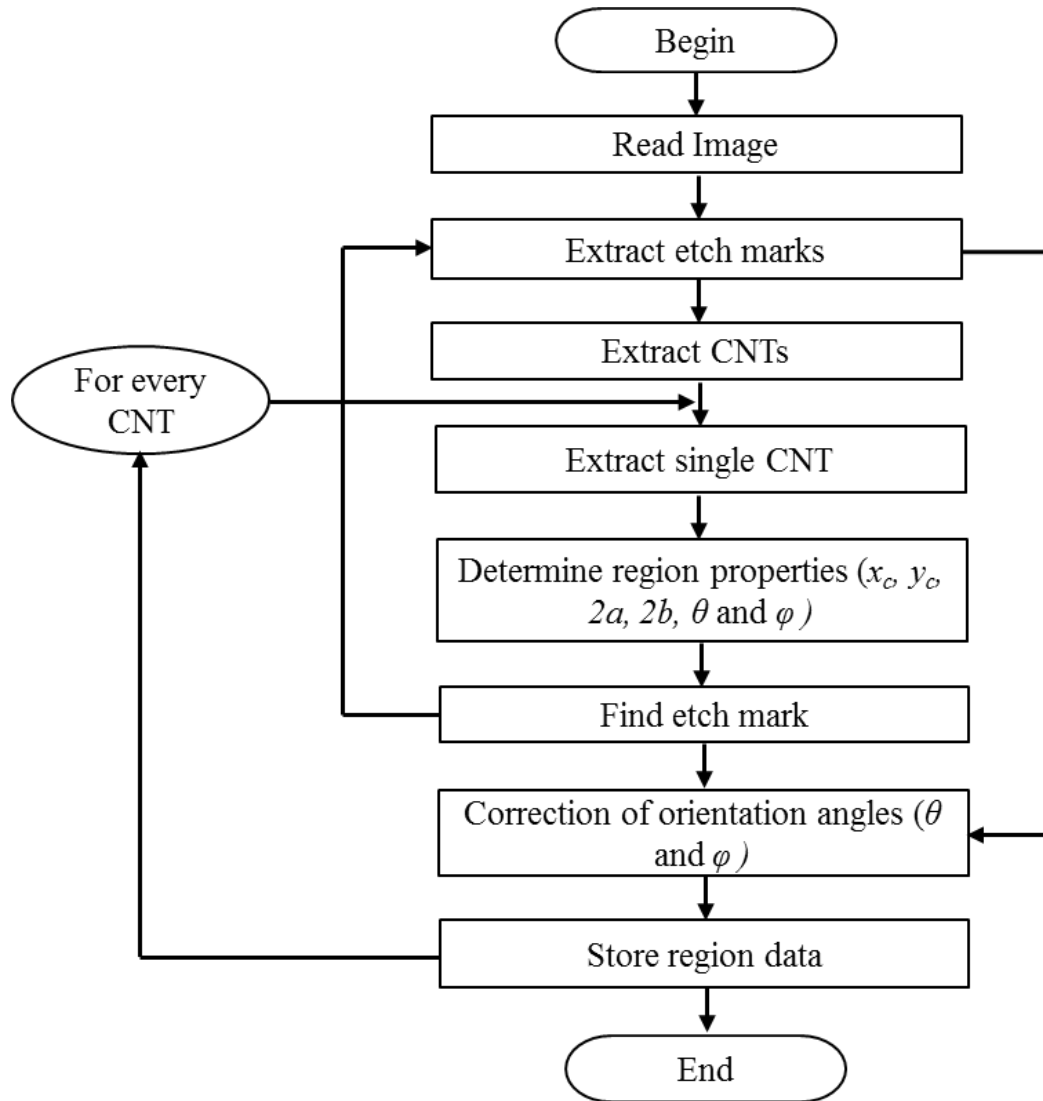
Figure 4.6 Image analysis algorithm implemented to determine the distribution of CNT orientation, diameter and spatial distribution in polymers
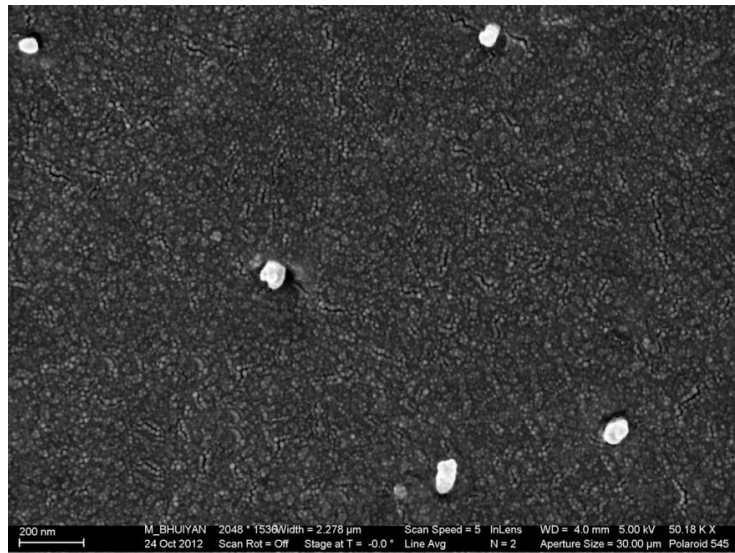
Figure 4.7 Representative SEM image used in the image analysis (the image is captured from the polished and etched surfaces of 4 wt.% (non-treated) CNT/PP composites
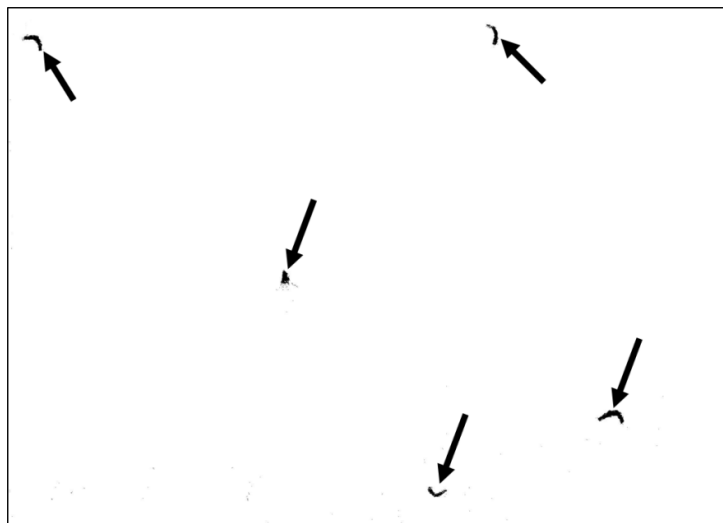
Figure 4.8 Extraction of etch marks through binary conversion of SEM images

The next step is to extract the cross-section of CNT from the original SEM image, which is also done by using binary conversion. The contrast between the relatively white color of the CNT makes it easy to extract them from the original image. Figure 4.9 shows the cross-sections of CNT extracted from the original SEM image shown in Figure 4.7.
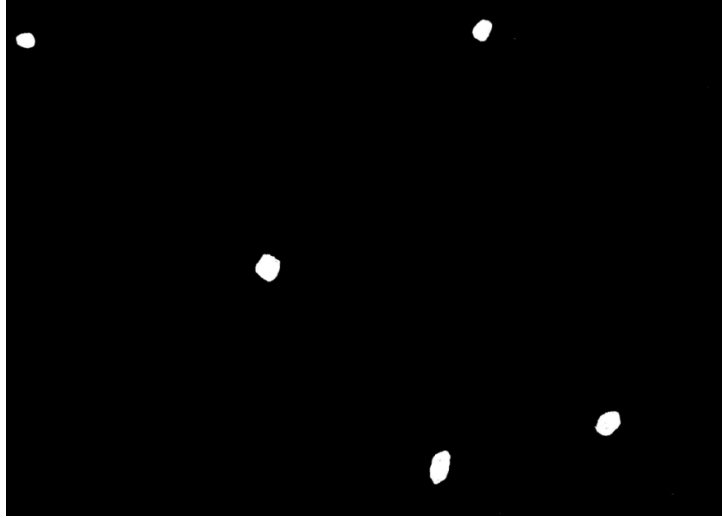
Figure 4.9 Cross-sections of CNT extracted from the original SEM image shown in Figure 4.7

The next step is to determine the region properties for each CNT i.e., the location of centroid (x_c, y_c) of each CNT, major ($2a$) and minor ($2b$) axes of CNT cross-section and orientation angles (θ and φ). In order to be able to obtain the region properties, the boundary/outline of each CNT is determined first using the morphological operation available in MATLAB®, which is explained next. First, the SEM image is refined using 'majority' and 'fill' commands which help reduce noise and fill small areas with the appropriate pixels. Finally, the 'remove' command is used to remove all the white pixels except those located at the boundary, which defines the cross-sections of all the CNT. The cross sections of the CNT obtained after the morphological operation of the SEM image are shown in Figure 4.10. From the cross-sections of the CNT, five geometrical parameters (the location (x_c,y_c) of the centroid of the cross-section, the major ($2a$) and minor axes ($2b$), and the orientation angles, θ (out-of angle) and φ (in-plane angle) are measured for each CNT cross-section using the '*regionprops*' command available in MATLAB®. The out-of-plane angle is calculated using equation 4.1 (see section 4.1.1). The in-plane orientation angle is defined as the angle between the CNT's major axis (2a) and the x-axis in the x-y plane.
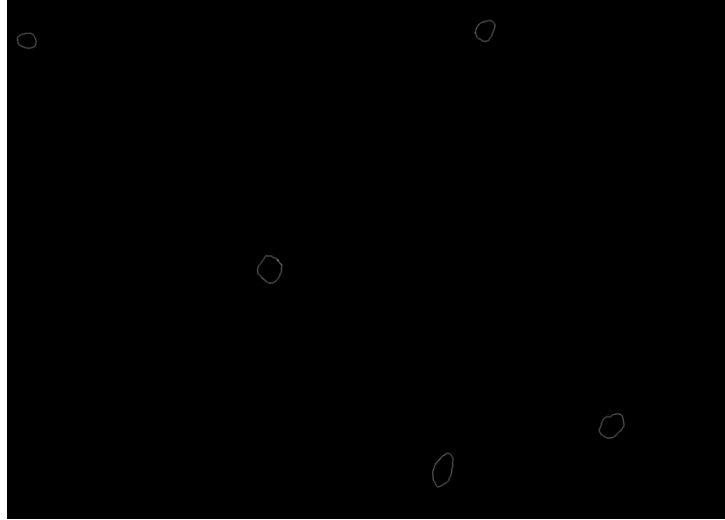
Figure 4.10 CNT boundaries obtained from the SEM image through morphological operations

The final step is the correction of in-plane orientation angle (φ) because for the same cross-section this angle can have two different configurations, φ and $\varphi+\pi$. This ambiguity is removed with the help of the etch marks (shown in Figure 4.8) and its' location with respect to the CNT cross-sections. If the etch mark is located at the opposite side with respect to the measured in plane angle then no correction is required but if it is located at the same side then a correction of in-plane angle is needed. The code is written in such a way that the in-plane angle is measured with respect to the right side of the CNT cross-section. Therefore, it searches for etch marks next to the left side of the CNT cross-section.

If the code finds an etch mark to the left side of the CNT cross-section, and if it matches the etch marks obtained in the etch image (see figure 4.8), then the in-plane orientation is the same as calculated in MATLAB® and no correction of in-plane angle is needed. But if the code does not find an etch mark in the left side, then either the etch mark is on the right side or there is no etch mark present next to the CNT boundary. The code then searches whether there is any etch mark present at the right side of the CNT boundary. If it finds an etch mark at the right side, a correction of in-plane angle is

applied by adding π with the measured angle. The corresponding out-of-plane angle (θ) is also corrected by adding $-\frac{\pi}{2}$ with the measured angle. If no etch mark is present around the CNT boundary, then the in plane angle is as calculated in MATLAB®. Once all information is determined, the data is stored and the code performs the same steps for the other CNTs in the same SEM images, and when analysis for one SEM image is done the code starts again from the step "Read Image" for the next SEM image. With all the information in hand the distribution functions for CNT orientation, diameter and spatial distribution can now be obtained. The distribution functions of the CNTs characteristics within the PP matrix are presented below for a composite system 4 wt.% CNT/PP composites with as received CNT.

4.1.4.2 CNT Waviness

The algorithm implemented to determine the distribution for CNT waviness within the PP matrix is based on the approach reported in (108) but with significant modifications for CNT composites. The flow chart presented in Figure 4.11 shows the outline of the process implemented. The image is first smoothed with a Gaussian filter and then binarized such that pixels of value one are CNT and pixels of value zero are polymer. It is noted that for the algorithm to be able to obtain that CNT in a way that exactly matches the SEM images, the threshold must be chosen appropriately. If it is too high, one long CNT may be broken into many shorter ones and if it is too low, the CNT that are clearly separated in the original image become blurred together. A representative SEM image and the corresponding binary form are shown in Figure 4.12a and b respectively.
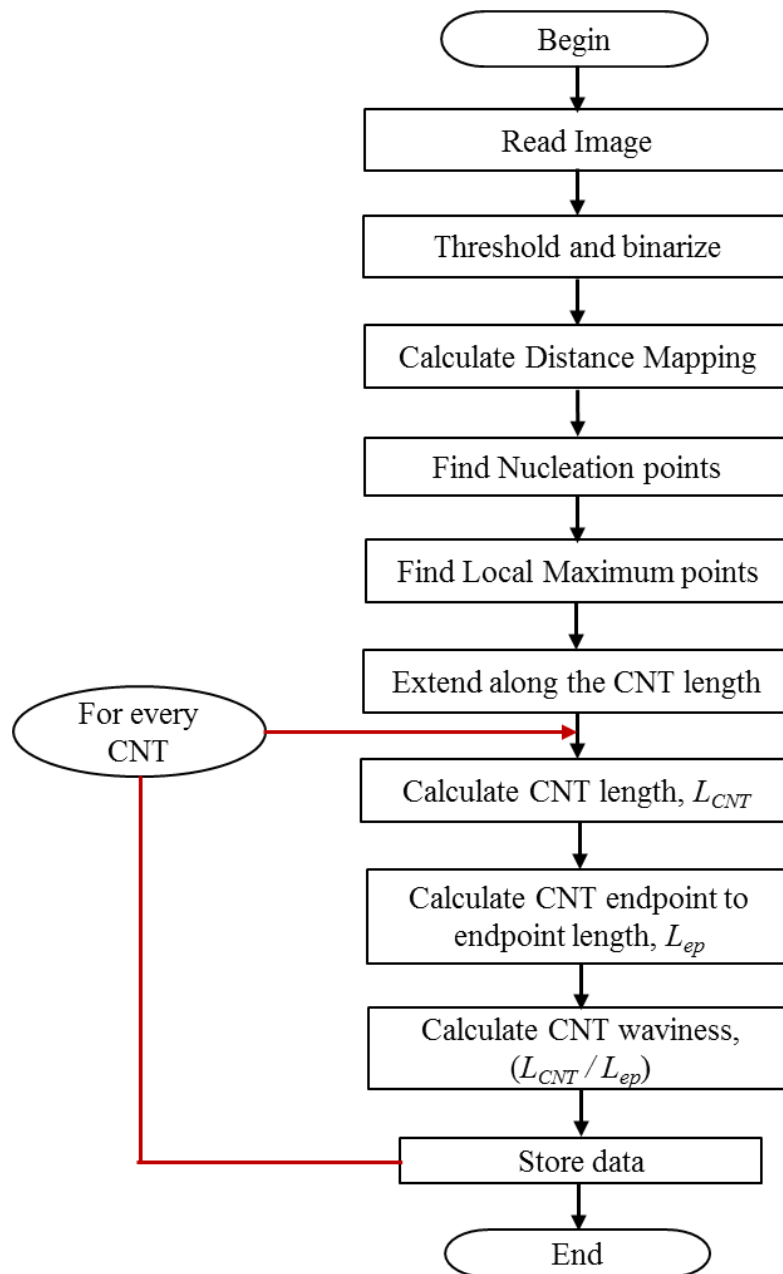
Figure 4.11 The outline of the tracing procedure to determine CNT waviness
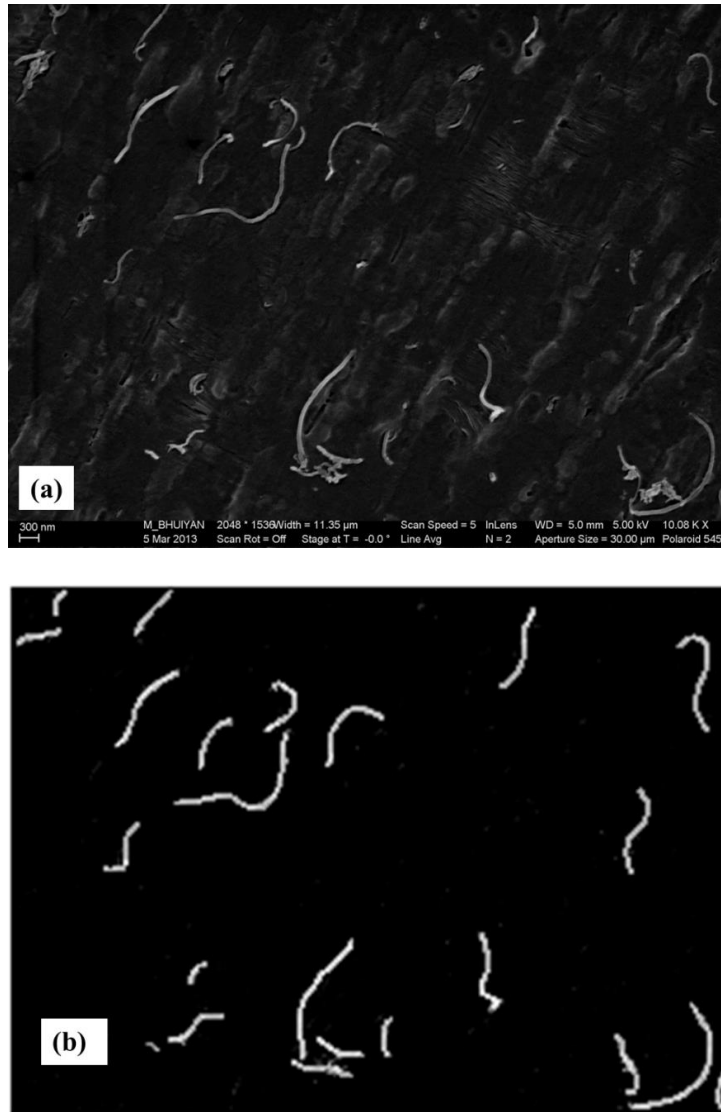
Figure 4.12 (a) Representative SEM image used to determined CNT waviness within the PP matrix; (b) SEM image after thresholding and binary conversion

The next step is to find the distance map/function from the binary image. The distance mapping that shows the distance of a CNT pixel (white in color in the binary image) from the PP pixels (black in color in the binary image) next to the CNT boundary is calculated using the '*bwdist.m*' function available in MATLAB®'s image processing toolbox and is then smoothed using Gaussian filter. The distance mapping of the SEM image presented in Figure 4.12a is shown in Figure 4.13a. The distance of the CNT pixels from the matrix pixels for a portion of CNT length (as pointed by arrow) is also presented

in Figure 4.13b. The nucleation points, the maximal ridges in the distance map, i.e. the farthest pixel on the CNT surface from the matrix pixels surrounding the CNT are then determined using the distance mapping. After identifying the nucleation points, the next step is to trace the CNT along its length extending from the nucleation points, which is done with the help of local maximum points (LMPs). To find the LMPs a box of radius r is drawn surrounding the nucleation point, where r is the distance of the nucleation point from the matrix, and the LMPs are defined as the pixels on the CNT surface that have the highest pixel value in the distance map and are located near the surface of the box. The process continues until it finds the end points of the CNT, and then calculation for CNT length (l_{CNT}) and CNT endpoint to endpoint distance (l_{ep}) is performed. CNT waviness, which is the ratio of l_{ep} to l_{CNT}, is also calculated. The nucleation points that are found along the length of CNT with the help of LMPs are shown in Figure 4.13b.Once the calculation for one SEM image is done, the algorithm looks for the next image and the process continues.
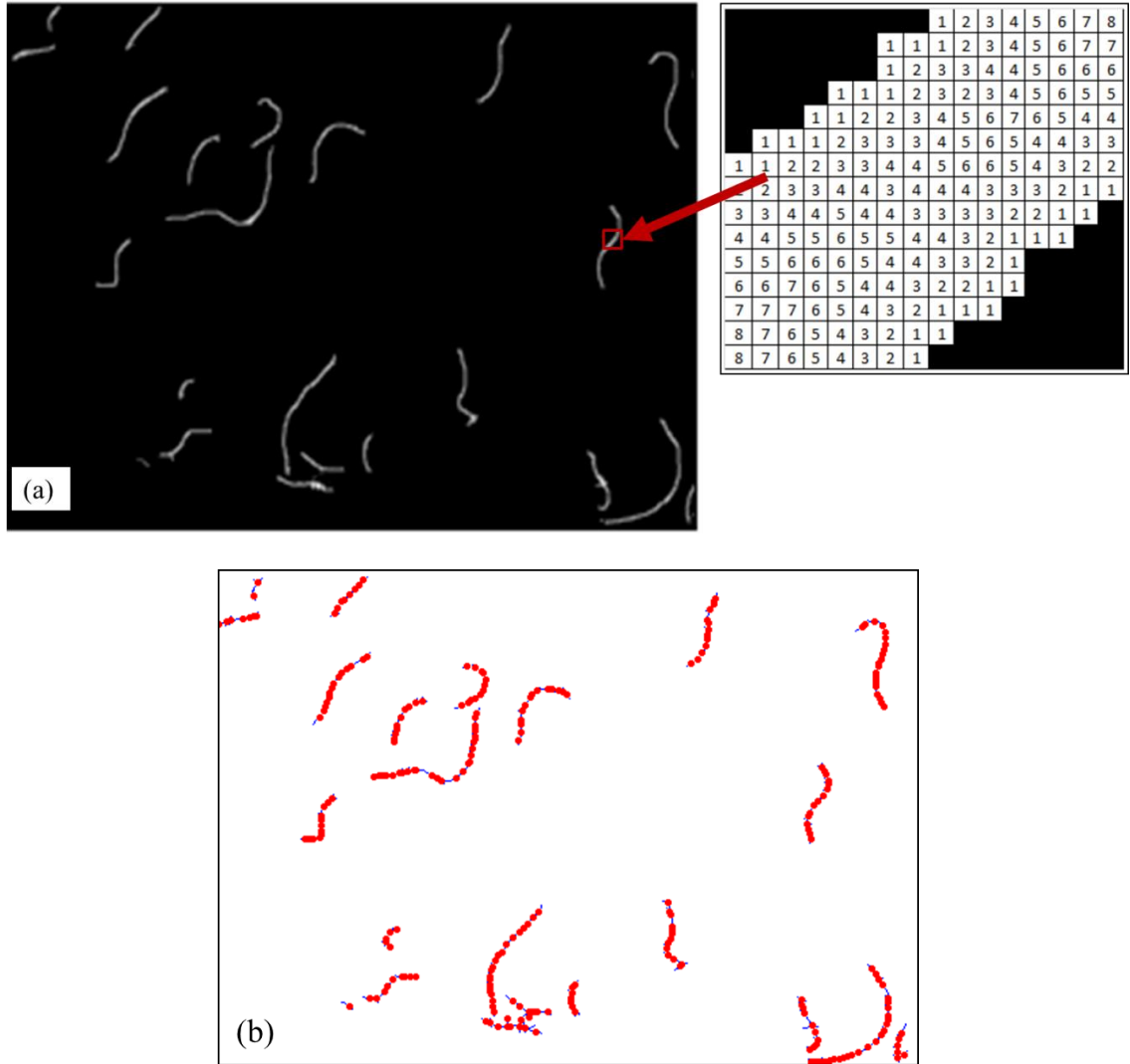
Figure 4.13 Distance mapping of the SEM image presented in Figure 4.12a; (b) Nucleation points found along the length of CNT

4.2 Finite Element Modeling

This section discusses the development of finite element models for PNCs containing up to 4 wt.% carbon nanomaterials; the models will be used to evaluate the tensile modulus of the PNCs. The effective Young's modulus of the PNCs is of particular interest and has been evaluated through numerical analysis of the generated models. Finite element analysis using ANSYS, which is commercially available, is used here to characterize PNCs. One of the main reasons for using this software is because of its computational efficiency with a vast database of elements and material models, and its

superior pre- and post-processing capabilities. The methodology used in evaluating PNCs' effective modulus is also discussed here.

4.2.1 Modeling the RVE

In order to determine the tensile modulus of the PNCs through FEA, an RVE of the PNCs is needed. The RVE must be large enough to represent the PNCs macroscopically and at the same time should be small enough to be computationally efficient. In this study, a 3D RVE is developed that consists of multiple CNT or xGnP embedded in PP matrix; PP matrix and nanomaterial/PP interphase and analyzed to evaluate the PNCs effective modulus using ANSYS 14. The dimensions of the RVEs used in this research are: 2000 nm (L) x 1000 nm (W) x 1000 nm (H) for CNT/PP (both bulk and fiber) and xGnP/PP (bulk) composites. The dimensions of the RVE are selected so that the finite element analyses are not computationally intensive. In addition to minimizing the computational complexity it is also made sure that the RVE size selected is sufficient enough to accommodate the nanomaterials' characteristics, such as orientation, dispersion, distribution, waviness and give converge results when FEA is repeated.

The RVE with different weight fractions of carbon nanomaterials are generated automatically using a programming code written in MATLAB®. The centers of mass of the nanomaterials' within the RVE are selected based on the spatial distribution function obtained from the SEM image analysis. Similarly, the 3D orientation of nanomaterials within the RVE is modeled by using the distribution functions obtained for two angles, θ and φ, that describe the orientation of the nanomaterial axis with respect to the axial loading direction (z-axis) and with respect to a defined plane (x–z), see Figure 4.14, respectively. To make the model more realistic individual CNT as well as CNT agglomerates of different sizes are modeled within the RVE using the diameter distribution function. For the RVE with CNT, the waviness of CNT, as determined by

SEM image analysis, is also integrated into the model. To generate the wavy CNT geometry a discretization method described in (115) is used, in addition to the distribution function. It is noted that the distribution functions of nanomaterials characteristics are defined by using parameters such as mean and standard deviation. These quantities are then used to define the distribution of nanomaterials parameters within the RVE with the help of the programming code written in MATLAB®. The three dimensional RVE is then generated in Autodex Inventor before importing the geometry to ANSYS for FEA. The flow chart presented in Figure 4.14 outlines the process of RVE generation for FEA. While generating the RVE, a contact algorithm is used to make sure that the CNT are not overlapping with each other. The volume fraction is updated when a new nanomaterial is added and the process continues until the desired volume fraction is achieved. The representative RVE of the composite systems generated for FEA are shown in Figure 4.15.

Begin

Step 1: Define the distribution functions of nanomaterials parameters in the code by mean and standard deviation

Step 2: Generate the nanomaterials geometry inside the RVE dimensions following the defined distribution functions

Step 3: Create the model for FEA in Autodex Inventor

Step 4: Import the RVE into ANSYS for FEA

Step 5: Perform FEA
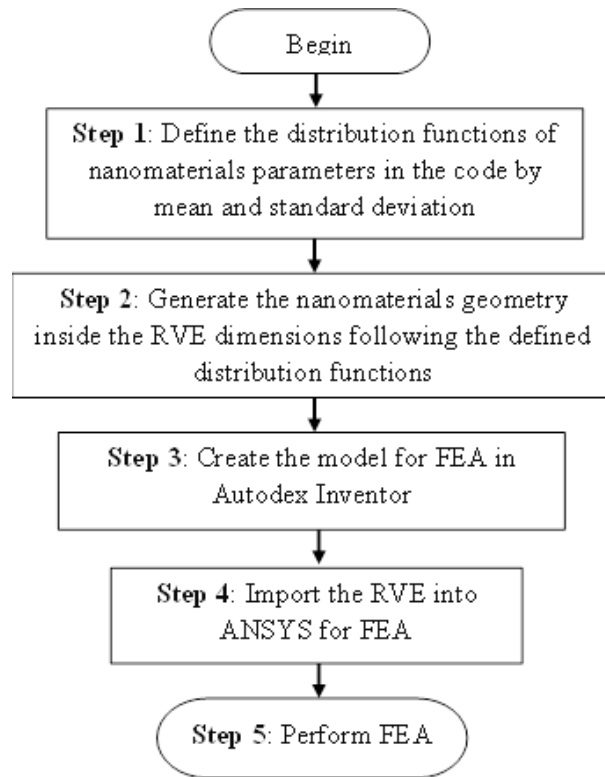
Figure 4.14 Flowchart showing the steps used to generate RVE for the composites for FEA
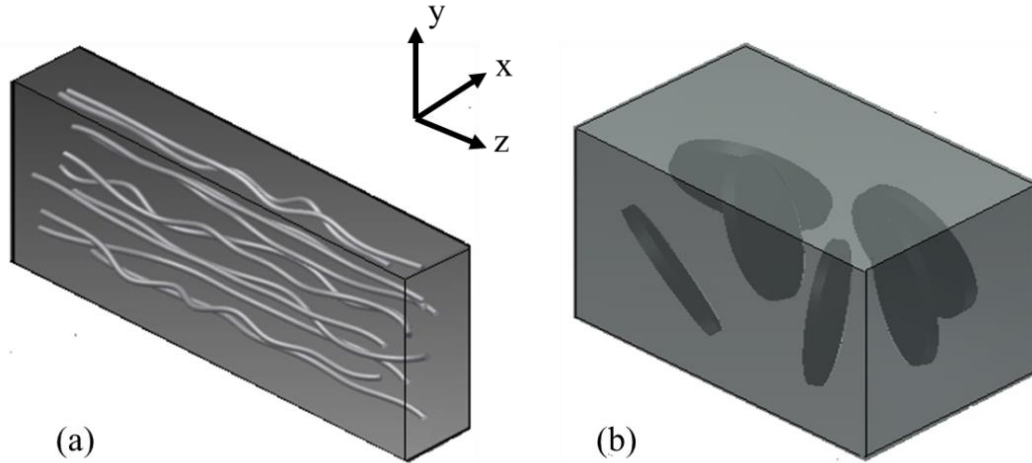
Figure 4.15 RVEs generated for FEA reinforced with (a) CNT, and (b) xGnP

4.2.2 Geometry and Properties of the Nanomaterials

For modeling the RVE with xGnP, discs of cylindrical shape with diameter = 1000 nm and thickness = 15 nm are used. These dimensions are chosen based on the specifications provided by the supplier. AFM experiment also supports the above xGnP dimensions. For the RVE with CNT embedded in PP, a CNT length of 1500 nm is used, which is the critical length of the CNT and is chosen based on a FEA parametric study. According to the supplier the CNT have an aspect ratio of 750. Therefore, the range of aspect ratio (length, l to diameter, d ratio) considered for the FEA parametric study is ~ 35 to 750. The results of the parametric study including the variation of effective modulus of the CNT/PP composites as a function of CNTs aspect ratio are presented in Figure 4.16. Accordingly the critical aspect ratio of CNT, above which there is no effect of the CNT aspect ratio (l/d) on the composites tensile modulus is ~ 60, which gives a CNT length of 1500 nm, using CNT diameter of 25 nm. Therefore, in this study, CNT length of 1500 nm is used for modeling the RVE and subsequent FEA.
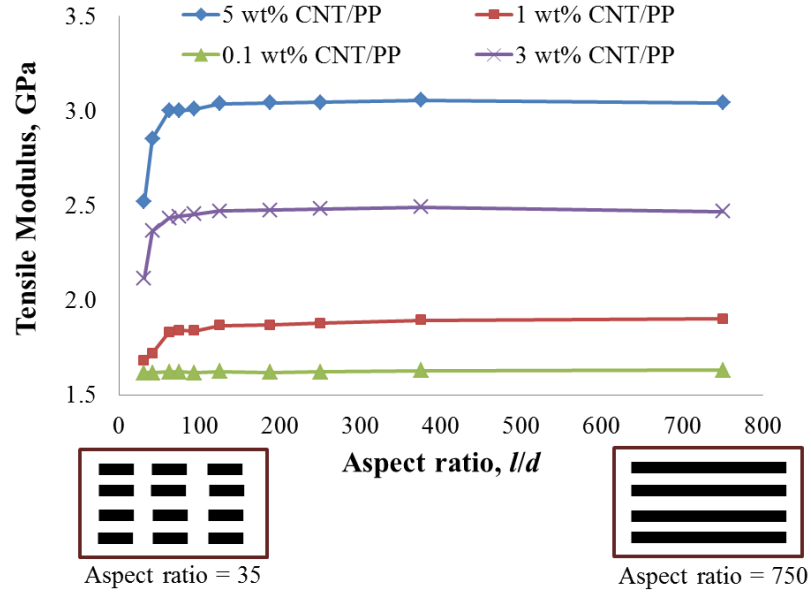
Figure 4.16 FEA predictions to determine the critical aspect ratio (*l/d*) on the CNT

In addition to simplifying the models using the critical length, another simplification is made by modeling the CNT within the RVE as solid cylinders of circular cross-sectional area. Continuum mechanics based FEM requires that the structurally discrete CNT be replaced by a continuum phase. Therefore, in this study CNT are represented as effective (solid) fibers with diameter equal to the outer diameter of the CNT (58, 75, 116, 117), as shown in Figure 4.17. The modulus of the effective fiber is calculated using equation 4.3, which is derived based on the assumption that an applied external force (F) on the CNT and the effective fiber (Figure 3.8) will result in an iso-strain condition (58).

$$E_{eff} = \frac{r_f^2 - (r_f - t)^2}{r_f^2} * E_{CNT} \tag{4.3}$$

where, r_f (=d/2) is the radius of effective fiber, t (= ~0.34 nm) is the thickness of CNT outer layer and E_{CNT} = 1250 GPa is the average modulus of the CNT as provided by the supplier.
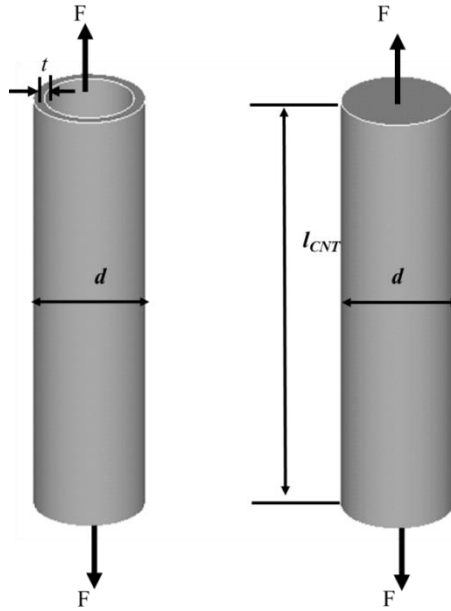
Figure 4.17 Schematic of the CNT and effective fiber used to evaluate the effective
elastic modulus of CNT in composites

4.2.3 Interphase Characteristics

The nanomaterial/polymer interphase is introduced in the RVE by replacing an equivalent volume of polymer matrix, while maintaining the nanomaterials volume. Both the width and modulus of the interphase are characterized by analyzing AFM phase images. The width of the interphase used in the modeling is 20 nm for the CNT/PP composite system and 30 nm for the xGnP/PP composite system as obtained from AFM. The AFM results also suggest that the modulus of the interphase is not constant across the interphase; instead it varies from $E_{int} = E_{nanomaterials}$ at the nanomaterials surface and $E_{int} = E_{polymer}$ at the interface surface adjacent to the polymer. The modulus variation across the interphase is used as input to the FEM model during FEA. The details of the interphase characterization are explained in chapter 3. The dimensions and mechanical properties of all the phases used in this FEA are presented in Table 4.1.

Table 4.1 Mechanical properties and the geometric characteristics of all the phases used in FEA

	Modulus, GPa	Poisson's Ratio	Characteristic Length, nm
CNT	70 (equation 4.3)	0.3 (118)	Diameter, d = 25
xGnP	70(119)	0.3 (118)	Diameter, d =1000, Thickness, t =15
PP	1.4 (experiment)	0.36(118)	
CNT agglomerates	Vary with CNT diameter	0.30(118)	CNTs diameter distribution
Interphase	Property gradient profile (AFM)	0.36(118)	width: CNT/PP = 20, xGnP/PP = 30 (AFM)

4.2.4 Loading, boundary conditions and assumptions for FEA

The RVE is subjected to uniform extension within the linear regime of the stress-strain curve as determined experimentally. The loading and boundary conditions applied to the RVE for FEA are presented in Figure 4.18. The RVE model is for CNT/PP composites and is presented here as a representative for all the composite systems used in this study. For each model, the z=0 end (Figure 4.18a) is constrained in the axial direction (z direction) and is free to move in the lateral directions. The free edges (Figure 4.18a) are constrained to their respective normal directions in order to allow contraction of the RVE due to tension. An axial displacement, equivalent to the experimental strain, is applied to all nodes on the end surface (z=L) (Figure 4.18c), where L is the length of the RVE. Periodic boundary conditions are applied on the other faces (Figure 4.18b). A higher order 3D structural brick element (SOLID185 -8-node quadratic element with three degrees of freedom per node) is used. An optimum element size (mesh density) that leads to a fully converged solution with minimum computational time is determined based on a FEA parametric study, presented in Appendix A. The assumptions made are

that there is perfect contact at the interfaces of all the phases (120-122), and that all the phases are homogeneous, isotropic, and linearly elastic. The effective modulus of the composite system is calculated as the ratio of the average stress generated at z = L (i.e., the surface at which the displacement, ΔL is applied) to the applied strain ($\Delta L/L$) on the RVE model. The same methodology has been used throughout this research to evaluate the effective modulus of the PNCs.

a) Constrained surface (z=0) , (u = 0)	b) Free surface (periodic boundary condition)	c) End surface (z=L); (u = ΔL)
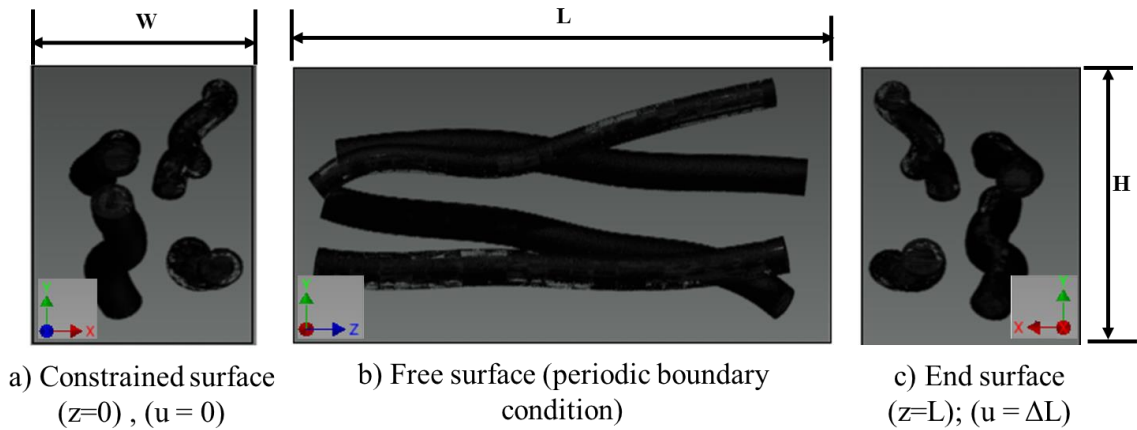
Figure 4.18 Applied loading and boundary conditions on the different surfaces of the 3D-RVE

4.2.5 Validation of the FEM Model

4.2.5.1 Validation of using FEA approach for PNC

FEA parametric study is performed first, using a simple case, to validate the use of FEA to predict the tensile modulus of the CNT/PP composites. For this study, a 3D quarter symmetry RVE of 5 wt.% CNT/PP composites, presented in Figure 4.19, is used. The RVE consists of only two phases: CNT and PP. The dimensions of the RVE used are: 200 nm x 74 nm x 74 nm (L x W x H). The geometric dimensions of the CNT used are: hollow CNT with outer diameter 25 nm and inner diameter 7.5 nm, length 200 nm. By changing the mesh density of the different phases (CNT and PP) within the RVE it is investigated whether FEA predictions matches with the theoretical predictions or not.
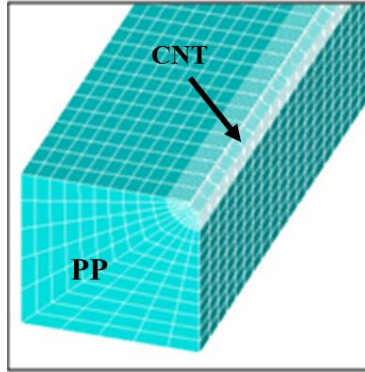
Figure 4.19: 3D quarter symmetry RVE with the generated mesh for 5 wt.% CNT/PP composites

The tensile modulus of 5 wt.% CNT/PP composites as obtained from FEA as a function of number of elements or mesh density is presented in Figure 4.20. To check the convergence of the model the model predictions are compared with the Rule of Mixture (ROM) predictions. From the results presented it can be seen that FEA prediction increases as the number of elements increases, and it reaches ROM predictions with a number of elements of 22200, therefore justifying the use of FEA to predict he tensile modulus of the CNT/PP composites.

Figure 4.20 FEA predictions of tensile modulus as a function of number of elements: validation of the use of FEA for predicting tensile modulus of PNC

4.2.5.2 Validation of the proposed FEM model

The next step is to validate the proposed FEM model. In order to validate the proposed model, the modulus predicted through FEA is compared with the predictions of theoretical micromechanical models as shown in Figure 4.21. The micromechanical models used for the comparison are Halpin–Tsai (H–T) (94) and Tandon–Weng (T–W) (95) models, and the comparison is performed for the CNT/PP composite system with CNT concentration of 5 wt.%. As shown in the figure the FEM model predictions follow the same trend, with the moduli predicted by the micromechanical models, thus validating the proposed FEM model. It is noted that the FEM model used for comparison consists of only CNT and PP and that all the CNT are straight, individual and aligned along the applied load direction. It can be seen that the H–T model results to lower modulus compared to FEA. This is because the H–T equation does not account for the maximum packing fraction and the arrangement of the reinforcement in the composite. A modified H–T model that accounts for this has been proposed in the literature (123). The effect of the maximum packing fraction and the arrangement of the reinforcement within the composite become less significant at higher aspect ratios (124).
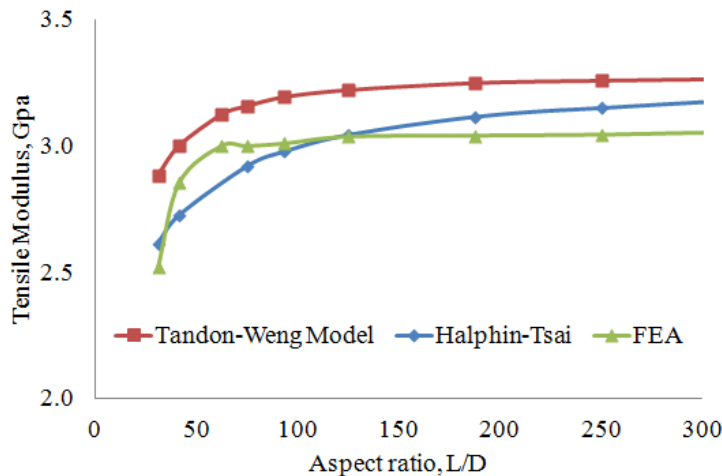
Figure 4.21 Validation of the FEM model: theoretical models vs. FEA

CHAPTER 5

EFFECTS OF NANOMATERIALS CHARACTERISRICS ON

TENSILE MODULUS OF PNCs

The tensile modulus of polymeric composites is one of the most important material properties for engineering applications. This chapter describes the development of a design tool able to predict the tensile modulus of PNCs based on the integration of finite element modeling coupled with SEM image analysis and thorough experiments. The proposed design tool can provide significant flexibility in terms of understanding both the individual and the combined effects of various nano- and micro-scale parameters on the tensile modulus of the composites. Critical parameters that are accounted for are nanomatrials' dispersion, spatial distribution, and orientation and shape changes due to processing such as waviness of CNT within the polymer. Effects of geometry and properties of nanomaterial/polymer interphase are also investigated. These parameters, in terms of their probability distribution functions obtained directly from SEM images of the composites through an elaborated image analysis, are used as input to the finite element models. The details of the image analysis technique and the finite element modeling are discussed in chapter 4. These distribution functions, as obtained from the composites' SEM images and their effect on the tensile modulus of carbon reinforced PNCs, are presented in this chapter. CNT reinforced PP composites are used as a model composite system to perform the analysis. Finite element modeling predictions of the tensile modulus are then compared with the experimentally determined values in order to validate the proposed design tool. Experimentally the parameters considered in the model are altered by using i) bulk and fiber composites, ii) as received and surface modified CNT and iii) CNT and xGnP and the accuracy and sensitivity of the proposed FEM model in capturing these differences is demonstrated.

5.1 Distribution Functions of nano- and micro-scale Parameters

Before studying the effects of nanomaterials parameters on the tensile modulus of PNCs, their distribution functions within the polymer must be known. This section presents the distribution functions of the various parameters that were obtained from the SEM images and that are accounted for in the model. The algorithm used to determine the distribution functions for nanomaterials parameters are discussed in Chapter 4.

5.1.1 CNT/PP Composites

Figure 5.1 shows the resulting histograms for the CNT 3D orientation (θ and φ) within the PP matrix along with the corresponding distribution curves. The out-of-plane (θ) orientation angle is presented in Figure 5.1a, from which it can be seen that the CNT out-of-plane angle follows normal distribution with mean and standard deviation of ~16º, and ~14º, respectively. The distribution for CNT in-plane angle (φ), as presented in Figure 5.1b also follows normal distribution with mean and standard deviation of ~150̊, and ~ 50̊, respectively. From the obtained out-of-plane distribution of CNT, it can be seen that most them are inclined to the right with respect to the applied load/injection direction (i.e, θ is positive), which means the in-plane angle for most of the CNT is more than $\frac{\pi}{2}$. The distribution for CNT in-plane angle within PP as shown in Figure 5.6b supports this argument. As shown the in-plane angle for most of the CNT is $> \frac{\pi}{2}$.
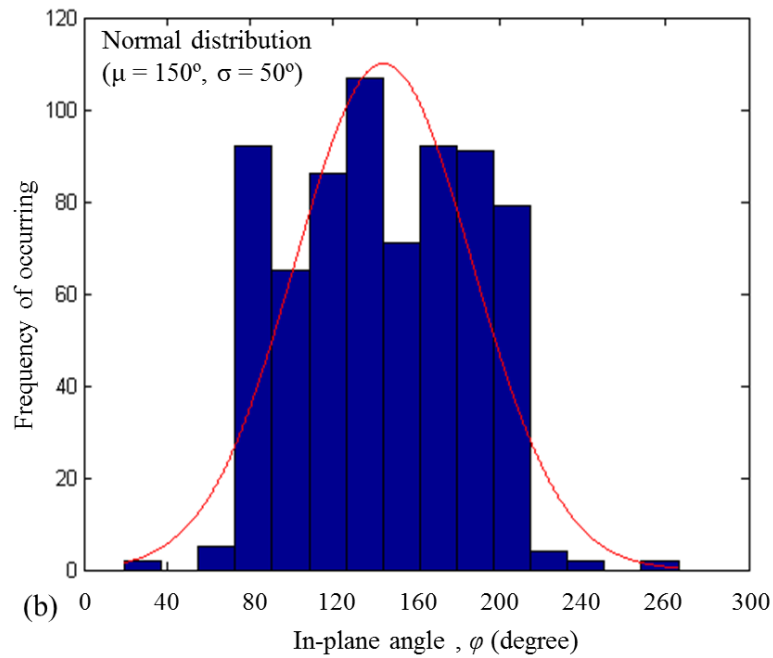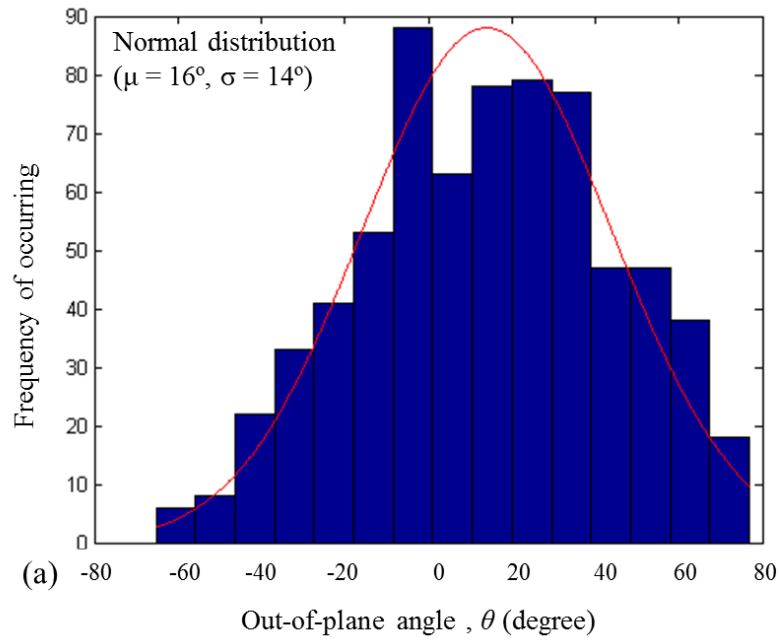
Figure 5.1 CNT orientation distribution within the PP matrix: (a) Out of plane distribution; and (b) in-plane angle orientation

The diameter distribution of CNT, both the histogram and the corresponding distribution curve, within the PP matrix is presented in Figure 5.2. As shown, CNT

diameter follows lognormal distribution with an average CNT diameter of ~ 50 nm, which is larger than the average CNT diameter, provided by the supplier, of ~25 nm. From the distribution obtained for CNT diameter, it can be seen that most of the CNT present within the PP matrix are in the form of agglomerates with diameters ranging from 40 nm to 180 nm due mainly to the strong van der Waals attractions among the CNT and their large aspect ratio.
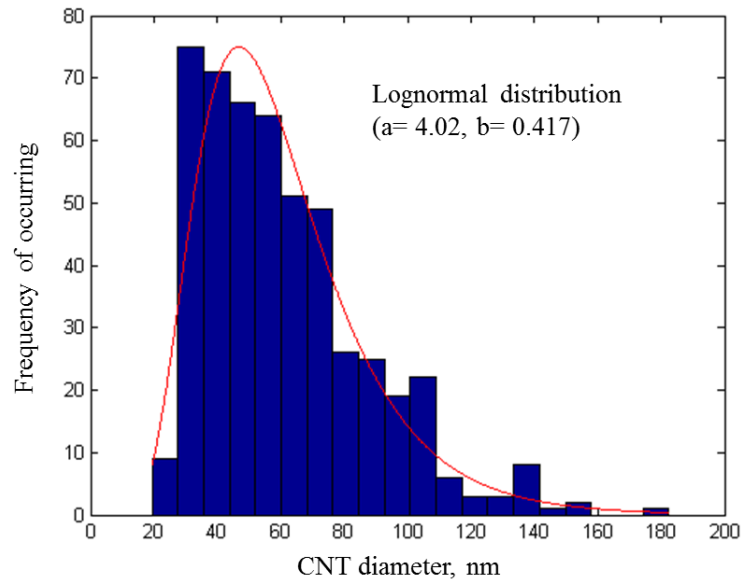
Figure 5.2 CNT diameter distribution obtained from the SEM images image analysis.

The spatial distribution of CNT within the polymer is described by two parameters, R (distance of the centroid (x_c, y_c) of CNT cross-section from the origin in nm) and α (angular position of the centroid of CNT cross-section with respect to the horizontal axis in degrees). As the centroid location for each CNT cross-section is known, the position of each CNT within the PP matrix can now be determined easily. The spatial distribution of CNT within the PP matrix in terms of their distance from the origin (0,0) of the specimen is shown in Figure 5.3a,whereas, the distribution for CNT angular position, with respect to the horizontal axis, is shown in Figure 5.3b. By observing the distribution for R and α, it can be seen that the spatial distribution of CNT

within the PP matrix is non-homogeneous. SEM observation of the fracture surfaces of CNT/PP composites also supports the CNT non-homogeneous distribution.

(a)

(b)
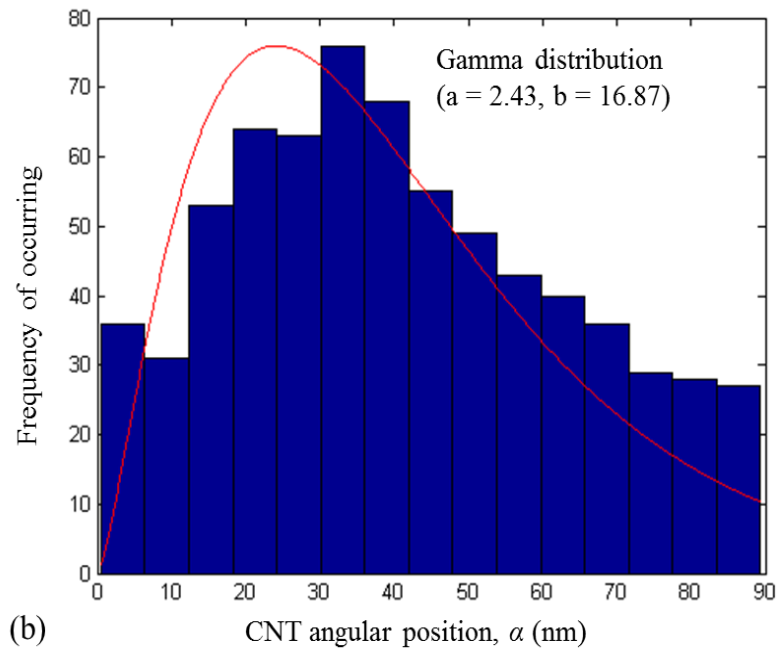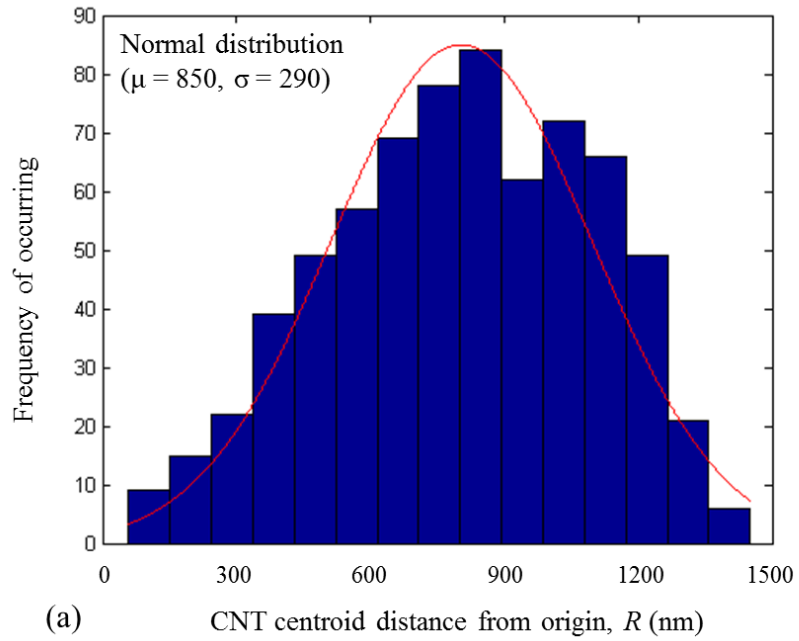
Figure 5.3 CNT Spatial distribution in PP extracted from the SEM images of 4 wt.% CNT/PP composites: (a) CNT spatial location; (b) CNT angular location in the x-y plane

Figure 5.4 shows the histogram along with the distribution curve (extreme value distribution, $\mu = 0.945$ and $\sigma = 0.0575$) for CNT waviness. The histogram presented in Figure 5.4 is obtained by analyzing a set of 15 SEM images. As shown, almost all the CNT present within the PP matrix show some kind of curvature along the length of the CNT.
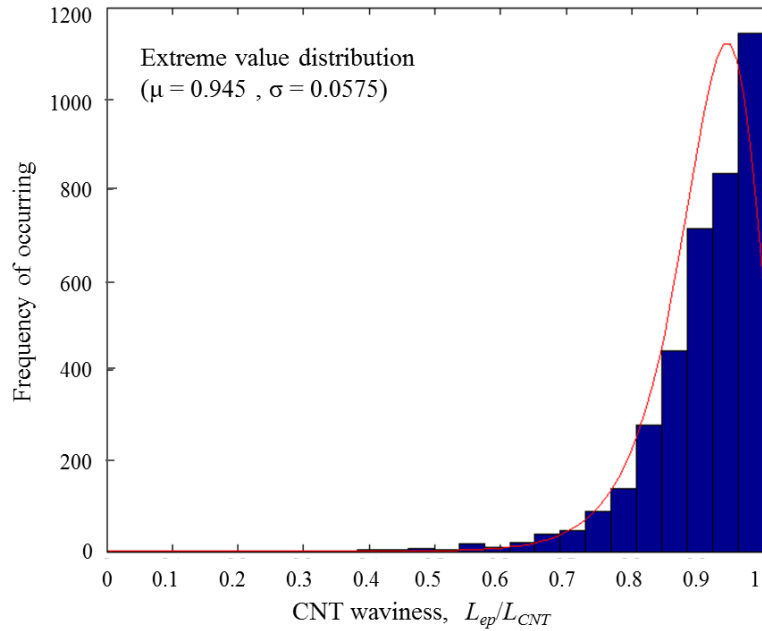
Figure 5.4 CNT waviness distribution obtained from the SEM image analysis.

5.1.2 SDBS-CNT/PP Composites

The CNT-PP interactions and consequently the dispersion of CNT within the polymer are altered by using SDBS surfactant. SEM study of the fracture surfaces of CNT/PP composites with as received and SDBS-treated CNT indicates that the size of the CNT agglomerate is greatly reduced and uniform dispersion is achieved upon addition of SDBS; this is mainly due to the reduction of interfacial tension between PP matrix and CNT (125, 126). The image analysis algorithm discussed above is also used without any modification for the case of SDBS-CNT/PP composites. Figure 5.5 shows the distribution of CNT diameter within the PP matrix as obtained from the SEM images

74

of 4 wt.% SDBS-CNT/PP composites. Similarly to the case of CNT/PP composites, the CNT diameter distribution follows lognormal distribution function but the mean CNT diameter is 30 nm for SDBS-CNT whereas it was 50 nm for as received CNT. Again, the distribution range of CNT diameter is also reduced. The maximum CNT diameter, the maximum size of the CNT agglomerate, present in the SDBS-CNT/PP composites is ~80 nm, which is much lower than the size of the agglomerates (~ 180 nm) obtained in the CNT/PP composites.
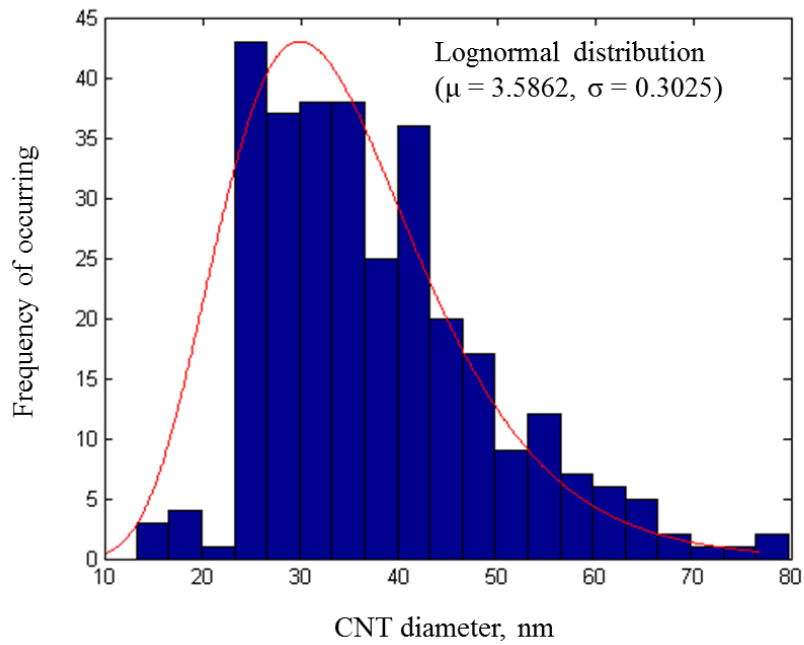
Figure 5.5 CNT diameter distribution obtained for SDBS-CNT/PP composites

The distribution functions for other CNT parameters such as CNT orientation, spatial distribution, and waviness within the PP matrix are also determined for SDBS treated CNT/PP composites. However, the distribution of these parameters within the PP matrix follows approximately the same trend as obtained for non-treated CNT/PP composites and therefore is not presented here. This is expected since no special effort has been undertaken to control the distribution of these CNT parameters within the PP matrix.

5.1.3 CNT/PP Fiber Composites

CNT characteristics such as their orientation and waviness are dictated by the processing conditions including for example the shear or elongational stress present during melt mixing, injection molding. To significantly alter the CNT orientation CNT/PP composite were made in fiber form by melt spinning. As the melt is stretched during the drawing step CNT and polymer chains are expected to stretch and align along the drawing direction. The distribution of CNT parameters within the CNT/PP fiber composites is also determined through image analysis, using images of fracture surface of 3 wt.% CNT/PP fiber composites. Figure 5.6 shows the CNT orientation $(\theta$ and $\varphi)$ distribution of in the CNT/PP fiber composites: As shown most CNT are oriented within $\pm 35°$ range with respect to the applied load/spinning direction. It is noted that this range is broad (from -40° to 70°) for CNT/PP bulk composites.
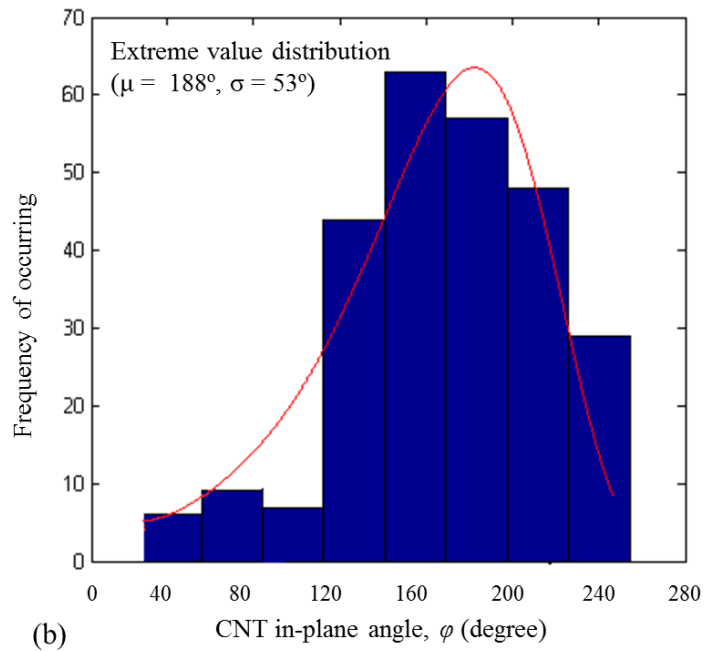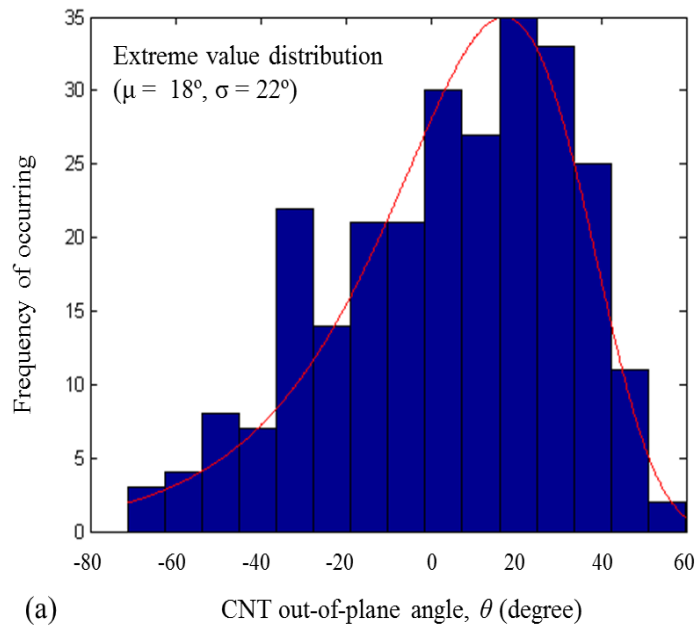
Figure 5.6 CNT orientation distribution in CNT/PP fiber composites: a) CNT out-of-plane angle distribution; b) CNT in-plane angle distribution

The diameter distribution function for CNT in CNT/PP fibers, presented in Figure 5.7, shows that the CNT diameter varies from 20 nm to 100 nm with a mean of ~ 30 nm which is very close to the diameter of a single CNT as provided by the supplier. Although

no surface treatment of CNT is performed, the size of the CNT agglomerates present in the CNT/PP fiber composites is much lower than the size of the agglomerates present in the CNT/PP bulk composites, which is the effect of processing. In the fiber spinning process, CNT are always under tension, which helps CNT alignment and dispersion. The alignment of CNT along the applied load direction, as well as small CNT diameter (better dispersion) results in CNT/PP fibers with tensile properties better than those of the CNT/PP bulk composites.
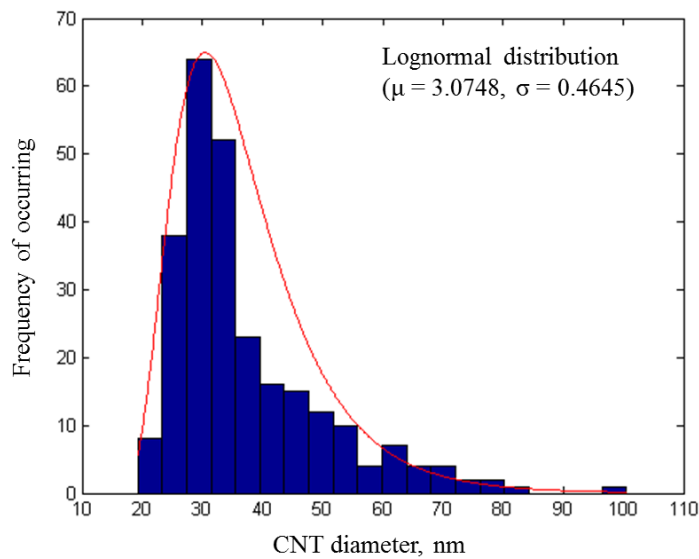
Figure 5.7 CNT diameter distribution in CNT/PP fiber composites

The CNT spatial distribution (R and α) within the fiber composites is presented in figure 5.8. As shown, both R and α follow normal distribution, and the CNT distribution within the PP matrix are almost homogeneous. Therefore it can be concluded that the distribution of CNT parameters in CNT/PP fiber composites is much closer to the ideal case compared to the CNT/PP bulk composites.
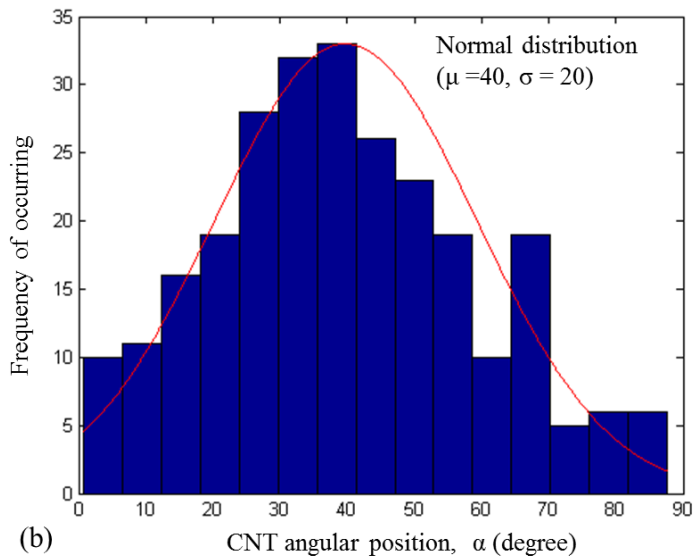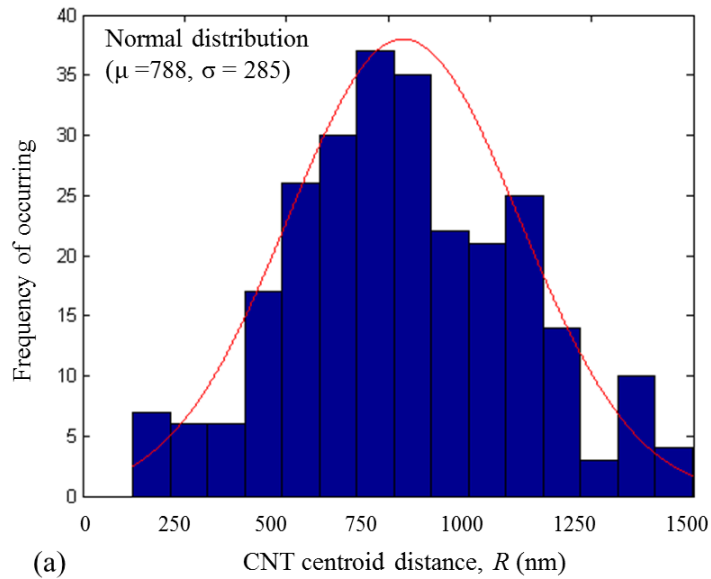
Figure 5.8 CNT spatial distribution in CNT/PP fiber composites: (a) CNT spatial location; (b) CNT angular location in the x-y plane

The distribution of CNT waviness within the PP matrix for CNT/PP fiber composites cannot be determined, since the number of CNT present within the SEM images captured from the surface of CNT/PP fiber composites are not enough to find a distribution. However, the SEM images confirmed the presence of wavy CNT in the CNT/PP fiber composites.

5.2 Finite Element Model Results

This section presents the effects of CNT parameters/characteristics, expressed in terms of the probability distribution functions determined in the previous section, on the tensile modulus of CNT/PP composites. Effect of CNT/PP interphase characteristics (thickness and modulus) is also studied. Finite element models accounting initially only for a single parameter at a time and then for all of them at the same time are generated and analyzed in order to explore potential synergistic effects and provide a design tool that can be used to predict the modulus range of PNC depending on the processing parameters and material characteristics. The details of the modeling of CNT/PP composites are presented in Chapter 4.

5.2.1. Effect of CNT Spatial Distribution on the Modulus of CNT/PP Bulk Composites

The effect of CNT spatial distribution within the PP matrix on the modulus of CNT/PP composites is presented in Figure 5.9 as a function of CNT content ranging from 0 to 5 wt.%. Spatial distribution of CNT within the PP matrix is modeled following the distribution functions for R and α obtained from the SEM image analysis (Figure 5.3). It is noted that the same distribution function is used for all CNT contents (0 to 5 wt.%). This is a conservative assumption that will lead to under-prediction of the modulus because the probability distribution function, estimated for 4 wt.% CNT/PP composites, that is employed in the FEM is expected to deviate more from the ideal case compare to the probability distribution function of composites with lower CNT content. Comparison of the experimentally obtained tensile modulus and the FEA results, considering the CNT homogeneous distribution (ideal case) and the non-homogeneous distribution (NHD) presented in Figure 5.9, indicate that at low CNT content the modeling predictions for both the homogeneous and non-homogeneous distribution cases agree well with the experimental data. This is because at low CNT content the dispersion of CNT within the

polymer is uniform (127) minimizing the effect of CNT non homogeneous distribution. As shown in Figure 5.9, the presence of CNT non homogeneous distribution results in reduction of composites modulus of more than 7% for composites with 4 wt.% CNT compared to the ideal case. This is because at higher CNT content, CNT non-homogeneous distribution leads to uneven stress transfer from the polymer to the CNT. From the results presented in Figure 5.9, two important conclusions can be made: i) the reduction in modulus due to the presence of CNT NHD, which is ~ 7%, is not really significant since it can be within the experimental error bar. This means distribution alone does not play an important role in determining the tensile modulus of PNCs; (ii) the modulus determined experimentally is much lower than the modulus predicted by FEA indicating that the modulus is more sensitive to the other CNT characteristics that are considered in the following.
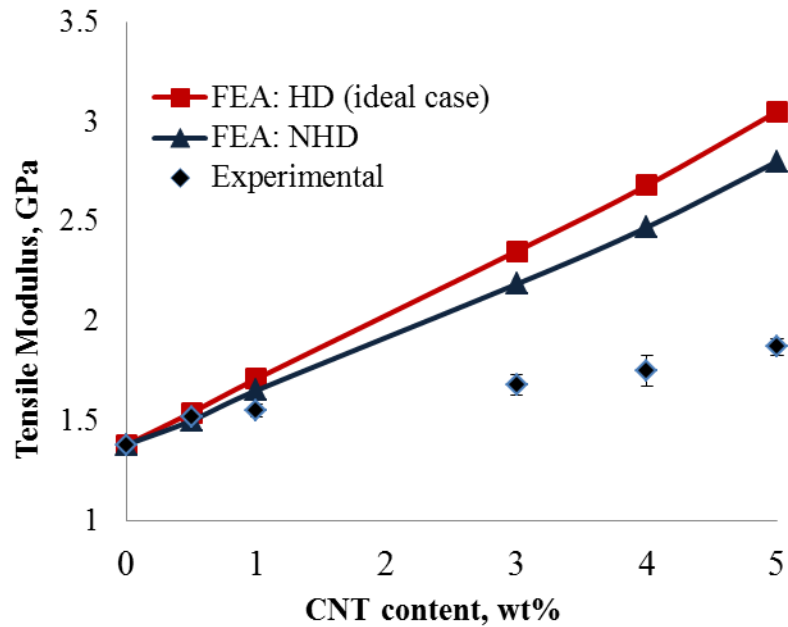
Figure 5.9 Effect of CNT spatial distribution on the tensile modulus of CNT/PP composites (HD: homogeneous distribution, ideal case: NHD: non-homogeneous distribution as determined by image analysis)

5.2.2 Effect of CNT Non-uniform Dispersion/agglomeration on the Modulus of CNT/PP Composites

FEA is performed to understand the effect of presence of CNT agglomerates (CNT non-uniform dispersion) within the PP matrix on the effective modulus of CNT/PP composites. Considering that the size of the CNT agglomerates is defined by their diameter, the probability distribution function for CNT diameter obtained from the SEM images of CNT/PP composites (Figure 5.2) is used to model the state of CNT dispersion within the PP matrix. The modulus of CNT (both individual and agglomerates) present within the RVE is calculated using equation 3.1(58) as shown below:

$$E_{eff} = \frac{r_f^2 - (r_f - t)^2}{r_f^2} * E_{CNT} \tag{3.1}$$

where, r_f (=d/2) is the radius of the CNT, which varies according to the distribution curve for CNT diameter, t (=~0.34) is the thickness of CNT outer layer and E_{CNT} (=1250 GPa) is the average modulus of the CNT as provided by the supplier.

The effect of CNT non-uniform dispersion (NUD) on the tensile modulus of CNT/PP composites is presented in Figure 5.10. FEA results considering uniform dispersion of CNT (individual CNT with diameter ~ 25 nm, which is the average diameter as provided by the supplier) within the PP, referred to as ideal case in Figure 5.10, is also presented to quantify the effect of CNT non-uniform dispersion on the composites tensile modulus. It is noted that the FEA analysis is performed only for 4 wt.% CNT/PP composites since it is expected that higher CNT contents will exhibit the largest extent of CNT agglomeration and therefore the effect on the composites effective modulus will be stronger. Although 5 wt.% is the highest CNT content used in the experiment it is observed that the tensile modulus reached a plateau value at 4 wt.% of CNT.
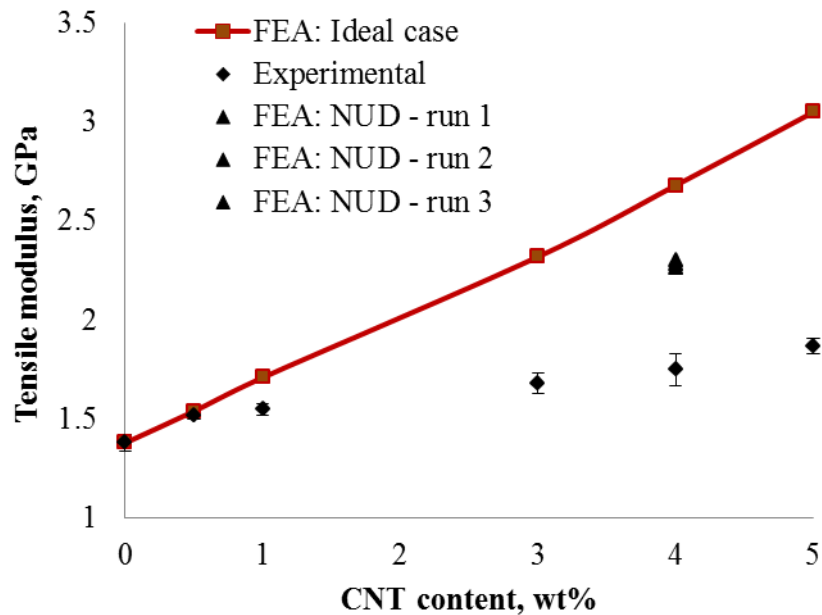
Figure 5.10 FEA prediction of the tensile modulus of CNT/PP composites: effect of CNT non-uniform dispersion (NUD: non-uniform dispersion)

As expected, CNT agglomerates significantly reduce the modulus of the CNT/PP composites and the reduction is around 15% compared to the ideal case. This is because agglomerates have significantly lower modulus than individual CNT (118) and their presence drastically reduces the reinforcing efficiency of CNT and thus the modulus of the composite. Slippage of CNT within the CNT agglomerates along with the reduced aspect ratio of the agglomerates compared to that of individual CNT is responsible for the lower modulus of the agglomerates. Since the FEM models generated are using the distribution function, FEA predictions are expected to vary. Therefore, FEA simulations are performed for three models generated using the same distribution function to verify that the FEA predictions are reliable. As shown in Figure 5.10, FEA predictions are approximately same (with a standard deviation of 0.2) for all three of the models generated

5.2.3 Effect of CNT Orientation on the Modulus of CNT/PP Composites

The FEA models presented so far are based on the assumption that all the CNT are aligned along the applied load direction. However, the elastic property of CNT/polymer composites is determined largely by the orientation of CNT within the polymer matrix. Random orientation of CNT within the RVE is modeled automatically using the distribution function for CNT orientation (θ and φ) as obtained from the SEM image analysis (Figure 5.1). Figure 5.11 shows the FEA predictions for tensile modulus of 4 wt.% CNT/PP composites with CNT oriented randomly. FEA prediction for ideal case (where all CNT are aligned along the applied load direction) is also presented for the same composite system for comparison. As expected when CNT are randomly oriented with respect to the applied load direction the modulus of the composites is reduced because of the reduced effective length of CNT along the applied load direction. It is noted that when all CNT are randomly oriented with respect to the applied load direction the reduction in modulus is more than 6%. However this is not significant since it can be within the experimental error bar. So, it is the combined effect of all the parameters that results in composites with lower modulus. As explained before, FEA simulation is performed three times to verify the consistency of the FEA predictions.
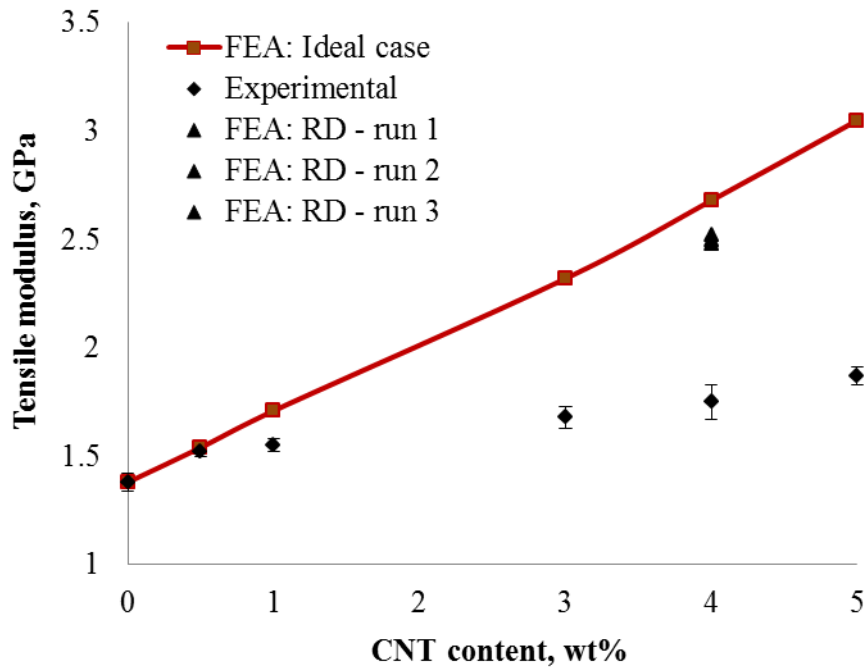
Figure 5.11 FEA predictions for tensile modulus of CNT/PP composites: effect of CNT orientation (RD: random distribution of CNT within the PP)

5.2.4 Effect of CNT Waviness on the Modulus of CNT/PP Composites

Another parameter that affects the reinforcing efficiency of CNT is their waviness. The presence of wavy CNT within the PP matrix is confirmed by SEM and AFM observations. The effect of presence of wavy CNT within the PP matrix as compared to the ideal case (all CNT are straight) is presented in Figure 5.12. CNT waviness distribution function obtained from SEM image analysis (Figure 5.4) is used to model the CNT waviness within the RVE. As shown in Figure 5.12, presence of CNT waviness results in a reduction of the composite modulus by approximately ~ 8%. This is because CNT waviness reduces the effective length of the CNT along the applied load direction; this in effect reduces the reinforcing efficiency of CNT.
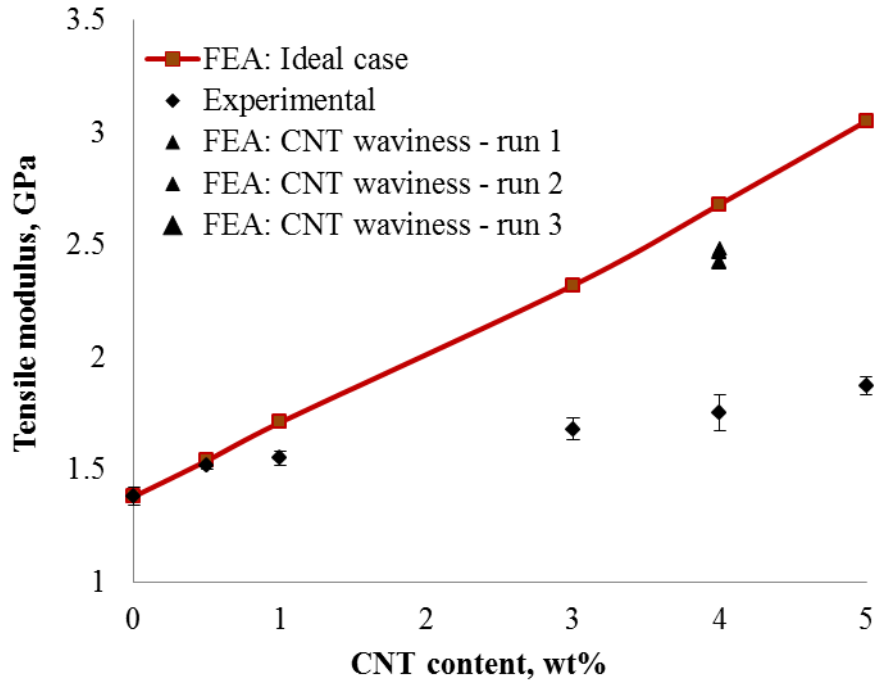
Figure 5.12 FEA predictions for tensile modulus of CNT/PP composites: effect of CNT waviness

5.2.5 Effect of CNT/PP Interphase on the Modulus of CNT/PP Composites

5.2.5.1 Defining the modulus variation across the interphase

The interphase is introduced in the RVE by replacing an equivalent volume of polymer matrix, while maintaining the CNT volume. The width of the interphase used is in average ~ 20 nm as determined by AFM. AFM and SEM observations support the presence of soft CNT/PP interphase (i.e. interphase modulus is less than that of the polymer); however, the true value of the interphase modulus cannot be calculated. Therefore, the interphase modulus is defined by the property gradient profile across the CNT/PP interphase as obtained from the AFM phase lag image. From the phase lag gradient profile it can be seen that the stiffness, and thus the modulus of the interphase (E_{int}), is a function of r, where r varies along the thickness t, of the interphase. And it can be described by the following 4th-order polynomial equation:

$E_{int} = Ar^4 - Br^3 + Cr^2 - Dr + E_{CNT}$, where A, B, C & D are constants

(5.1)

at $r = 0$ *(*$t = 0$*)*; $E_{int} = E_{CNT}$ (modulus of CNT), and

at $r = t$; $E_{int} = E_{PP}$ *(modulus of PP matrix)*

The values of the constants used in this study are: A = 0.0005; B = -0. 0247; C = 0.4928; and D = -4.0909 obtained by drawing a trend line, with a R^2 value of 0.9937, that matched the property gradient profile obtained from AFM phase images. A schematic showing the interphase thickness in between CNT and PP matrix and the direction of *r* used in equation 5.1 is presented in Figure 5.13.
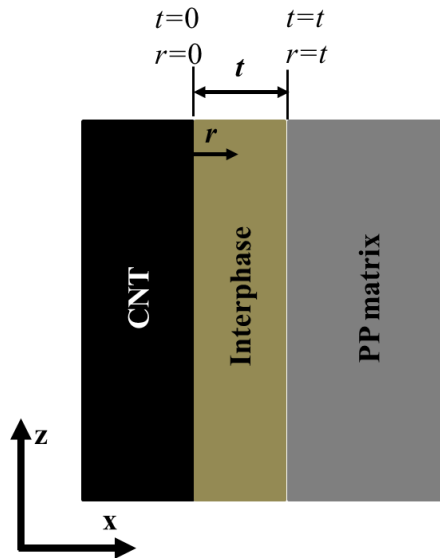
Figure 5.13 Definition of *r* and its' direction across the thickness, *t* of CNT/PP interphase

In order to define the interphase modulus, the interphase volume is first divided into twenty divisions along the radial direction. A FEA parametric study is performed to find the number of interphase thickness divisions that gives convergent results, and the distance *r,* of the centroid of all the elements from the surface of the CNT, is calculated. The final optimum mesh at the interphase region that provided converged results is also shown in Figure 5.14.
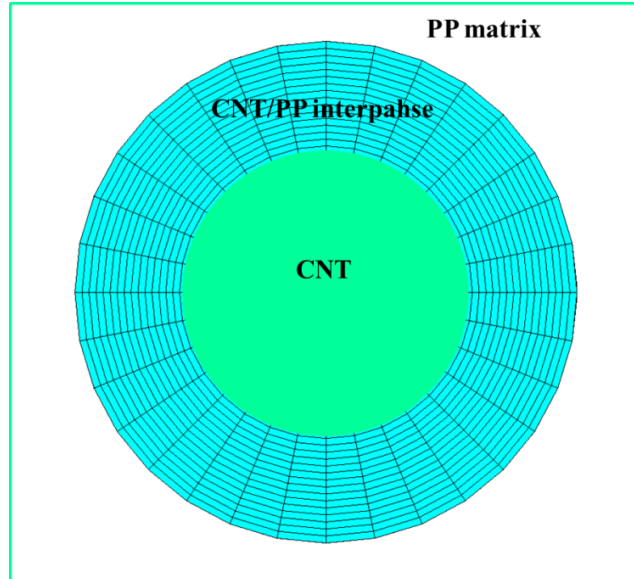
Figure 5.14 CNT/PP interphase with the modeled optimum mesh.

5.2.5.2 Why 4th order polynomial equation is used instead of linear equation to define interphase modulus?

The goal of this section is to check whether it is required to use a 4th order polynomial equation to define the variation of interphase modulus across the interphase or whether using a linear equation is sufficient. Figure 5.15 presented below shows the effect of interphase modulus on the tensile modulus of 5 wt.% CNT/PP composites, where four different cases are considered to define the interphase modulus: (i) ideal case (no interphase); (ii) Interphase modulus lower than PP (soft interphase); (iii) interphase modulus varies linearly (hard interphase); and (iv) interphase modulus varies exponentially.

Tensile modulus of 5 wt% CNT/PP composites, effect of interphase			
Ideal Case (no interphase)	Interphase modulus lower than PP (soft interphase)	Interphase modulus varies linearly (hard interphase)	Interphase modulus varies exponentially
3.27 GPa	3.10 GPa	4.50 GPa	2.91 GPa
compared to ideal case	5% reduction	38% improvement	11% reduction

Figure 5.15 Effect of interphase modulus on the tensile modulus of 5 wt.% CNT/PP composites

From the results presented it can be seen that when linear variation of the interphase modulus (column 4) is considered in the model the predicted modulus is even higher (38% higher) than the modulus obtained for the ideal case (column 2). This is because when linear variation of the modulus is considered across the interphase, the interphase is considered hard (modulus higher than that of matrix).

On the other hand, when exponential variation of the interphase modulus, as obtained from AFM experiments, is considered in the model a reduction in tensile modulus of 11% compared to the ideal case prediction is observed. This supports the experimental trends. Therefore, it is important to use a higher order polynomial equation to represent the modulus variation across the interphase, since use of the linear equation over-predicts the tensile modulus of the composites. Although, 2nd and 3rd order polynomial equations are also available, 4th order polynomial equation is used in this study since it gives the exact representation of the property gradient profile across the CNT/PP interphase as obtained from the AFM phase image.

5.2.5.3 Effect of interphase on the tensile modulus of CNT/PP composites

Figure 5.16 shows the effect of interphase on the tensile modulus of CNT/PP composites as a function of CNT content. The same interphase thickness and modulus is used in the FEA for all the CNT contents used, since the width of interphase is independent of the CNT nanomaterials content, as confirmed by AFM experiments (see Chapter 3). As shown, at low CNT content, the interphase has no significant effect on the tensile modulus of CNT/PP composites; however, the effect is more pronounced as the CNT content increases. The trend is expected because the amount of interphase, and thus its effect on the modulus, increases with CNT content. A reduction in tensile modulus of more than 11% is observed for the case of 5 wt.% CNT/PP composites when the interphase is considered in the FEA.
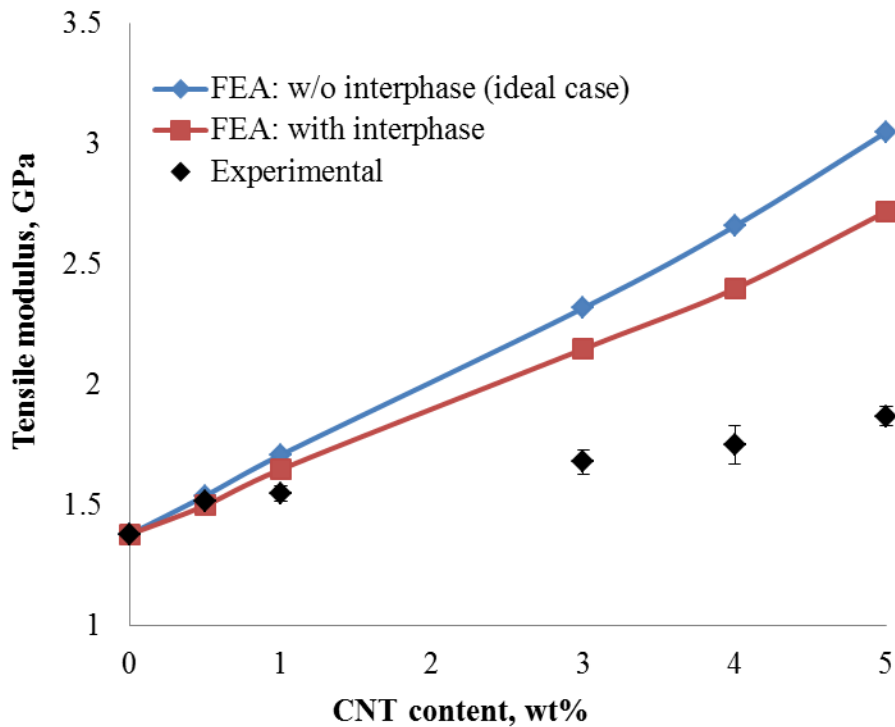
Figure 5.16 FEA predictions of the tensile modulus of CNT/PP composites: effect of CNT/PP interphase

5.2.6 Synergistic Effect of CNT Characteristics on the Tensile Modulus of CNT/PP Composites

The effect of each CNT parameter including dispersion, distribution, waviness and interphase on the modulus of the CNT/PP composites was determined using FEA by introducing the corresponding probability distribution function into the FEM. It was found that the effect of each parameter alone cannot justify the big difference between the theoretically expected and the experimentally determined values of the modulus. Therefore, an FEA study, considering all the parameters together into the finite element modeling is performed. This section presents the FEA predictions for tensile modulus of 4 wt.% CNT/PP composites where the distribution functions for all the CNT parameters obtained from the SEM image analysis (Figure 5.1, 5.2, 5.3 and 5.4) are incorporated into the model. A representative 3D RVE used in the FEA is shown in Figure 5.17.

3D view

Right end view
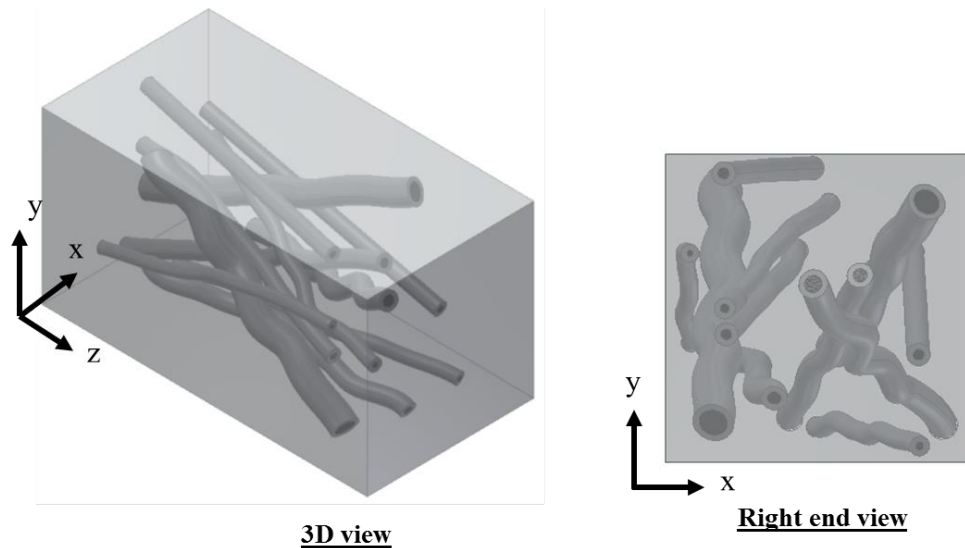
Figure 5.17 3D RVE for 4 wt.% CNT/PP composite using the distribution functions for CNT dispersion, distribution and waviness obtained from the SEM image analysis. Phases in the RVE (CNT: dark, interphase: dark gray and matrix: light gray)

While generating the RVE, every time the weight fraction (or volume fraction) of CNT within the RVE is also calculated, based on the geometric dimensions (length, l and diameter, d) of CNT and RVE, as shown below. This is done to confirm that the RVE

contains the exact amount of CNT. For example, the RVE presented in Figure 5.17 contains 11 CNTs. The length of each CNT is 1500 nm, and the diameters of the CNTs are presented in the Table 5.1.

Table 5.1: Diameter of CNTs within the RVE presented in Figure 5.17

CNT no	1	2	3	4	5	6	7	8	9	10	11
Diameter, *d*	23	30	32	39	40	41	49	49	61	93	102

Total volume of CNTs $= (\pi/4) * (d_1^2 + d_2^2 + d_3^2 + d_4^2 + d_5^2 + d_6^2 + d_7^2 + d_8^2 + d_9^2 + d_{10}^2 + d_{11}^2) * l = 41034305 \text{ nm}^3$

Volume of RVE (or, volume of PP) $= 2260125000 \text{ nm}^3$

Volume fraction of CNT = (Total volume of CNT/ volume of RVE) = 0.0181 or 1.81%, which is equivalent to 4 wt.% of CNT in PP matrix.

The FEA predictions for tensile modulus of 4 wt.% CNT /PP composites are presented in Figure 5.17. The modulus obtained considering a unit cell (single CNT RVE) model (118) and multi-CNT RVE models, where the distribution of CNT orientation, dispersion, spatial distribution and waviness within the RVE are considered random (128) are also presented for comparison. The simulations are repeated six times for multi-CNT RVE models with random distribution of CNT various parameters (128) and for models considering the distribution functions of CNT parameters obtained from image analysis. The modulus of 4 wt.% CNT/PP composites obtained experimentally is also presented as a horizontal dotted line in Figure 5.18 for comparison. The corresponding modulus values and standard deviation are also presented in Table 5.2.
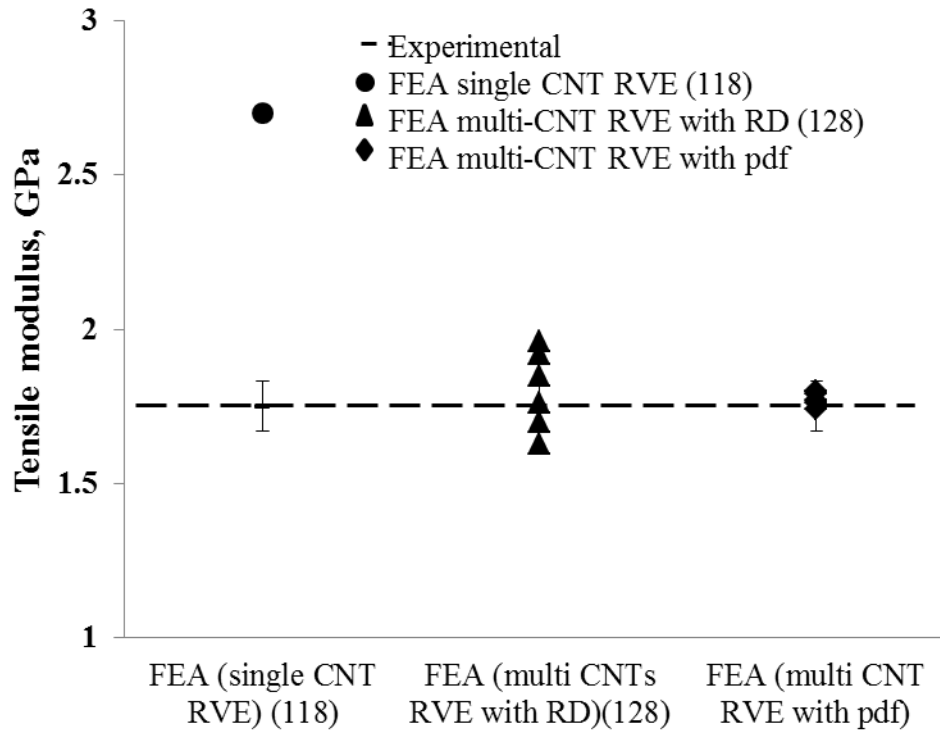
Figure 5.18 FEA predictions for tensile modulus of 4 wt.% CNT/PP composites: validation of the proposed modeling technique. (RD: random distribution; and pdf: statistical distribution of CNT orientation, diameter, spatial distribution and waviness in PP as determined by image analysis)

As shown in Figure 5.18 and Table 5.2, when single CNT RVE is considered, the FEA prediction is much higher than the modulus obtained experimentally. This is expected since no CNT parameters are incorporated in these models. However, when the CNT parameters are included in the FEA, using a random approach and a pdf approach (statistical distribution of CNT parameters obtained from SEM image analysis), the predicted modulus varies for each FEA simulation. As can be seen, when a random distribution of CNT parameters is considered, FEA predictions show large variation (shown as triangles in Figure 5.18) with a standard deviation of 0.13 (see Table 5.2, column 3). When the distribution of CNT parameters obtained from SEM image analysis is considered, the FEA predictions show less variation (shown as diamonds in Figure 5.18) with a standard deviation of 0.024 (see Table 5.2, column 4). The FEA predictions

obtained from the present approach also falls within the range of the experimental error bar as shown in Figure 5.18. Therefore, it can be concluded that the proposed integrated images analysis and FEA supported by experiments can be successfully applied to extract the information on CNT orientation, agglomeration, spatial distribution and waviness of CNTs to model the composites. The strong dependence of the composite's modulus on the distribution of these parameters justifies the need of an integrated approach to accurately determine and to model these parameters in order to develop CNT-based composites with engineered properties.

Table 5.2: Tensile modulus of 4 wt.% CNT/PP composites: Experimental vs. FEA predictions

Tensile modulus of 4 wt.% CNT/PP composites, GPa			
Experimental	FEA (single CNT RVE) (118)	FEA (multi CNT RVE with RD) (128)	FEA (multi CNT RVE with pdf)
1.67		1.85 (run 1)	1.77 (run 1)
1.68	2.7	1.96 (run 2)	1.79 (run 2)
1.82		1.92 (run 3)	1.74 (run 3)
1.74		1.76 (run 4)	1.8 (run 4)
1.83		1.63 (run 5)	1.8 (run 5)
		1.70 (run 6)	1.76 (run 6)
Average ± Stdev	1.75 ± 0.08	2.7 ± 0	1.8 ± 0.13	1.77 ± 0.024

5.2.7 Ability of FEM to Distinguish Between Two Different Dispersion and Orientation States

As mentioned earlier, SDBS is used in this study to alter/improve the dispersion of CNT within the PP matrix. As shown by the corresponding SEM images the use of SDBS improves the dispersion of CNT within the PP matrix and this improvement is quantified through image analysis (see section 5.1.2). The goal of this section is to

demonstrate the ability of the FEM to capture the changes in the CNT dispersion state within the PP matrix. SDBS- CNT/PP composites are modeled using the corresponding probability distribution function for the CNT diameter. All other parameters are held constant as in the case of the CNT/PP composites, since it is found based on the SEM image analysis that the probability distribution functions of the other CNT parameters do not change significantly due to the addition of SDBS. The interphase characteristics (thickness and modulus) are also kept constant. A representative 3D RVE for 4 wt.% SDBS treated CNT/PP composite is presented in Figure 5.18 with new distribution for CNT diameter (Figure 5.5).

As shown in Figure 5.19, the number of CNT within the RVE for the same CNT content increases when the new distribution function for the CNT diameter (see Figure 5.17 for comparison) is used. This is expected since the distribution range of CNT diameter for SDBS modified CNT/PP composites is narrow (~20 nm to 80 nm, see Figure 5.14) compared to the distribution range obtained from non-modified CNT/PP composites (~20 nm to 180 nm, see Figure 5.7) and therefore, for the same CNT content and RVE size, more CNT are required for SDBS-CNT/PP composites to fulfill the CNT wt.% requirements. Visual observation of the RVE also supports the presence of CNT with smaller diameter in the case of the SDBS-CNT/PP composites compared to the CNT diameter of the CNT/PP composite case (Figure 5.217). Therefore, it can be concluded that the model could capture the change of CNT dispersion within the PP matrix. Figure 5.20 shows the FEA predictions for 4wt.% SDBS-CNT/PP composites. As in the case of CNT/PP composites, the simulations are repeated six times and the experimentally determined modulus is also presented for comparison. As shown, FEA predictions are in good agreement with the experimental data.

3D view

Right end view
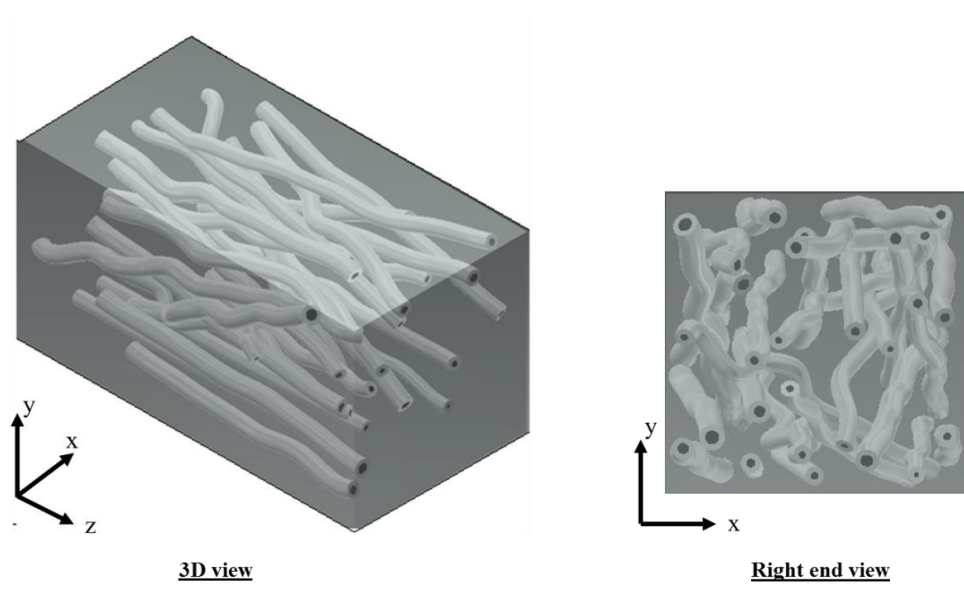
Figure 5.19 3D RVE for 4 wt.% SDBS-CNT/PP composite using the distribution function for CNT parameters as obtained from the SEM image analysis. (CNT: dark, interphase: light gray and matrix: dark gray)
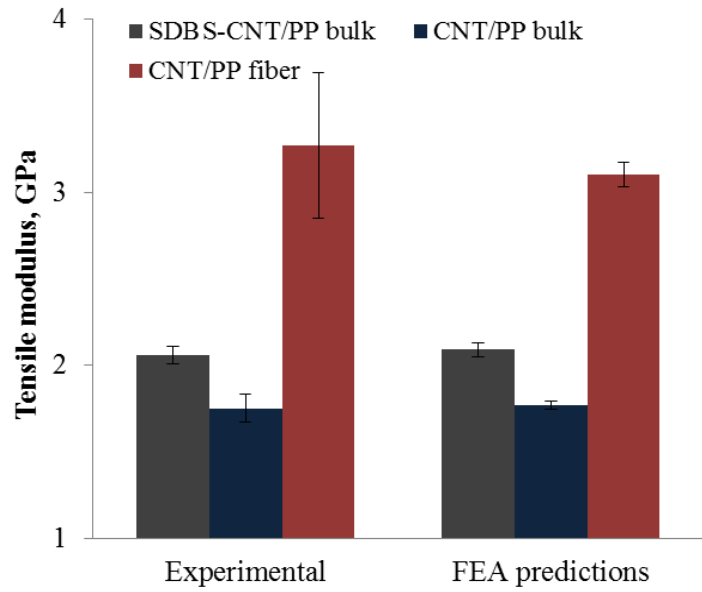
Figure 5.20 FEA predictions for tensile modulus of CNT/PP bulk composites (both modified and non-modified CNT) and CNT/PP fiber composites.

The ability of the FEM to capture the difference in CNT alignment is verified by modeling CNT/PP fiber composites and accounting for the probability distribution function of CNT distribution/alignment within the fibers, as estimated using image

analysis. It was not possible to determine the probability distribution function of the CNT waviness in the CNT/PP fiber composites, so the waviness is modeled using a random distribution. The same RVE geometry and loading and boundary conditions, with those used in the CNT/PP bulk composites, are used in the FEA. Defining the material properties for all the phases is also done following the same method used for CNT/PP bulk composites. The FEA results and a comparison with the experimentally determined modulus of 3 wt.% CNT/PP fiber composites are presented in Figure 5.20. Like CNT/PP bulk composites, FEA simulations for CNT/PP fiber composites are also repeated six times, where all the RVEs are generated for the same CNT content and the same distribution functions for CNT parameters. The variations in FEA predictions are also presented in Figure 5.20 using error bars. As shown, although the modulus predicted by the FEA is within the experimental deviation, the model under-predicts the tensile modulus of CNT/PP fiber composites for CNT content of 3 wt.%. One thing that might contribute to this is the random distribution assumption for CNT waviness. In addition, modeling of the interphase, which is modeled based on the observation made for bulk composites, could be another factor that results to FEA predictions.

5.2.8 Ability of the proposed model to predict the tensile modulus for different CNT loading other than 4 wt.%

The ability of the proposed model to predict the tensile modulus for different CNT loading other than 4 wt.% is also investigated. In order for that, 3D RVE for 3 wt.% CNT/PP composite is generated, as shown in Figure 5.21, using the same distribution functions for CNT parameters as obtained from the SEM images captured from the polished and etched surfaces of 4 wt.% CNT/PP composites.
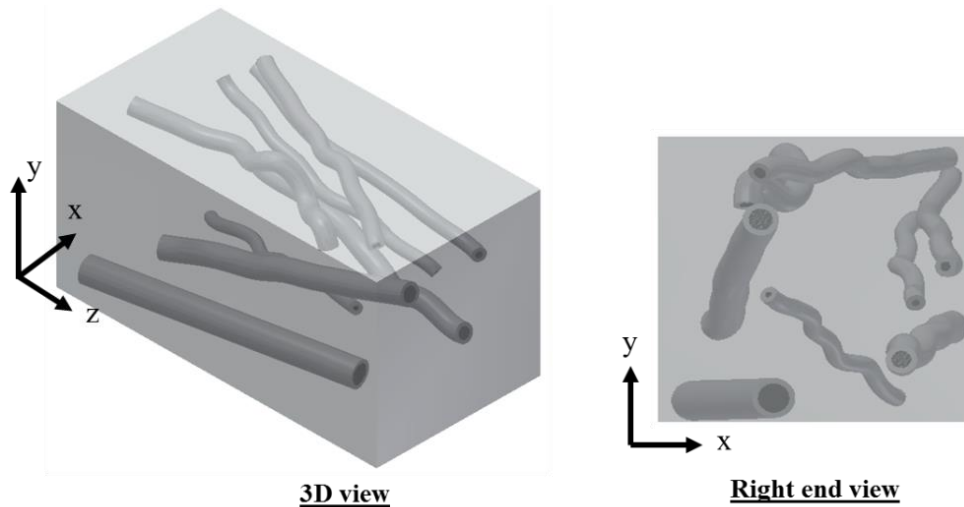
Figure 5.21 3D RVE for 3 wt.% CNT/PP composite using the distribution function for CNT parameters as obtained from the SEM images of 4 wt.% CNT/PP composites. (CNT: dark, interphase: dark gray and matrix: light gray)

Tensile modulus of 3 wt.% CNT/PP composites as obtained from FEA is presented in Table 5.3. Tensile Modulus predicted from FEA considering ideal case and from experiments is also presented for comparison. As expected, the model slightly under-predicts the tensile modulus of the composites when CNT parameters are considered. Since the distribution of CNT parameters used in generating the model is obtained from SEM images captured from 4 wt.% CNT/PP composites, these distributions represent the worst case scenario for 3 wt.% CNT/PP composites and the model provides the lower limit of the modulus.

Table 5.3: FEA predictions of tensile modulus of 3 wt.% CNT/PP composites

Tensile modulus of 3 wt.% CNT/PP composites, GPa		
Experiment	FEA: Ideal case	FEA: with pdf of CNT parameters
1.68 ± 0.05	2.32	1.58 ± 0.04

*pdf: probability distribution functions of CNT parameters as obtained from image analysis

5.3 Conclusions

The elastic properties of CNT/PP composites, for given CNT type; grade and content, are particularly sensitive to various parameters, such as CNT/polymer interfacial interactions, which dictate the CNT orientation, dispersion, distribution, and waviness. An image analysis technique, based on MATLAB® and 3D info extracted from SEM images, was employed to determine the probability distribution function of these CNT characteristics. In this study, the image analysis technique coupled with FEA, presented in details, is able to predict the effective tensile modulus of CNT/PP composites and to determine the effect of each of the parameters considered on the tensile modulus of the composites. In summary, the probability distribution function for CNT orientation within PP, obtained from the SEM images, indicates that most of the CNT make an angle of ~20˚ with the applied load direction. This is expected for the CNT/PP composite presented in this work, as the injection pressure forces the CNT to align along the injection/applied load direction. The CNT diameter distribution function for CNT/PP composites shows the presence of CNT agglomerates of size varying from ~40 nm to 180 nm. Although the use of SDBS improved the dispersion (size of CNT agglomerates obtained ranges from ~40 nm to 80 nm), uniform dispersion could not be achieved. A realistic spatial distribution (non-homogeneous) of the CNT within the PP matrix is modeled for FEA by using the spatial distribution function (parameters R and α) obtained from the SEM images. Finally from the distribution function of CNT waviness, it can be observed that all CNT exhibit a high degree of waviness. It is noted that for measuring CNT waviness, in this study we have used the length of the CNT in the 2D SEM images assuming that the rest of the CNT below the imaged surface follow the same waviness distribution. Study of the AFM phase images shows that the interphase modulus across the width of the interphase is not constant; instead it varies exponentially, with the higher modulus being at the nanomaterials side and the lowest modulus being at the polymer side. Therefore, an equation is defined that represents the property gradient profile across

the interphase as observed in the AFM phase lag images and used in the FEA to find the interphase material property.

3D FE models accounting for the CNT/PP interphase and the probability distribution functions for CNT orientation, diameter, spatial distribution and waviness are generated for CNT/PP composites (bulk and fiber) and are analyzed for their tensile modulus. A good agreement between the model predictions and the experimental data for the same composite system is observed. Therefore, it can be concluded that the random orientation and distribution of wavy CNT within the polymers as well as presence of CNT agglomerates within the polymer and voids at the CNT/PP contact area are the main factors that reduce the reinforcing efficiency of the CNT when they are added to the polymers. It is noted that an error in the SEM image analysis is introduced by defining the distribution curves that describe the histograms. The range of FEA predictions is narrow when distribution functions for the CNT parameters are used in the FE models instead of average value for these parameters.

The integrated approach of image analysis coupled with FEA and supported by experimental characterization can account for all the CNT characteristics at the nano- and micro-scale, which can be altered by tuning the processing conditions, and that it provides a tool for the design and development of CNT based polymer composites with engineered properties for targeted applications.

CHAPTER 6

EFFECT OF GEOMETRY OF NANOMATERIALS ON THE TENSILE MODULUS OF PP BASED NANOCOMPOSITES

This chapter presents a comparative study to understand the effect of nanomaterials geometry and modulus on the tensile modulus of carbon reinforced PNCs. The purpose of this study is to compare both experimentally and computationally through finite element analysis (FEA) the reinforcing efficiency of two different types of nanomaterials that have similar surface chemistries but different geometries. The nanomaterials are CNT which are tubes of diameter ~ 20 to 30 nm and length ~10 µm and xGnP which are platelets ~ 10-15 nm thick with a diameter of ~ 1 µm). Only three important parameters, the nanomaterials' geometries, their orientation and the nanomaterial/polymer interphase, are considered in the analysis. The modulus of CNT considered for the analysis is 70 GPa, which is calculated using equation 4.3 (see Chapter 4), and it is assumed that xGnP has also a modulus of 70 GPa considering the two materials have the same chemistry and thus similar properties.

6.1 Effect of Nanomaterials Geometry and Orientation

In order to study the reinforcing efficiency of CNT and xGnP in polymer, 3D RVE of CNT- and xGnP-reinforced PP composites are generated first. FEA is then performed to evaluate the modulus enhancement of the PNCs due to the addition of nanomaterials. As mentioned before in Chapter 4, in this study, CNT is considered as a solid cylinder with diameter, d_{CNT} and length, l_{CNT}, whereas xGnP is considered as a round disk with a thickness of t_{xGnP} and diameter of d_{xGnP}. The geometries of both the CNT and the xGnP used in the analysis are presented in Figure 6.1. More detailed

information about the geometry and properties of all the phases used in the FEA is presented in chapter 4.
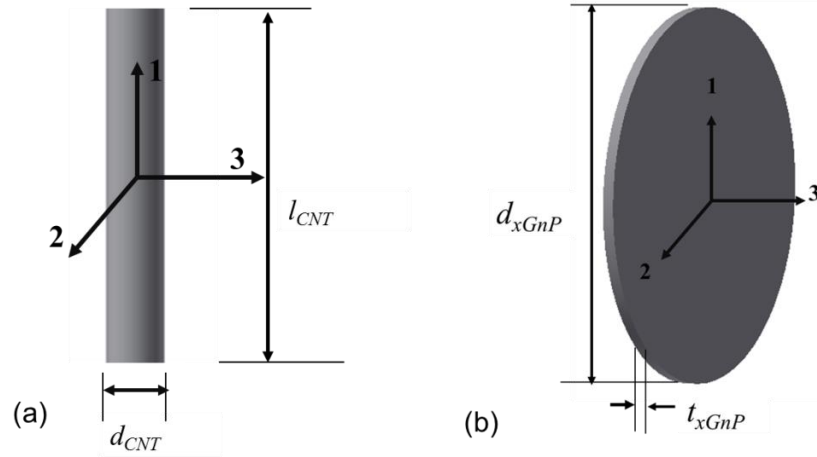
Figure 6.1 Schematic of (a) CNT and (b) xGnP used in this study to model CNT/PP and xGnP/PP composites

6.1.1 Effect of Nanomaterials Geometry on the Composites' Tensile Modulus

The RVEs used in the FEA consist of two phases only i.e., nanomaterials (CNT or xGnP) and PP. It is assumed that the nanomaterials are dispersed uniformly and aligned along the applied load direction. Figure 6.2 shows the representative RVEs used in the FEA for CNT/PP and xGnP/PP composites.
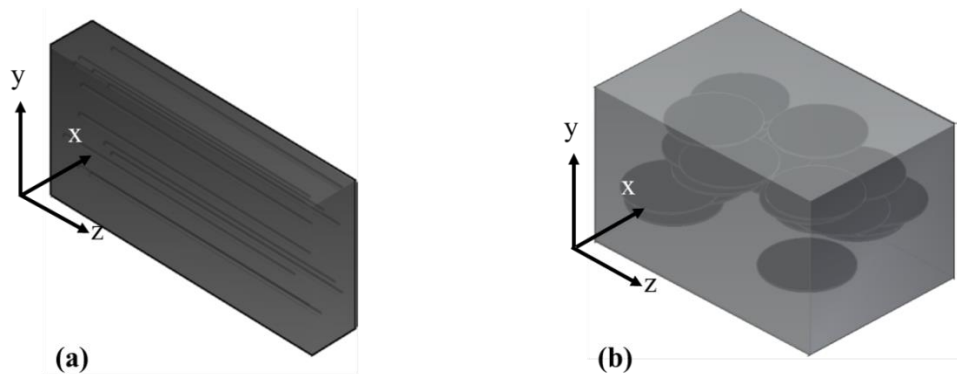
Figure 6.2 RVEs with (a) CNT and (b) xGnP aligned along the applied load direction

The tensile modulus of CNT/PP and xGnP/PP composites as determined by the FEA and experimentally for nanomaterial content of 0-5 wt.% is presented in Figure 6.3. As shown, the composites' modulus increases with the increase of the nanomaterials content for both cases. However, for constant wt.% of nanomaterials, the modulus increase is higher for CNT/PP composites compared to xGnP/PP composites. Tensile modulus of CNT/PP and xGnP/PP composites obtained from experiment is also presented in Figure 6.3. Experimental results also show improvement in tensile modulus with the increase of nanomaterials content, therefore supporting FEA predictions, although the modulus improvement is much lower than that obtained by the FEA. This is expected since there are other factors in addition to the geometry such as agglomeration, orientation, waviness/buckling etc. that affects the tensile modulus of the composites during tensile experiments. The difference in modulus improvement for the two composite systems, for a constant wt.% of nanomaterials, is also insignificant, which means that with the presence of all the nanmaterials parameters the reinforcing efficiency of CNT and xGNP is approximately same.
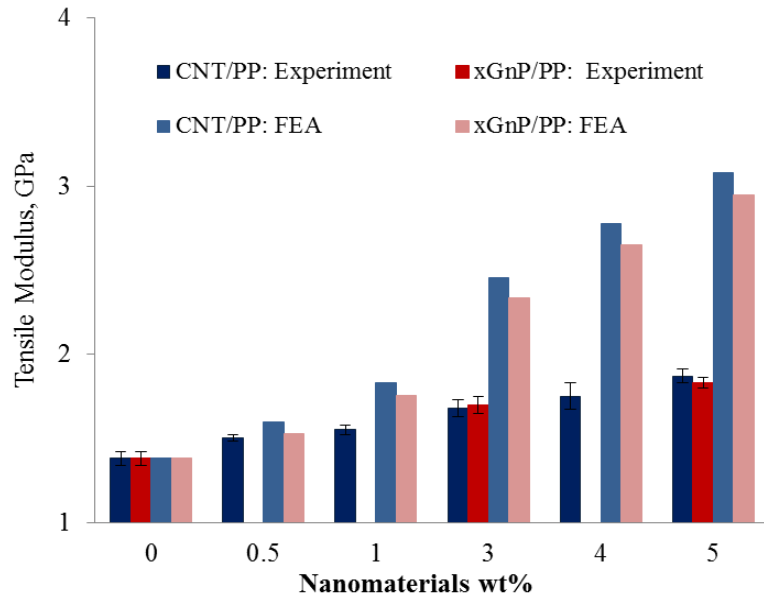
Figure 6.3 Effect of nanomaterials (CNT and xGnP) geometry on the tensile modulus of PNCs

The higher tensile modulus obtained for the case of CNT/PP composites in FEA can be explained by the presence of large number of CNT within the PP matrix, for a constant wt.% of nanomaterials, compared to xGnP. Since the aspect ratio of both the CNT and xGnP is same (~ 65) and thickness of xGnP (15 nm) is comparable to the diameter of CNT (25 nm), the volume of xGnP is significantly larger than that of the CNT; thus, at the same wt.% of nanomaterials content, the number of CNT present in the CNT/PP composites is significantly larger than the number of xGnP presents in the xGnP/PP composites. As the stiffening effect happens through the interaction between the reinforcing phase and the host polymer matrix, a larger number of CNT within the PP results in a better reinforcing effect.

Another important factor that contributes to this improvement is the effective surface area per unit volume of nanomaterials. Considering the dimensions of nanomaterials mentioned above, the effective surface area per unit volume of a CNT is higher than that of an xGnP, as shown in Table 6.1. With a larger number of CNT the surface area available for the surrounding matrix for the case of CNT/PP composites is even higher. This high surface area increases the efficiency of the stress transfer along the CNT–PP interface resulting in higher modulus for the case of CNT/PP composites.

Table 6.1 Effective surface area per unit volume of nanomaterials used in the FEA

Nanomaterials	Surface area of a single nanomaterial (nm^2)	Volume of a single nanomaterial (nm^3)	Surface area to volume ratio
CNT	118.79×10^{-3}	736.31×10^{-3}	0.16
xGnP	1.617×10^{-6}	11.78×10^{-6}	0.13

6.1.2 Effect of Nanomaterials Orientation

FEA is also performed for the case of randomly, with respect to the applied load direction, oriented nanomaterials within the PP matrix. The orientation of both CNT and xGnP is modeled randomly without using probability distribution functions and image

analysis. Representative RVEs of xGnP/PP composites and CNT/PP composites used in FEA to study the orientation effect are presented in Figure 6.4.
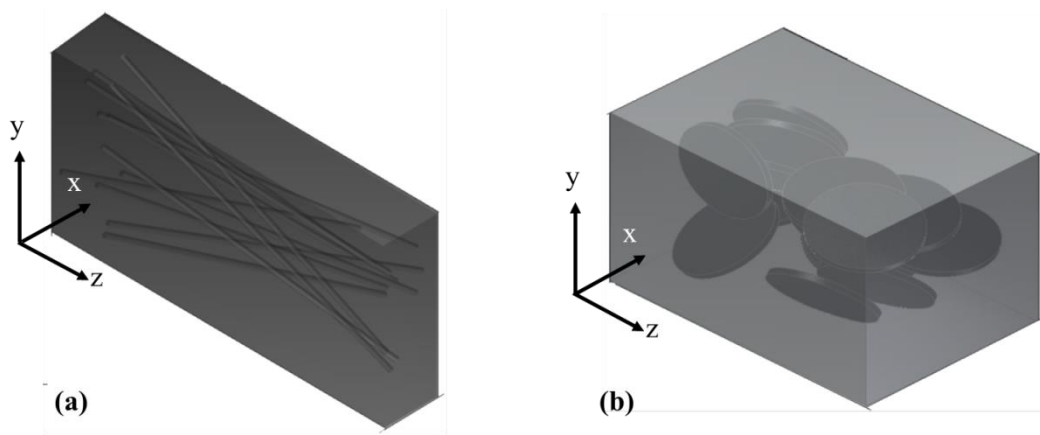
Figure 6.4 Representative RVEs for (a) CNT/PP and (b) xGnP/PP composites used in the FEA to study nanomaterials random orientation effect on the tensile modulus of PNCs

The effect of CNT and xGnP orientation on the tensile modulus of PNCs is presented in Figure 6.5. It is noted that, since the orientation of nanomaterials within the PP matrix is modeled randomly, variations in FEA predictions are expected. Therefore, FEA simulations are repeated three times for each nanomaterial's content and the variations in FEA predictions are presented using error bars in in Figure 6.5. The modulus of the composites for uniform dispersion of nanomaterials and when aligned along the applied load direction (ideal case) is also presented for comparison. As shown in Figure 6.5, the tensile modulus of CNT/PP composites reduces significantly due to the random orientation of CNT within the PP. The random orientation of CNT with respect to the direction of applied load direction reduces the effective length of the CNT, thus reducing their reinforcing efficiency. However, the effect is not significant for the case of xGnP/PP composites. Another important observation that can be made from Figure 6.5 is that the modulus of randomly oriented xGnP reinforced PP composites is higher than the modulus of randomly oriented CNT reinforced PP composites for all nanomaterials content. This can be explained by the xGnP's ability to provide multidirectional reinforcement. The geometry of the xGnP allows it to offer uniform reinforcement

isotropically in the 1-3 plane (see Figure 6.1), while the CNT offers only superior reinforcement as the loading approaches in the longitudinal-1 direction (see Figure 6.1). The reinforcement potential for the CNT in the other directions (direction 2 and 3) is two orders of magnitude lower than that in the longitudinal direction (106). Thus for PNCs with randomly oriented nanomaterials, the xGnP's ability to reinforce the polymer in 2-D compared to the 1-D reinforcing ability of CNT comes into play.
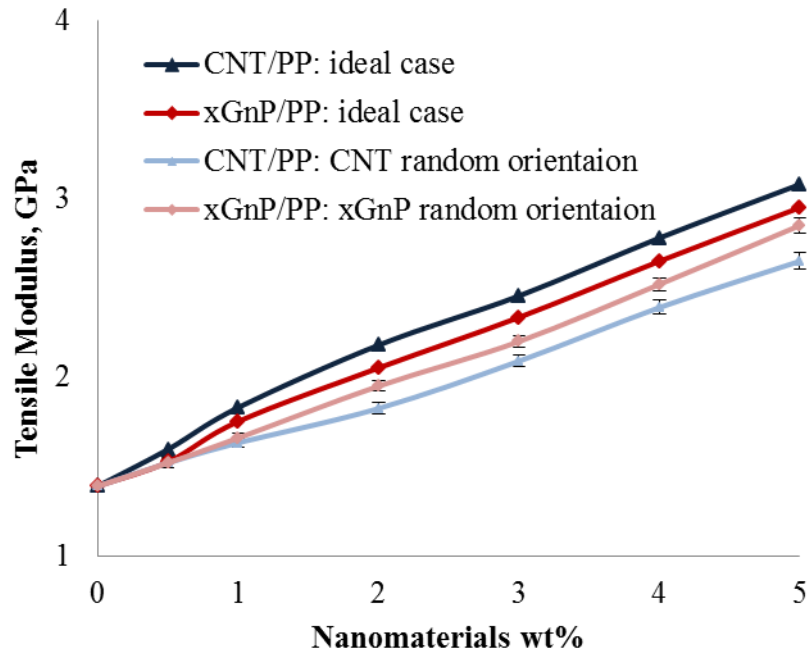
Figure 6.5 Effect of CNT and xGnP random orientation on the tensile modulus of PNCs

6.2 Effect of Nanomaterials/polymer Interphase

Another important factor that needs to be studied in terms of its effect on the tensile modulus of PNCs is the nanomaterial/polymer interphase, which is also related to the geometry of the nanomaterials. Due to the enormous specific surface area of nanomaterials, the amount of interphase generated by the addition of a small volume fraction of nanomaterials can be extensive and thus can have a remarkable impact on the bulk properties of the nanocomposites. As mentioned in chapter 5, the interphase is introduced in the RVE by replacing an equal volume of polymer matrix, while

maintaining the nanomaterials volume. The thickness and the modulus of the nanomaterial/polymer interphase for both the CNT/PP composites and xGnP/PP composites are determined using AFM experiments. The details of the measurement of interphase thickness and modulus through AFM experiments are explained in Chapter 3. Figure 6.6 shows the representative RVEs used in the FEA to study the effect of the nanomaterial/polymer interphase on the tensile modulus of PNCs.
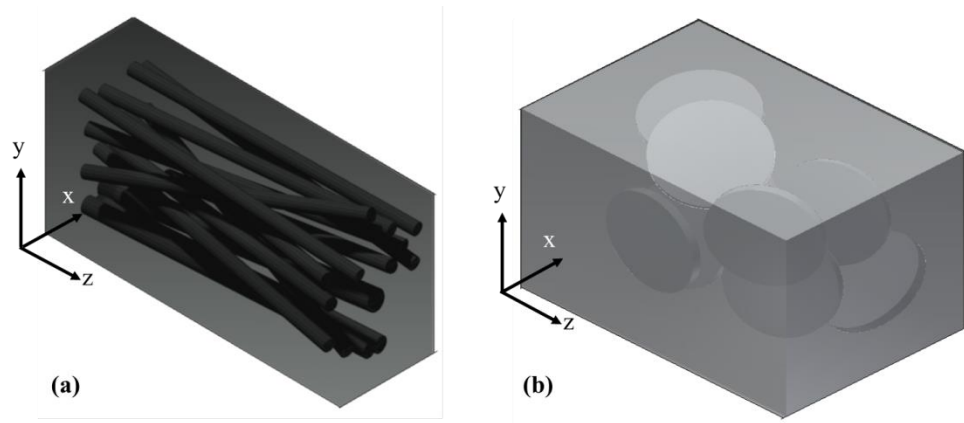
Figure 6.6 Representative RVEs of (a) CNT/PP and (b) xGnP/PP composites used in the FEA to study the effect of interphase on the PNCs tensile modulus

FEA, accounting for the CNT-PP and xGnP-PP interphase and considering random nanomaterial orientation, was performed to determine the tensile modulus of the CNT/PP and xGnP/PP composites. Since the orientation of the nanomaterials within the RVE is random, for each nanomaterial's content the FEA simulations are repeated three times. The results are presented in Figure 6.7. The moduli predictions for ideal case (nanomaterial alignment along the applied load direction and no consideration of interphase) are also presented for both composite for comparison. As shown in Figure 6.7, the interphase results in reduction of the modulus for both composite systems. However, the effect is more significant for CNT/PP composites, which is due to the presence of large amount of interphase. For a constant wt.% of nanomaterials, the number of CNT within the composites is higher than the number of xGnP, this helps to generate a large amount of interphase. In addition, CNT have high specific surface area compared to

xGnP and therefore have higher potential to generate interphase, assuming identical surface chemistries and identical dispersion. The large amount of interphase, which is soft in nature i.e, the modulus of interphase is lower than the modulus of neat PP, present in CNT/PP composites compared to xGnP/PP composites is responsible for the significant reduction in the tensile modulus of CNT/PP composites.
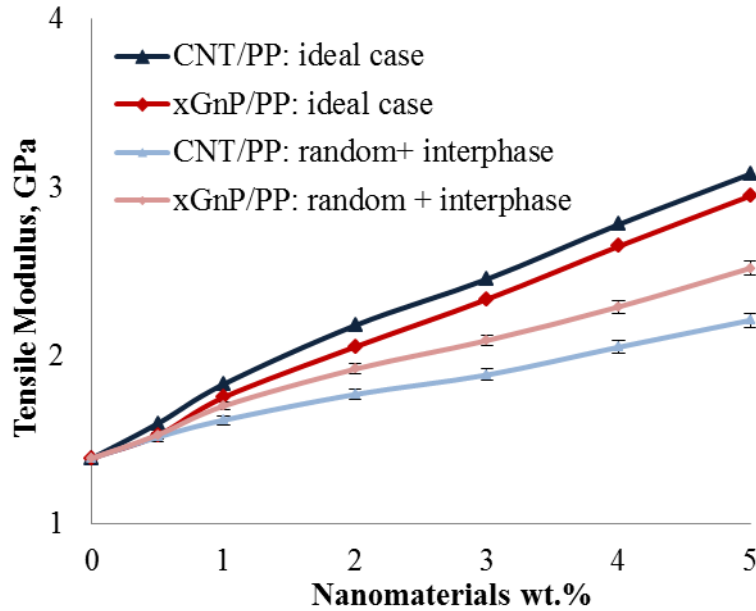
Figure 6.7 Effect of interphase on the tensile modulus of CNT/PP and xGnP/PP composites

6.3 Conclusions

The mechanical reinforcing efficiency of two types of nanomaterials, CNT and xGnP, that have similar surface chemistries and modulus is studied using FEA. Additionally, the effect of interphase, developed in the vicinity of the nanomaterials, on the tensile modulus of PNCs is also studied. As expected the mechanical reinforcing efficiency of CNT is higher than that of xGnP when the nanomaterials are aligned along the applied load direction and when random orientation is considered, the reinforcing efficiency of xGnP is higher due to the 1-D versus 2-D geometry of CNT and xGnP, respectively and to the inherited anisotropy.

In addition, for the same weight fraction of nanomaterials and for uniform dispersion of nanomaterials within the PP matrix, CNT can generate significantly larger amount of soft interphase compared to the interphase generated in case of xGnP which results in higher reduction of tensile modulus of the composites. The presented results highlight the need for considering various aspects of nanomaterials such as geometry, anisotropic reinforcing ability and their influence on the formation of interphase in order to develop better design tools to fabricate PNCs with engineered properties.

CHAPTER 7

CONCLUSIONS AND SUGGESTIONS FOR FUTURE WORK

7.1 Conclusions

In this study, an integrated modeling technique that combines experimental characterization and finite element modeling to determine the tensile modulus of PP composites (bulk and fiber) reinforced with carbon nanomaterials (CNT and xGnP) has been presented. The novelty of the proposed technique is that it can capture the distribution states of various nanomaterials' parameters within the polymer matrix using 2D SEM and AFM images of the composites and it can quantify the effect of these parameters on the tensile modulus of PNCs. The various nanomaterials parameters that are of interest of this study are nanomaterials dispersion, spatial distribution, orientation and waviness. The proposed model is also capable of capturing the effect of the nanomaterials' geometry and of nanomaterial-polymer interphase on the tensile modulus of PNCs.

As a first step of the modeling technique, the distribution of the nanomaterials parameters, mentioned above, within the polymer matrix is characterized using an image analysis technique. For the image analysis technique, SEM images captured from the polished and etched surfaces of PNCs are used. The effect of these parameters on the tensile modulus of PNCs is then investigated quantitatively through finite element analysis. 3D RVEs of the composites are developed using the determined distribution functions of nanomaterials parameters. The distribution of these parameters is incorporated within the RVE with the help of a programming code written in MATLAB$^{®}$ and the corresponding RVEs are generated using Autodesk$^{®}$ Inventor$^{®}$ 3D modeling software. Nanomaterial/polymer interphase of constant width and property that varies across the interphase as obtained from the AFM experiments is also incorporated into the

model. The model is then imported to finite element software, ANSYS 14, and analyzed to predict the tensile modulus of carbon reinforced PP composites.

A systematic study to understand the effect of each individual parameter first, and then all the parameters together on the tensile modulus of PNCs performed. It is found that the modulus of the composites is more sensitive to the presence of nanomaterials agglomerates. A reduction of tensile modulus of approximately 16% is observed when the presence of nanomaterials agglomerates is considered in the analysis. The next important parameters in terms of effect on the tensile modulus of PNCs are the nanomaterial/polymer interphase (tensile modulus reduction is ~ 11%). The effect of other parameters on the modulus, such as the nanomaterials' non-homogeneous distribution, random orientation and waviness, is approximately same, that is in the range of ~ 6 to 8%. Although the individual effect of these parameters is not significant, their combined effect, when considered together in the model, is significant. It is found that when all the parameters are considered in the model at the same time, the reduction in tensile modulus is approximately 40%. A validation of the proposed model is performed by comparing the model predictions with the data obtained from tensile experiment performed according to ASTM D638. The results are in complete agreement revealing that the proposed model can be an excellent approximate in estimating the tensile modulus of PNCs.

The ability of the proposed integrated model to capture the change in distribution states of nanomaterials parameters within the polymer matrix is also investigated. The distribution of nanomaterials' parameters within the PP matrix is altered by using surfactants (for bulk composites) and by changing the processing conditions (fiber composites). Determined distribution functions through image analysis are then incorporated into the finite element model, analyzed and compared with the corresponding experimental data to see if the model can capture the change in distribution state of nanomaterials parameters within the PP matrix. A good agreement

between the model predictions and the experimental data is observed, therefore supporting the ability of the proposed model to capture the change of the nanomaterials' distribution state, if there is any, within the polymer matrix accurately.

In summary, a finite element model that can capture the nanomaterials characteristics that are observed experimentally within the polymer is developed and proposed in this study. The model proposed herein can reliably simulate the tensile modulus of PNCs and provides quantitative information regarding the impact of nanomaterials' parameters and their geometry on the composites tensile modulus. The model can also capture the relative impact and influence of every experimentally observed characteristic that is related to the manufacturing of PNCs. Although several models have been proposed in the literature to calculate the tensile properties of PNCs, finite element model considering all the parameters determined through image analysis has not been proposed to date, which is the fundamental contribution of this study.

The proposed model can have significant impact in the development of PNCs as structural composites. It can be used as a design tool to validate the PNCs' experimental results, as well as a means to explore approximate properties of composite systems without going for the nanocomposites experimentation that are both costly and time intensive due to the equipment and method that must be used.

The presented combined experimental and finite element modeling technique can also be extended to determine the non-linear mechanical behavior i.e., stress-strain relationships of PNCs. The stress-strain curve, which is one of the most important characteristics of PNCs, can easily be obtained by using the proposed model where the only input needed, in addition to the nanomaterials characteristics, is the non-liner elastic properties of the polymer matrix and the nanomaterials. The model is also flexible enough to use for determining other PNCs properties such as electrical and thermal conductivity, percolation threshold, etc. Finally, this model can also be used for other

composite systems providing upfront design guidelines for manufacturing of nanocomposites with engineered properties.

7.2 Future Work

Based on the work presented, several recommendations for future work can be made. The image analysis approach proposed in this study to determine the distribution of nanomaterials parameters within the polymer is suitable only for nanomaterials with cylindrical and circular shapes. Approach to determine the distribution of these parameters for nanomaterials with other geometric shapes such as platelet is therefore needed to be explored. In addition, to determine the waviness of CNT only the visible length of the CNT as observed in the SEM images is considered assuming that the rest of the length follows the same waviness. Future studies in this direction to resolve this issue are therefore needed. Quantifying the modulus of the nanomaterial-polymer interphase is another issue. In this study the property gradient profile across the nanomaterial-polymer interphase is used to approximate the modulus variation across the interphase. However, a direct approach to determine the exact modulus of interphase needs to be explored.

Finally, the focus of this study was mainly to evaluate the tensile modulus of PNCs. Studies on other properties such as tensile strength, Poisson's ratio, vibration damping, transverse shear and compressive buckling, etc. and approach to evaluate these properties for PNCs, through finite element modeling, need to be introduced. Little work has also been performed on non-linear mechanical behavior e.g., fracture or failure of PNCs. The present work can also be directed to evaluate the electrical and thermal properties of PNCs. Based on all these studies to be performed, constitutive equations to calculate the mechanical, electrical and thermal properties of PNCs can be developed as a function of nanomaterials content and geometry and experimentally observed factors including but not limited to the nanomaterials/polymer interphase, nanomaterials dispersion, distribution, orientation, waviness/buckling etc.

APPENDIX A

FEA PARAMETRIC STUDY TO SELECT THE OPTIMUM

ELEMENT SIZE

A FEA parametric study has been performed to select the optimum mesh/element sizes for the three phases (neat PP, nanomaterials and nanomaterial/PP interphase) used in the finite element modeling that give converging solution with minimum computational time. It is noted that only CNT/PP composites were investigated for finding the optimum mesh size and a RVE that consists of CNT embedded within the PP matrix and interphase around the CNT was used. The dimensions of the RVE were: 2000 nm (L) x 250 nm (W) x 250 nm (H). Individual CNT, aligned along the applied load direction, were considered in the model. Figure A.1 presents the FEA predictions of tensile modulus of CNT/PP composites for different CNT wt.% as a function of number of elements. As shown in Figure A.1, for all the wt.% of CNT used in the FEA, the FEA predictions give converging results when the number of elements within the RVE are ~ 70,000 or above. Since, less computational time is desired; element sizes that gave 70,960 elements are selected in this study to perform FEA. The aspect ratio (height to weight ration) of the elements that gave a total of 70,960 elements are as follows:

(i)   For the elements in CNT the element aspect ratio was 1;

(ii)   For the elements in CNT/PP interphase, the element aspect ratio varied for 0.0333 (elements next to the CNT) to 0.0625 (elements next to the PP matrix); and

(iii)   For the elements in PP matrix, the element aspect ratio was also ~ 1 but with higher mesh density next to the CNT/PP interphase and lower mesh density next to RVE boundary.

An illustration of the 3D finite element mesh used in this study is presented in Figure A.2.
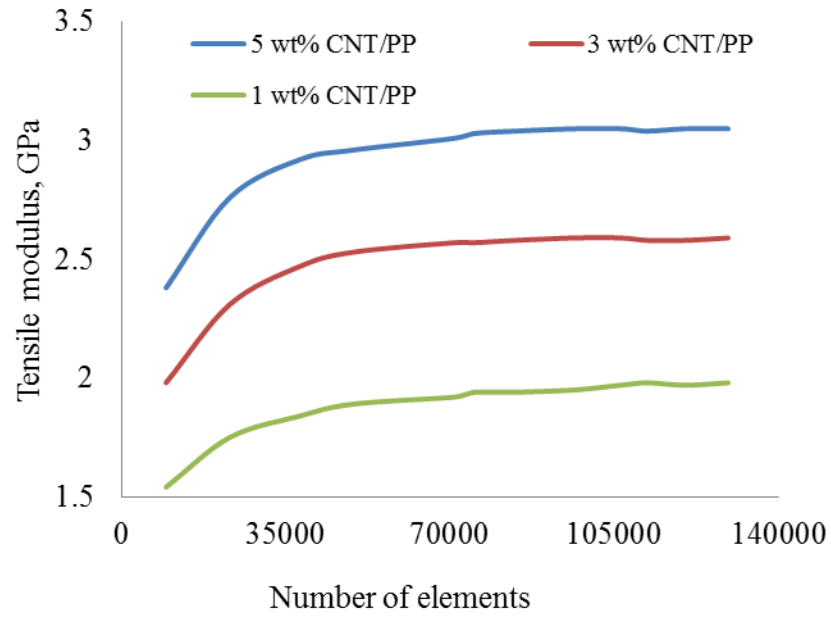
Figure A.1: FEA parametric study to find the optimum mesh size with converging solution
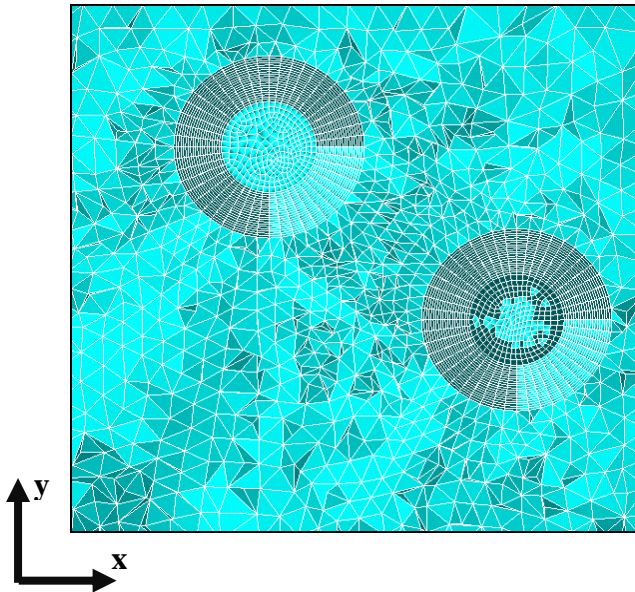
Figure A.2: Illustration of 3D finite element mesh used in this study

REFERENCES

[1]   Godovsky, D.Y., "Device applications of polymer-nanocomposites," Advances in Polymer Science, vol. 153, pp. 163-205, 2000.

[2]   Mylvaganam, K., and Zhang, L.C., "Fabrication and application of polymer composites comprising carbon nanotubes," Recent Patents on Nanotechnology, vol. 1, pp. 59-65, 2007.

[3]   Jancar, J., Douglas, J. F., Starr, F. W., Kumar, S. K., Cassagnau, P., and Lesser, A. J., "Current issues in research on structureeproperty relationships in polymer nanocomposites," Polymer, vol. 51, pp. 3321-3343, 2010.

[4]   Du, J. H., Bai, J., and Cheng, H. M., "The present status and key problems of carbon nanotube based polymer composites," eXPRESS Polymer Letters, vol. 1(5), pp. 253-273, 2007.

[5]   Li, B., and Zhong, W. H., "Review on polymer/graphite nanoplatelet nanocomposites," Journal of Materials Science, vol. 46, pp. 5595-5614, 2011.

[6]   Dusza, J., Blugan, G., Morgiel, J., Kuebler, J., Inamd, F., Peijs, T., et al. "Hot pressed and spark plasma sintered zirconia/carbon nanofiber composites," Journal of the European Ceramic Society, vol. 29, pp. 3177- 3184, 2009.

[7]   Gall, K., Dunn, M. L., and Liu, Y., "Internal stress storage in shape memory polymer nanocomposites," Applied Physics Letters, vol. 84(2), pp. 290-292, 2004.

[8]   Liu, H., and Webster, T. J., "Mechanical properties of dispersed ceramic nanoparticles in polymer composites for orthopedic applications," International Journal of Nanomedicine, vol. 5, pp. 299-313, 2010.

[9]   Patel, H. A., Somani, R. S., Bajaj, H. C., and Jasra, R. V., "Nanoclays for polymer nanocomposites, paints, inks, greases and cosmetics formulations, drug delivery vehicle and waste water treatment," Bulletin of Materials Science, vol. 29(2), pp. 133-145, 2006.

[10]   Kim, H., Abdala, A. A., and Macosko, C. W., "Graphene/Polymer Nanocomposites," Macromolecules, vol. 43(16), pp. 6515-6530, 2010.

[11]   Wanjun, L., Inhwan, D., Hiroyuki, F., and Drzal, L. T., "Influence of Processing on Morphology, Electrical Conductivity and Flexural Properties of Exfoliated Graphite Nanoplatelets–Polyamide Nanocomposites," Carbon Letters, vol. 11(4), pp. 279-284, 2010.

[12]   Moniruzzaman, M., and Winey, K. I., "Polymer Nanocomposites Containing Carbon Nanotubes," Macromolecules, vol. 39(16), pp. 5194- 5205, 2006.

[13]   Choi, Y.K., Sugimoto, K. I., Song, S. M., Gotoh, Y., Ohkoshi, Y., and Endo, M., "Mechanical and physical properties of epoxy composites reinforced by vapor grown carbon nanofibers," Carbon, vol. 43(10), pp. 2199-2208, 2005.

[14]   Advani, S.G., "Proessing and properties of Nanocomposites," Singapore: World Scientific Publish Co. Pte. Ltd; 2007.

[15]   Nafigate nanofibers gateway (www.nafigate.com).

[16]   Meo, M., and Rossi, M., "A molecular-mechanics based finite element model for strength prediction of single wall carbon nanotubes," Materials Science and Engineering: A, vol. 454-455, pp. 170-177, 2007.

[17]   Tserpes, K., Papanikos, P., and Tsirkas, S., "A progressive fracture model for carbon nanotubes," Composites Part B: Engineering, vol. 37, pp. 662-669, 2006.

[18]   Yu, M. F., Lourie, O., Dyer, M.J., Moloni, K., Kelly, T. F., and Ruoff, R. S., "Strength and breaking mechanism of multiwalled carbon nanotubes under tensile loads," Science, vol. 287, pp. 637-640, 2000.

[19]   Berber, S., Kwon, Y., and Tomanek, D., "Unusually High Thermal Conductivity of Carbon Nanotubes," Physical Review Letters, vol. 84(20), pp. 4613-4616, 2000.

[20]   Du, F., Guthy, C., Kashiwagi, T., Fischer, J. E., and Winey, K. I., "An infiltration method for preparing single-wall nanotube/epoxy composites with improved thermal conductivity," Journal of Polymer Science Part B: Polymer Physics, vol. 44, pp. 1513-1519, 2006.

[21]   Moisala, A., Li, Q., Kinloch, I., and Windle, A., "Thermal and electrical conductivity of single- and multi-walled carbon nanotube-epoxy composites," Composites Science and Technology, vol. 66, pp. 1285-1288, 2006.

[22]   Luo, D., Wang, W. X., and Takao, Y., "Effects of the distribution and geometry of carbon nanotubes on the macroscopic stiffness and microscopic stresses of nanocomposites," Composites Science and Technology, vol. 67(14), pp. 2947-2958, 2007.

[23]   Odegard, G. M., Frankland, S. J. V., and Gates, T. S., "The effect of chemical functionalization on mechanical properties of nanotube/polymer composites," American Institute of Aeronautics andAstronautics, 2003.

[24]   Ciprari, D. J., and Tannenbaum, R., "Characterization of polymer nanocomposite interphase and its impact on mechanical properties," Macromolecules, vol. 39(19), pp. 6565-6573, 2006.

[25]   Jancar J., "Review of the role of the interphase in the control of composite performance on micro- and nano-length scales," Journal of Materials Science, vol. 43(20), pp. 6747-6757, 2008.

[26]   Mader, E., Gao, S., "Prospect of nanoscale interphase evaluation to predict composite properties," Journal of Adhesion Science and Technology, vol. 15, pp. 1015-1037, 2001.

[27]   Ajayan, P. M., and Tour, J. M., "Materials science: nanotube composites," Nature, vol. 447(7148), pp. 1066-1068, 2007.

[28]   Calvert, P., "Nanotube composites: a recipe for strength," Nature, vol. 399(6733), pp. 210–211, 1999.

[29]   Endo, M., Strano, M. S., and Ajayan, P. M., "Potential applications of carbon nanotubes," Berlin/Heidelberg: Springer; 2008.

[30]   Kevin, D. A., Piner, R., Lourie, A. O., Ruoff, R. S., and Korobov, M., Organic "Solvent Dispersions of Single-Walled Carbon Nanotubes: Toward Solutions of Pristine Nanotubes," September, 2000.

[31]   Thostenson, E. T., Li. C., Chou, T.W., "Nanocomposites in context," Composites Science and Technology, vol. 65, pp. 491-516, 2005.

[32]   Andrews, R., Jaques, D., Qian, D., and Rantell, T., "Multiwall Carbon Nanotubes: Synthesis and Application," Accounts of Chemical Research, vol. 35(12), pp. 1008-1017, 2002.

[33]   Sideridis, E., "The in plane shear modulus of fiber reinforced composites as defined by the concept of interphase," Composites Science and Technology, vol. 31, pp. 35-53, 1988.

[34]   Dasgupta, A., and Bhandarkar, S. M., "A Generalized Self-Consistent Mori-Tanaka Scheme for Fiber Composites with Multiple Interphases," Mechanics of Materials, vol. 14, pp. 67-82, 1992.

[35]   Tsagaropoulos, G., and Eisenbere, A., "Direct observation of two glass transitions in silica-filledpolymers. Implications to the morphology of random ionomers," Macromolecules, vol. 28(1), pp. 396-398, 1995.

[36]   Kim, J. K., Sham, M. L., and Wu, J., "Nanoscale characterization of interphase in silane treated glass fibre composites," Composites Part A: Applied Science and Manufacturing, vol. 32(5), pp. 607-618, 2001.

[37]   Kim, J. K., and Hodzic, A., "Nanoscale characterisation of thickness and properties of interphase in polymer matrix composites," The Journal of Adhesion, vol. 79(4), pp. 383-414, 2003.

[38]   Williams, J. G., Donnellan, M. E., James, M.R., and Morris, W. L., "Properties of the Interphase in Organic Matrix Composites," Materials Science and Engineering, A., vol. 126(1-2), pp. 305-312, 1990.

[39]   Munza, M., Sturma, H., Schulza, E., and Hinrichsenb, G., "The scanning force microscope as a tool for the detection of local mechanical properties within the interphase of fibre reinforced polymers," Composites Part A: Applied Science and Manufacturing, vol. 29(9-10), pp. 1251–1259, 1998.

[40]   VanLandinghama, M., Dagastinea, R., Eduljeea, R., McCullougha, R., and Gillespie, J. W., "Characterization of nanoscale property variations in polymer composite systems: 1. Experimental results," Composites Part A: Applied Science and Manufacturing, vol. 30(1), pp. 75-83, 1999.

[41]   Bogetti, T., Wang, T., VanLandingham, M. and Gillespie, J. W., "Characterization of nanoscale property variations in polymer composite systems: 2. Numerical modeling," Composites Part A: Applied Science and Manufacturing, vol. 30(1), pp. 85-94, 1999.

[42]   Gao, S. L., and Mader, E., "Characterisation of interphase nanoscale property variations in glass fibre reinforced polypropylene and epoxy resin composites," Composites Part A: Applied Science and Manufacturing, vol. 33(4), pp. 559-576, 2002.

[43]   Ajayan, P.M., "Nanotubes from carbon. Chemical Reviews," vol. 99(7), pp. 1787-1800, 1999.

[44]   Qian, D., Dickey, E. C., Andrews, R., and Rantell, T., "Load transfer and deformation mechanisms in carbon nanotubepolystyrene composites," Applied Physics Letters, vol. 76(20), pp. 2868-2870, 2000.

[45]   Thostenson, E. T., and Chou, T. W., "Aligned multi-walled carbon nanotube-reinforced composites: processing and mechanical characterization," Journal of Physics D: Applied Physics, vol. 35, pp. 77-80, 2002.

[46]   Kalaitzidou, K., Fukushima, H., and Drzal, L. T., "A Route for Polymer Nanocomposites with Engineered Electrical Conductivity and Percolation Threshold," Materials, vol. 3, pp. 1089-1103, 2010.

[47]   Fisher, F. T., Bradshaw, R. D., and Brinson, L. C., "Effects of nanotube waviness on the modulus of nanotube-reinforced polymers," Applied Physics Letters, vol. 80(24), pp. 4647- 4649, 2002.

[48]   Shi, D. L., Feng, X. Q., Huang, Y. Y., Hwang, K. C., and Gao, H., "The Effect of Nanotube Waviness and Agglomeration on the Elastic Property of Carbon Nanotube-Reinforced Composites," Journal of Engineering Materials and Technology, vol. 126, pp. 250-257, 2004.

[49]   Anumandla, V., and Gibson, R.F., "A comprehensive closed form micromechanics model for estimating the elastic modulus of nanotube-reinforced composites," Composites Part A: Applied Science and Manufacturing, vol. 37(12), pp. 2178-2185, 2006.

[50]   Andrews, R., Jacques, D., Minot, M., and Rantell, T., "Fabrication of carbon multiwalled nanotube/polymer composites by shear mixing," Macromolecular Materials and Engineering, vol. 287(6), pp. 395-403, 2002.

[51]   Xia, H., Wang, Q., Li, K., and Hu, G.H., "Preparation of propylene/carbon nanotube composite powder with a solid-state mechanochemical pulverization process," Journal of Applied Polymer Science, vol. 93, pp. 378-86, 2004.

[52]   Song, Y. S., and Youn, J. R., "Influence of dispersion states of carbon nanotubes on physical properties of epoxy nanocomposites," Carbon, vol. 43, pp. 1378-85, 2005.

[53]   Zhu, J., Peng, H., Rodriguez-Macias, F., Margrave, J., Khabashesku, V., and Imam, A., "Reinforcing Epoxy Polymer Composites Through Covalent Integration of Functionalized Nanotubes," Advanced Functional Materials, vol. 14, pp. 643-648, 2004.

[54]   Zhu, J., Kim, J., Peng, H., Margrave, J., Khabashesku, V., and Barrera, E., "Improving the Dispersion and Integration of Single-Walled Carbon Nanotubes in Epoxy Composites through Functionalization," Nano Letters, vol. 3, pp. 1107-1113, 2003.

[55]   Vaia, R., Koerner, H., Lu, W., and Manias, E., "Polymer Nanocomposites With Prescribed Morphology: Going Beyond Nanoparticle-filled Polymers," Chemistry of Materials, vol. 19(11), pp. 2736-2751, 2007.

[56]   Wang, Z., and Stein, A., "Morphology Control of Carbon, Silica, and Carbon/Silica Nanocomposites: From 3D Ordered Macro-/Mesoporous Monoliths to Shaped Mesoporous Particles," Chemistry of Materials, vol. 20(3), pp. 1029-1040, 2008.

[57]   Okamoto, M., Nam, H.P., Maiti, P., Kotaka, T., Hasegawa, N., and Usuki, A., "A House of Cards Structure in Polypropylene/Clay Nanocomposites under Elongational Flow," Nano Letters, vol. 1(6), pp. 295-298, 2001.

[58]   Thostenson, E. T., and Chou, T. W., "On the elastic properties of carbon nanotube-based composites: modelling and characterization,." Journal of Applied Physics D: Applied Physics, vol. 36(5), pp. 573-582, 2003.

[59]   Dresselhausa, M. S., Dresselhausb, G., Saitoc, R., and Joriod, A., "Raman spectroscopy of carbon nanotubes," Physics Reports, vol. 409, pp. 47-99, 2005.

[60]   Shaffer, M. S. P., and Windle, A. H., "Fabrication and characterization of carbon nanotube/poly(vinyl alcohol) composites," Advanced Materials, vol. 11, pp. 937-941, 1999.

[61]   Fan, Z., and Advani, S. G., "Characterization of orientation state of carbon nanotubes in shear flows," Polymer, vol. 46, pp. 5232-5240, 2005.

[62]   Andrews, R., Jacques, D., Rao, A. M., Rantell, T., Derbyshire, F., an d Chen, Y., "Nanotube Composite Carbon Fibers," Applied Physics Letters, vol. 75(9), pp. 1329-1331, 1999.

[63]   Kumar, S., Dang, T. D., Arnold, F. E., Bhattacharyya, A. R., Min, B. G., and Zhang, X., "Synthesis, Structure and properties of PBO/SWNT composites," Macromolecules, vol. 24, pp. 9039-9043, 2002.

[64]   Liang, J., Huang, Y., Zhang, L., Wang, Y., Ma, Y., and Guo, T., "Molecular-level dispersion of graphene into poly(vinyl alcohol) and effective reinforcement of their nanocomposites," Advanced Functional Materials, vol. 19, pp. 2297-2302, 2009.

[65]   Kalaitzidou, K., Fukushima, H., and Drzal, L. T., "A new compounding method for exfoliated graphite–polypropylene nanocomposites with enhanced flexural properties and lower percolation threshold," Composites Science and Technology, vol. 67, pp. 2045-2051, 2007.

[66]   Kalaitzidou, K., Fukushima, H., Drzal, L. T., "Mechanical properties and morphological characterization of exfoliated graphitepolypropylene nanocomposites," Composites Part A: Applied Science and Manufacturing, vol. 38, pp. 1675-1682, 2007.

[67]   Wakabayashi, K., Pierre, C., Dikin, D. A., Ruoff, R. S., Ramanathan, T., and Brinson, L. C., "Polymer-graphite nanocomposites: effective dispersion and major property enhancement via solid-state shear pulverization," Macromolecules, vol. 41, pp. 1905-1908, 2008.

[68]   Kim, S., Do, I., and Drzal, L.T., "Multifunctional Exfoliated Graphite Nanoplatelets-LLDPE Nanocomposites Fabricated By Solution Compounding

Method And Various Screw Rotating Systems," Macromolecular Materials and Engineering, vol. 3, pp. 196-205, 2009.

[69]   Kim, S, and Drzal, L. T., "Improvement of electric conductivity of LLDPE based nanocomposite by paraffin coating on exfoliated graphite nanoplatelets," Composites Part A: Applied Science and Manufacturing, vol. 41, pp. 1581-1587, 2010.

[70]   Chen, X. L., and Liu, Y. J., "Square Representative Volume Elements for Evaluating the Effective Material Properties of Carbon Nanotube-Based Composites," Computational Materials Science, vol. 29, pp. 1-11, 2004.

[71]   Griebel, M., and Hamaekers, J., "Molecular dynamics simulations of the elastic modulii of polymer-carbon nanotube composites," Computer methods in applied mechanics and engineering, vol. 193, pp. 1773-1788, 2004.

[72]   Frankland, S. J. V., Caglar, A., Brenner, D.W., and Griebel, M., "Reinforcement mechanisms in polymer nanotube composites: Simulated non-bonded and crosslinked system," MRS Fall Meeting, 2000.

[73]   Frankland, S. J. V., Harik, V. M., Odegard, G. M., Brenner, D. W., and Gates, T.S., "The stress-strain behavior of polymer-nanotube composites from molecular dynamics simulations," Composites Science and Technology, vol. 63(11), pp. 1655-1661, 2003.

[74]   Odegard, G. M., Gates, T. S., Nicholson, L. M., and Wise. K. E., "Equivalent-Continuum Modeling of Nano-Structured Materials," Composites Science and Technology, vol. 62(14), pp. 1869-1880, 2002.

[75]   Odegard, G. M., Gates, T. S., Wise, K.. E., "Constitutive Modeling of Nanotube-Reinforced Polymer Composites," American Institute of Aeronautics andAstronautics, 2002.

[76]   Valavala, P. K., and Odegard, G. M., "Modeling Techniques for Determination of Mechanical Properties of Polymer Nanocomposites," Reviews on Advanced Materials Science, vol. 9, pp. 34-44, 2005.

[77]   Wan, H., Delale, F., and Shen, L., "Effect of CNT length and CNT-matrix interphase in carbon nanotube (CNT) reinforced composites," Mechanics Research Communications, vol. 32(5), pp. 481-489, 2005.

[78]   Hernández-Pérez, A., and Avilés, F., "Modeling the influence of interphase on the elastic properties of carbon nanotube composites," Computational Materials Science, vol. 47, pp. 926-933, 2010.

[79]   Pantano. A., Modica, G., and Cappello, F., "Multiwalled carbon nanotube reinforced polymer composites," Materials Science and Engineering, A, vol. 486, pp. 222-227, 2008.

[80]   Ashrafi. B., and Hubert, P., "Modeling the elastic properties of carbon nanotube array/polymer composites," Composites Science and Technology, vol. 66, pp. 387-396, 2006.

[81]   Gade, S., "Characterization of the Mechanical properties of carbon nanotube based composites using the finite element method," M. S. Thesis, University of Cincinnati, 2005.

[82]   Liu, Y. J., and Chen, X. L., "Evaluation of the Effective Material Properties of Carbon Nanotube-Based Composites Using a Nanoscale Representative Volume Element," Mechanics of Materials, vol. 35, pp. 69-81, 2003.

[83]   Schadler, L. S., Giannaris, S. C., and Ajayan, P. M., "Load transfer in carbon nanotube epoxy composites," Applied Physics Letters. vol. 73(26), pp. 3842-3844, 1998.

[84]   Wagner, H. D., Lourie, O., Feldman, Y., and Tenne, R., "Stress-induced fragmentation of multiwall carbon nanotubes in a polymer matrix," Applied Physics Letters, vol. 72(2), pp. 188-190, 1998.

[85]   Bower, C., Rosen, R., Jin, L., Han, J., and Zhou, O., "Deformation of carbon nanotubes in nano-tube composites," Applied Physics Letters, vol. 74(22), pp. 3317-3319, 1999.

[86]   Hu, N., Fukunaga, H., Lu, C., Kameyama, M., and Yan, B., "Prediction of elastic properties of carbon nanotube reinforced composites," Proceedings of the Royal Society A, vol. 461, pp. 1685-1710, 2005.

[87]   Xu, L. R., and Sengupta, S., "Interfacial stress transfer and property mismatch in discontinuous nanofiber/nanotube composite materials," Journal of Nanoscience and Nanotechnology, vol. 5(4), pp. 620-626, 2005.

[88]   Fisher. F. T., Bradshaw, R. D., and Brinson, L. C., "Fibre Waviness in Nanotube-Reinforced Polymer Composites- I: Modulus Predictions Using Effective Nanotube Properties," Composites Science and Technology, vol. 63, pp.1689-1703, 2003.

[89]   Li, C., and Chou, T. W., "Failure of carbon nanotube/polymer composites and the effect of nanotube waviness," Composites Part A: Applied Science and Manufacturing, vol. 40, pp. 1580-1586, 2009.

[90]   Teng, C. C., Ma, C. C. M., Huang, Y.W., Yuen, S.M., Weng, C.C., and Chen C.H., "Effect of MWCNT content on rheological and dynamic mechanical properties of multiwalled carbon nanotube/polypropylene composites," Composites Part A: Applied Science and Manufacturing, vol. 39, pp. 1869-1875, 2008.

[91]   Noll, A., and Knoer, N., "Crystallization Behaviour of TiO2 Nanoparticle Reinforced Polypropylene," Materials Science Forum, vol. 636-637, pp. 688-696, 2010.

[92]   Ton-That, M. T., Leelapornpisit, W., Utracki, L. A., Perrin-Sarazin, F., Denault, J., and Cole, K. C., "Effect of Crystallization on Intercalation of Clay-Polyolefin Nanocomposites and their Performance," Polymer Engineering and Science, vol. 46, pp. 1085-1093, 2006.

[93]   Zhang , S., Minus, M. L., Zhu, L., Wong, C. P., and Kumar, S., "Polymer transcrystallinity induced by carbon nanotubes," Polymer Composites, vol. 49, pp. 1356-1364, 2008.

[94]   Halpin, J. C., and Kardos, J. L., "The Halpin–Tsai equations: a review," Polymer Engineering and Science. vol. 16(5), pp. 344-352, 1976.

[95]   Tandon, G. P., and Weng, G. J., "The effect of aspect ratio of inclusions on the elastic properties of unidirectionally aligned composites," Polymer Composite, vol. 5(4), pp. 327-333, 1984.

[96]   Moore, E. M., Ortiz, D. L., Marla, V. T., Shambaugh, R. L., and Grady, B.P., "Enhancing the Strength of Polypropylene Fibers with Carbon Nanotubes," Journal of Applied Polymer Science, vol. 93, pp. 2926-2933, 2004.

[97]   Yang, J. P., Yang, G., Xu, G., and Fu, S.Y., "Cryogenic mechanical behaviors of MMT/epoxy nanocomposites," Composites Science and Technology, vol. 67, pp. 2934-2940, 2007.

[98]   Khalili, S. M., Soleimani, N., Farsani, R. E., and Hedayatnasab, Z., "Tensile Properties of Clay/PolypropyleneNanocomposites at Cryogenic Temperature," Advanced Materials Research, vol. 488-489, pp. 562-566, 2012.

[99]   Huang, C. J., Fu, S. Y., Zhang, Y. H., Lauke, B., Li, L. F., and Ye, L., "Cryogenic properties of SiO_2/epoxy nanocomposites," Cryogenics, vol. 45, pp. 450-454, 2005.

[100]   Cheng, H. K. F., Pan, Y., Sahoo, N. G., Chong, K., Li, L., and Hwa-Chan, S., "Improvement in properties of multiwalled carbon nanotube/polypropylene nanocomposites through homogeneous dispersion with the aid of surfactants," Journal of Applied Polymer Science, vol. 124(2), pp. 1117-1127, 2012.

[101]   Zhou, Z., Wang, S., Lu, L., Zhang, Y., and Zhang, Y., "Functionalization of multi-wall carbon nanotubes with silane and its reinforcement on polypropylene composites," Composites Science and Technology, vol. 68, pp. 1727-1733, 2008.

[102]   Micusık, M., Omastova, M., Pionteck, J., Pandis, J., Logakis, E., Pissis, P., "Influence of surface treatment of multiwall carbon nanotubes on the properties of polypropylene/carbon nanotubes nanocomposites," Polymers for Advanced Technologies, vol. 22, pp. 38-47, 2011.

[103]   Kim, J. K., and Mai, Y. W., "High Strength, High Fracture Toughness Fibre Composites with Interface Control A Review," Composites Science and Technology, vol. 41, pp. 333-378, 1991.

[104]   Drzal, L. T., and Madhukar, M., "Fibre-matrix adhesion and its relationship to composite mechanical properties," Journal of Materials Science, vol 28, pp. 569-610, 1993.

[105]   Fisher, F. T., "Nanomechanics and the viscoelastic behavior of carbon nanotube-reinforced polymers," PhD Thesis, Northwestern University, 2002.

[106]   Liu, H., and Brinson, L. C., "Reinforcing efficiency of nanoparticles: A simple comparison for polymer nanocomposites," Composites Science and Technology, vol. 68(6), pp. 1502-1512, 2008.

[107] Vélez-García, G. M., Wapperom, P., Baird, D. G., Aning, A. O., and Kunc, V., "Unambiguous orientation in short fiber composites over small sampling area in a center-gated disk," Composites Part A: Applied Science and Manufacturing, vol. 43, pp. 104-113, 2012.

[108] Stein, A. M., Vader, D. A., Jawerth, L. M., Weitz, D. A., and Sander, L. M., "An algorithm for extracting the network geometry of three-dimensional collagen gels," Journal of Microscopy, vol. 232, pp. 463-475, 2008.

[109] Bay, R.S., and Tucker, C. L., "Stereological measurement and error estimates for threedimensional fiber orientation," Polymer Engineering & Science, vol. 32(4), pp. 240-253, 1992.

[110] Clarke, A. R., and CN. E., "Microscopy techniques for materials science," Boca Raton: CRC, 2002.

[111] Gommes, C., Blacher, S., Masenelli-Varlot, K., Bossuot, C., McRae, E., and Fonseca, A., "Image analysis characterization of multi-walled carbon nanotubes," Carbon, vol. 41, pp. 2561-2572, 2003.

[112] Sarkar, A., and Banerjee, R., "A quantitative method for characterization of carbon nanotubes for hydrogen storage," International Journal of Hydrogen Energineering, vol. 29, pp. 1487-1491, 2004.

[113] Fischer. G., and Eyerer, P., "Measuring spatial orientation of short fiber reinforced thermoplastics by image analysis," Polymer Composites, vol. 9, pp. 297-304, 1988.

[114] Rezakhaniha, R., Agianniotis, A., Schrauwen, J. T. C., Griff, A., Sage, D., Bouten, C. V. C., van de Vosse, F. N., Unser, M., and Stergiopulos, N., "Experimental investigation of collagen waviness and orientation in the arterial adventitia using confocal laser scanning microscopy," Biomechanics and Modeling in Mechanobiology, vol. 11, pp. 461-473, 2012.

[115] Grujicic, M., Cao, G., and Roy, W.N., "A computational analysis of the percolation threshold and the electrical conductivity of carbon nanotubes filled polymeric materials," Journal of Materials Science, vol. 39(14), pp. 4441-4449, 2004.

[116] Selmi, A., Friebel, C., Doghri, I., and Hassis, H., "Prediction of the elastic properties of single walled carbon nanotube reinforced polymers: a comparative study of several micromechanical models," Composites Science and Technology, vol. 67, pp. 2071-2084, 2007.

[117] Gao, X. L., and Li. K., "A shear-lag model for carbon nanotube-reinforced polymer composites," International Journal of Solids and Structures, vol. 42(5-6), pp. 1649-1667, 2005.

[118] Bhuiyan, M. A., Pucha R. V., Karevan, M., and Kalaitzidou, K., "Tensile modulus of carbon nanotube/polypropylene composites - A computational study based on experimental characterization," Computational Materials Science, vol. 50(8), pp. 2347-53, 2011.

[119] Karevan, M., Pucha, R. V., Bhuiyan, M. A., and Kalaitzidou, K., "Effect of interphase Modulus and nanofiller Agglomeration on the Tensile Modulus of Graphite Nanoplatelets and Carbon Nanotube Reinforced Polypropylene Nanocomposites," Carbon letters, vol. 11(4), pp. 325-331, 2010.

[120] Zhang, W. X., Li, L. X., and Wang, T. J., "Interphase effect on the strengthening behavior of particle-reinforced metal matrix composites," Computational Materials Science, vol. 41(2), pp. 145-155, 2007.

[121] Hammeranda, D. C., Seidelb, G. D., and Lagoudasb, D. C., "Computational Micromechanics of Clustering and Interphase Effects in Carbon Nanotube Composites," Mechanics of Advanced Materials and Structures, vol. 14(4), pp. 277-294, 2007.

[122] Kumar, P., Chandra, R., and Singh, S. P., "Interphase Effect on Fiber-Reinforced Polymer Composites," Composite Interfaces, vol. 17(1), pp. 15-35, 2010.

[123] Nielsen, L.E., "Mechanical properties of polymers and composites," New York: Marcel Dekker; 1974.

[124] Tucker, C.L., and Liang, E., "Stiffness predictions for unidirectional short-fiber composites: review and evaluation," Composites Science and Technology, vol. 59(5), pp. :65-671, 1999.

[125] Lee, S. H., Cho, E., Jeon, S. H., and Youn, J. R., "Rheological and electrical properties of polypropylene composites containing functionalized multi-walled carbon nanotubes and compatibilizers," Carbon, vol. 45(14), pp. 2810-22, 2007.

[126] Peng, L., "Modifications of carbon nanotubes with polymers," European Polym er Journal, vol. 41, pp. 2693-2703, 2005.

[127] Jeefferie, A. R., Yuhazri, M. Y., Nooririnah, O., Haidir, M.M., Sihombing, H., and Salleh, M. A.M., "Thermomechanical amd morphological interrelationship of polypropylene-multiwalled carbon nanotubes (PP/MWNTs) nanocomposites, " International Journal of Basic & Applied Sciences, vol. 10(4), pp. 29-35,2010 .

[128] Bhuiyan, M. A., Pucha, R.V., Worthy, J., Karevan, M., and Kalaitzidou, K., "Defining the lower and upper limit of the effective modulus of CNT/polypropylene composites through integration of modeling and experiments," Composite Structure, vol . 95, pp. 80-87, 2013.

VITA

MD ATIQUR RAHMAN BHUIYAN

BHUIYAN started his doctoral education in the George W. Woodruff School of Mechanical Engineering at Georgia Institute of Technology (Atlanta, GA, USA) in the Spring semester of 2009. His research focuses on understanding the structure-property relationships in polymer nanocomposites in order to be able to manufacture polymer nanocomposites with engineered properties for targeted applications. He received his baccalaureate in Mechanical Engineering from Bangladesh University of Engineering and Technology (Dhaka, Bangladesh) in 2006. He received his Master's degree in Mechanical Engineering from Tuskegee University (Tuskegee Institute, AL, USA) in 2009, where he conducted research in developing sandwich structures for automotive, marine and aerospace applications. During his PhD he has published six journal papers (three as first author and three as co-author) and six conference papers (four as first author and two co- author).